SPOUTED BED HYDRODYNAMICS AT TEMPERATURES UP TO 580°C

by

YANG LI

B. Eng. East China University of Chemical Technology, 1985

M. Eng. East China University of Chemical Technology, 1988

A THESIS SUBMITTED IN PARTIAL FULFILLMENT OF

THE REQUIREMENTS FOR THE DEGREE OF

MASTER OF APPLIED SCIENCE

in

THE FACULTY OF GRADUATE STUDIES

DEPARTMENT OF CHEMICAL ENGINEERING

We accept this thesis as conforming

to the required standard

THE UNIVERSITY OF BRITISH COLUMBIA

August 1992

Abstract

A study of the hydrodynamics of spouted beds at temperatures ranging from room temperature to $580°C$ was carried out using a 0.156 m I.D. stainless steel conical-cylindrical half-column. Five narrowly sized fractions of Target sand with reciprocal mean diameters of 0.915 mm, 1.010 mm, 1.200 mm, 1.630 mm and 2.025 mm, and three orifices with internal diameters of 12.70 mm, 19.05 mm and 26.64 mm were used.

The main purpose of the present work was to obtain a wide range of experimental data at high temperatures and compare the results with existing equations, to establish new correlations under different circumstances. Aspects studied included minimum spouting velocity, U_{ms}, maximum spoutable bed height, H_m, and average spout diameter, D_s.

It was found that the stability of spouting decreased with increasing temperature. The value of U_{ms} increased with increasing temperature, especially for the large particles. The best of several empirical equations developed for U_{ms} is one which uses the free-settling terminal velocity of the particles as a correlating parameter.

The McNab - Bridgwater equation for H_m overpredicted H_m substantially at room temperatures and underpredicted H_m slightly at high temperatures. A similar equation with a slightly smaller value of U_m/U_{mf} than that recommended by McNab and Bridgwater gives better overall results.

The Wu *et al.* non-dimensional equation for D_s, which explicitly includes the effect of gas density and gas viscosity, hence of gas temperature, gave better absolute prediction of the average spout diameter, D_s, than did the dimensional McNab equation, especially at elevated bed temperatures.

Table of Contents

Abstract ii

List of Tables vii

List of Figures viii

Acknowledgement xi

1 Introduction 1

1.1 Rationale for the Present Work 1

1.2 Objectives of the Present Work 3

2 Literature Review 4

2.1 General Information 4

2.2 Spoutability 5

2.3 Minimum Spouting Velocity 5

2.3.1 Mathur and Gishler equation 6

2.3.2 Correlation of Grbavcic *et al.* 9

2.3.3 Wu *et al.* Modification of Equation (2.1) 10

2.3.4 The Maximum Value of U_{ms} 11

2.4 Maximum Spoutable Bed Height 11

2.5 Spout Diameter 15

2.6 Pressure Drop and Pressure Distribution 17

3 Experimental Apparatus **19**

3.1 Equipment 19

3.1.1 Choice and Description of Equipment 19

3.1.2 Heaters 20

3.2 Instrumentation 23

3.3 Bed Material 26

4 Experimental Procedures and Conditions **29**

4.1 Operating procedure 29

4.1.1 Operation 29

4.1.2 Measurement 30

4.1.3 Calculation of U_{ms} 31

4.2 Experimental Conditions 34

4.2.1 Range 34

4.2.2 Experimental Error Calculation 34

5 Results: Minimum Spouting Velocity **36**

5.1 Measurement difficulties 36

5.2 Effect of Particle Diameter 37

5.3 Effect of Orifice Diameter 37

5.4 Effect of Bed Height 42

5.5 Effect of Temperature 42

5.6 Data Correlation 47

5.6.1 First Option 47

5.6.2 Second Option 48

5.6.3 Third Option 49

5.6.4 Fourth Option 51

6 **Results: Maximum Spoutable Bed Height** 58

6.1 Spoutability 58

6.2 Maximum Spoutable Bed Height 60

6.2.1 Effect of Particle diameter on H_m 60

6.2.2 Effect of Orifice Diameter on H_m 64

6.2.3 Effect of Temperature on H_m 64

7 **Results: Average Spout Diameter** 74

7.1 Effect of Bed Temperature on D_s 74

7.2 Effect of Bed Height on D_s 74

7.3 Comparison with Existing Correlations 77

8 **Conclusions** 81

Bibliography 87

Appendices 92

A **Calibration of Rotameters** 92

B **Derivation of the Expression for $\frac{dH_m}{dAr}$** 96

C **Experimental Conditions** 97

D **Experimental Data** 100

E **Fortran Programs** 109

E.1 Program on U_{ms} correlation 109

E.2 Program to calculate average spout diameter 119

F Error % for the U_{ms} Values Predicted by Four Equations 121

G Error % for the Spout Diameter 128

List of Tables

3.1 Typical measurement of sand particles. 27

3.2 Mean diameters of sand particles 28

5.3 Constants in Equation (5.47) and root mean square errors for three correlations 48

5.4 Comparison of average and root mean square errors of U_{ms} by equations of Mathur and Gishler, Wu *et al.*, Grbavcic *et al.* and best fit by present work 54

6.5 Spoutability of sand particles 59

6.6 Change of critical value of d_p with temperature 63

List of Figures

1.1 Schematic diagram of a spouted bed. 2

2.2 Typical pressure drop versus velocity curve for a spouted bed of coarse particles. 7

3.3 Details of the spouted bed column. 21

3.4 Dimensions of the orifice plates. 22

3.5 Schematic of the experimental equipment. 24

3.6 Calibration curve for $-\Delta P_s$ versus $-\Delta P_a$. 26

4.7 Simplified flow diagram of the apparatus. 32

5.8 Effect of particle diameter on U_{ms}. (D_c=156 mm, D_i=19.05 mm, H=0.2 m) 38

5.9 Effect of particle diameter on U_{ms}. (D_c=156 mm, D_i=12.70 mm, H=0.2 m) 39

5.10 Effect of orifice diameter on U_{ms}. (D_c=156 mm, d_p=2.025 mm, H=0.3 m) 40

5.11 Effect of orifice diameter on U_{ms}. (D_c=156 mm, d_p=1.010 mm, H=0.2 m) 41

5.12 Effect of bed height on U_{ms}. (D_c=156 mm, D_i=26.64 mm, d_p=2.025 mm) 43

5.13 Effect of temperature on U_{ms}. (D_c=156 mm, D_i=19.05 mm) 44

5.14 Effect of temperature on U_{ms}. (D_c=156 mm, D_i=26.64 mm) 45

5.15 Effect of temperature on U_{ms}. (D_c=156 mm, D_i=12.70 mm) 46

5.16 Experimental values of U_{ms} vs. values predicted by Equation (5.75). . . . 53

5.17 Comparison of correlations for U_{ms} with experimental data. (D_c=156 mm, D_i=19.05 mm, d_p=2.025 mm) 56

5.18 Comparison of correlations for U_{ms} with experimental data. (D_c=156 mm, D_i=12.70 mm, d_p=1.630 mm) 57

6.19 Comparison between experimental data (points), prediction by Equation 2.10a (solid line) and prediction by modified equation (broken line). . . . 61

6.20 Comparison between experimental data (points), prediction by Equation 2.10a (solid line) and prediction by modified equation (broken line). . . . 62

6.21 Effect of particle diameter on H_m. Points represent experimental data, lines represent McNab - Bridgwater equation. (D_c=156 mm, D_i=26.64 mm) 65

6.22 Effect of particle diameter on H_m. Points represent experimental data, lines represent McNab - Bridgwater equation. (D_c=156 mm, D_i=19.05 mm) 66

6.23 Effect of particle diameter on H_m. Points represent experimental data, lines represent McNab - Bridgwater equation. (D_c=156 mm, D_i=12.70 mm) 67

6.24 Effect of orifice diameter on H_m. Points represent experimental data, lines represent McNab - Bridgwater equation. (D_c=156 mm, d_p=2.025 mm) . 68

6.25 Effect of orifice diameter on H_m. Points represent experimental data, lines represent McNab - Bridgwater equation. (D_c=156 mm, d_p=1.630 mm) . 68

6.26 Effect of orifice diameter on H_m. Points represent experimental data, lines represent McNab - Bridgwater equation. (D_c=156 mm, d_p=1.200 mm) . 69

6.27 Effect of orifice diameter on H_m. Points represent experimental data, lines represent McNab - Bridgwater equation. (D_c=156 mm, d_p=1.010 mm) . 69

6.28 Effect of temperature on H_m. Points represent experimental data, lines represent McNab - Bridgwater equation. (D_c=156 mm, D_i=26.64 mm) . 71

6.29 Effect of temperature on H_m. Points represent experimental data, lines represent McNab - Bridgwater equation. (D_c=156 mm, D_i=19.05 mm) . 72

6.30 Effect of temperature on H_m. Points represent experimental data, lines represent McNab - Bridgwater equation. (D_c=156 mm, D_i=12.70 mm) . 73

7.31 Effect of temperature on D_s. (D_c=156 mm, D_i=19.05 mm, d_p=1.630 mm) 75

7.32 Effect of temperature on D_s. (D_c=156 mm, D_i=26.64 mm, d_p=2.025 mm) 76

7.33 Effect of bed height on D_s. (D_c=156 mm, D_i=26.64 mm, d_p=2.025 mm) 78

7.34 Comparison of D_s measured experimentally with D_s predicted by McNab equation. (D_c=156 mm) 79

7.35 Comparison of D_s measured experimentally with D_s predicted by Wu *et al.* equation. (D_c=156 mm) 80

A.36 Schematic set-up for rotameter calibration. 93

A.37 Calibration curve (small rotameter). 94

A.38 Calibration curve (large rotameter). 95

Acknowledgement

I would like to express my appreciation to Dr. N. Epstein and Dr. C. J. Lim, under whose supervision and guidance this work was carried out.

Thanks are also due to the people of the Department of Chemical Engineering Workshop and Stores for their invaluable assistance.

Finally, to my parents for their encouragement and support.

Chapter 1

Introduction

1.1 Rationale for the Present Work

The spouted bed technique was developed by Mathur and Gishler [24] for drying wheat in the 1950's. Since then, spouted beds have been used as an alternative to fluidized beds for gas contacting of coarse particles ($d_p \geq 1\ mm$).

Figure 1.1 illustrates schematically a typical cylindrical spouted bed column with a conical base. Under the condition of stable spouting, the spouted bed consists essentially of two regions: a dilute phase central core of upward moving gas and particles called the *spout* and a surrounding dense phase region of downward moving particles and upward percolating gas known as the *annulus*. In a bed filled with coarse particles, fluid, usually gas, is injected vertically from the bottom of the bed through a centrally located small opening called the orifice. Particles are entrained in the spout by the gas at high velocity, and then penetrate somewhat above the bed level in a region called the fountain, where they fall back onto the annulus surface. In the annulus, particles slowly move downwards by gravity and, to some extent, radially inwards as a loosely packed bed. These particles are re-entrained into the spout through the spout wall over the entire bed height. The fluid from the spout seeps through the annular solids as it travels upwards. This systematic movement of the fluid and the solids leads to effective contact between them.

A complete review of spouted bed technology was presented in the monograph by Mathur and Epstein [1]. More recent reviews are given by Epstein and Grace [2] and by

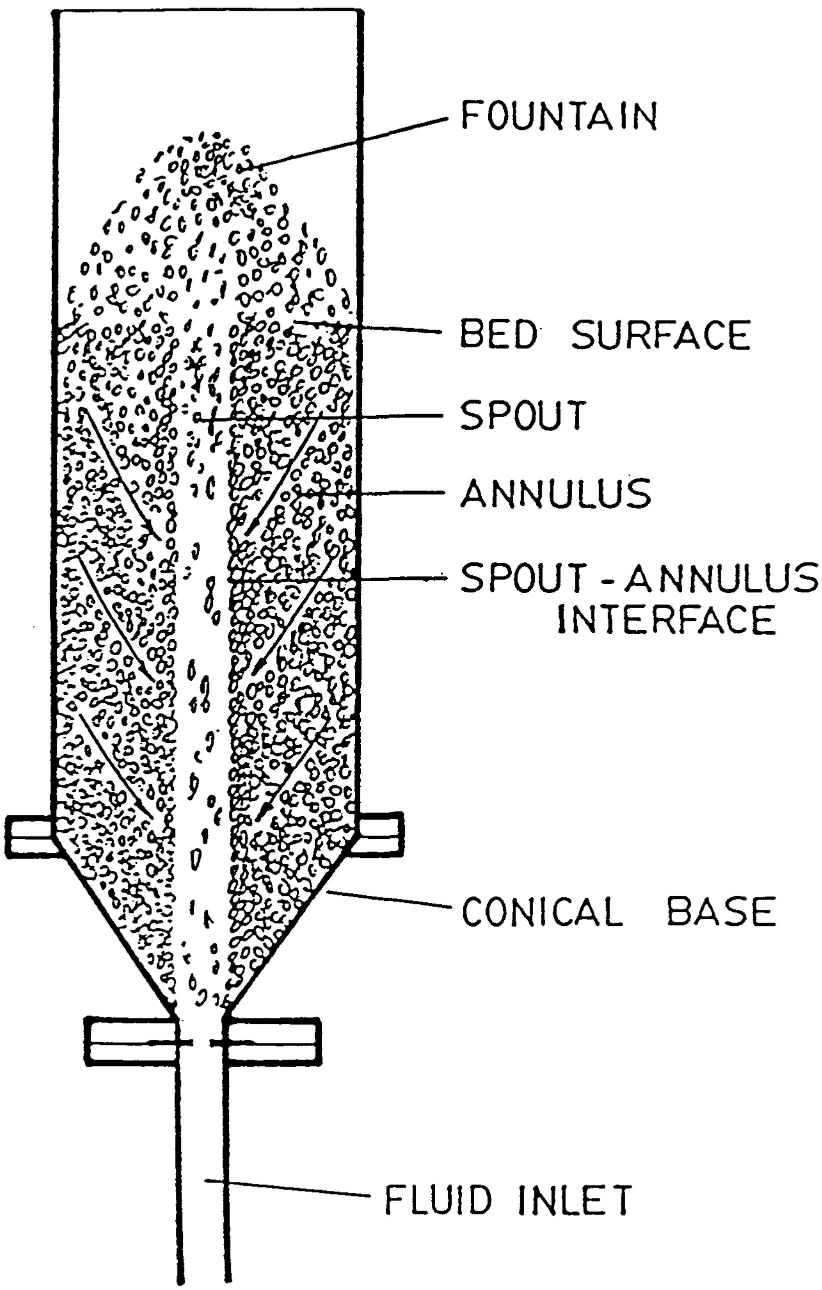

Figure 1.1: Schematic diagram of a spouted bed.

Bridgwater [3].

As pointed out by Lim *et al.* [11], spouted beds exhibit some advantages over conventional fluidized beds. They have been used for various physical and chemical processes and have achieved increasing recognition. Recently, high temperature spouting has attracted some attention because of its industrial applications, particularly in the energy field. These applications include not only carbonization of caking coal [4, 5, 6], drying of granular solids, slurries and solutions, and tablet coating [1], but also gasification , pyrolysis and combustion of caking coals [7, 8, 11, 14, 20, 21], and combustion of low heating value fuels and wastes [11, 15, 16, 17, 18].

While the hydrodynamics of spouted beds at ambient temperatures have been well studied in the past, knowledge of spouted bed hydrodynamics at high temperature is far from sufficient yet. The fragmentry information available on high temperature spouting differs from one worker to another and is sometimes even contradictory. The present work involves a detailed study of certain hydrodynamic features of spouted beds at high temperature.

1.2 Objectives of the Present Work

Some important hydrodynamic parameters of spouted beds are: spoutability, minimum spouting velocity, maximum spoutable height, spout shape and diameter, overall bed pressure drop, pressure profiles, fluid and particle velocities in the spout and annulus.

The primary objective of the present research is to collect experimental data on some of these hydrodynamic parameters at varying operating conditions, including a temperature range from room temperature to $580°C$. Using the data obtained, the validity of existing equations can be examined and, where indicated, new correlations can be developed and explanations offered for unanticipated results of the present work.

Chapter 2

Literature Review

2.1 General Information

With the increasing development of the spouted bed as a high temperature reactor, the need for better understanding of spouted bed hydrodynamics at high temperatures has become evident. Gas spouting at ambient conditions has been well studied in most aspects and many equations are available for predicting hydrodynamic parameters. Mathur and Epstein [1] and Epstein and Grace [2] have given complete reviews of spouted bed technology. However, information on high temperature spouting is scarce. A few published articles on this subject were mainly about reactor performance characteristics [8, 10, 11], reaction kinetics [12, 13, 14], and combustion models [15, 16, 17, 18, 19, 20, 21]. The hydrodynamics at high temperature are not well understood. Stanley Wu [22] studied the hydrodynamics of spouted beds at temperatures up to $420°C$. The temperature range of Wu's study was thus limited and only three particle sizes were investigated. Bogang Ye [21] made some investigations on spouted bed hydrodynamics in a 0.15 m internal diameter half-column spout-fluid bed at high temperature, by burning Minto coal. However, the combustion inside the spouted bed made it diffucult to study the hydrodynamics precisely. Minto coal caused serious sintering problems because of the poor micro-circulation of solids and the limited bed-to-wall heat transfer coefficient with air as external coolant. The limestone used for sulphur capture underwent a large change in its mean particle diameter after several hours of experimental operation, thus affecting the mean diameter of the bed solids.

The equations originally developed at room temperature conditions have been applied at high temperatures, with the assumption that these equations do not change significantly at elevated temperatures. Often, however, modification of the existing equations are required when they are used at elevated temperatures. It is thus important that the real features of gas spouting at high temperature, including the hydrodynamics, be investigated systematically.

2.2 Spoutability

Spoutability refers to those conditions for which stable spouting occurs in a spouted bed. Increasing bed temperature could shift the flow regime from stable spouting to pulsatory spouting [20, 22]. Chandnani and Epstein [23] proposed that stable spouting can occur only if $D_i/d_p < 25.4$. This criterion does not predict any effect of the bed temperature. Wu [22] showed that at some temperatures below $420°C$, this criterion sometimes failed. Zhao *et al.* [20] found that the hydrodynamic pattern and even the flow regime changed substantially with temperature, particularly with smaller particles. Hydrodynamic patterns of spouted beds are influenced by such conditions as fluid flow rates, solids properties, bed height and fluid properties, the last of which are affected by increasing the temperature. Particle density apparently has a negligible effect on spoutability [23].

2.3 Minimum Spouting Velocity

The minimum superficial fluid velocity at which a spouted bed will remain in the stable spouting state is called the minimum spouting velocity, U_{ms}. It is determined experimentally by reducing the fluid flow rate to a point at which a further decrease of flowrate will cause the spout to collapse and the bed pressure drop to increase suddenly. The spouting velocity at this point is taken as the minimum spouting velocity. It is sometimes only a relatively narrow region above incipient spouting where stable behavior prevails. Figure 2.2 shows a typical curve of pressure drop versus superficial velocity for spouting of coarse particles ($d_p > 1\ mm$). In a typical run, the fluid flowrate is first increased until point C is reached, which indicates stable spouting. However, this point is bed-history dependent and is not exactly reproducible. By decreasing the flowrate to point B, at which a further decrease of flowrate will cause the spout to collapse and the bed pressure to increase suddenly, it has been found that the velocity at this point is reproducible. Hence the minimum (superficial) spouting velocity U_{ms} is represented by point B.

It is generally known that U_{ms} depends on solid and fluid properties, column geometry and bed depth. For a given bed material and given fluid properties, U_{ms} increases with increasing bed depth and fluid inlet diameter, and with decreasing column diameter. For a given column geometry and bed height, U_{ms} increases with increasing particle diameter and decreasing fluid density.

2.3.1 Mathur and Gishler equation

The Mathur and Gishler [24] equation is the most widely used empirical equation for predicting the minimum spouting velocity [1]. This empirical equation was derived from data for both gas and liquid spouted beds with diameters up to 0.6 m starting with dimensional analysis. The equation is:

$$U_{ms} = \left[\frac{d_p}{D_c}\right]\left[\frac{D_i}{D_c}\right]^{1/3}\sqrt{\frac{2gH(\rho_p - \rho_f)}{\rho_f}} \tag{2.1}$$

Ghosh [29] derived a similar theoretical equation based on a momentum exchange

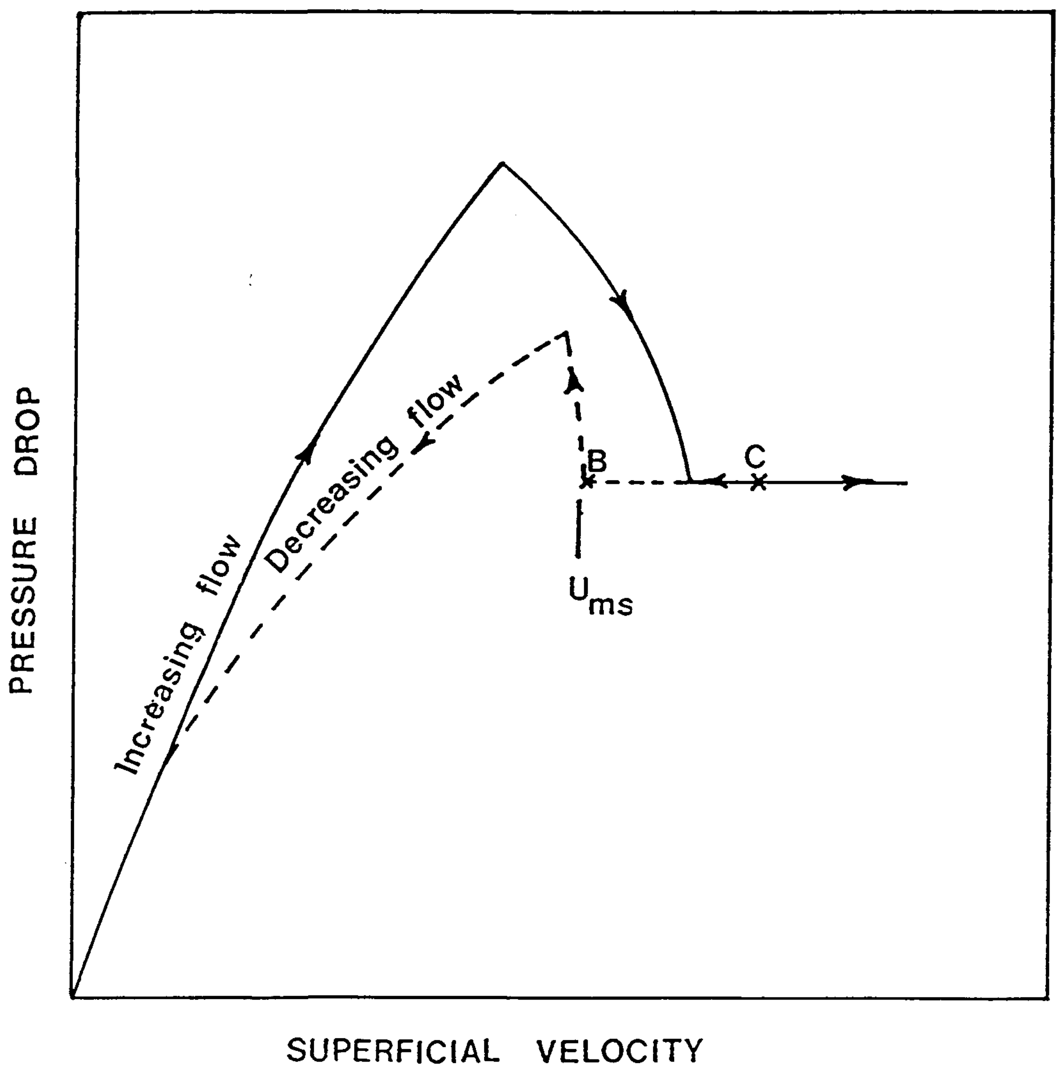

Figure 2.2: Typical pressure drop versus velocity curve for a spouted bed of coarse particles.

between the entering fluid and the entrained particles:

$$U_{ms} = \sqrt{\frac{2n}{3k}} \left[\frac{d_p}{D_c}\right] \left[\frac{D_i}{D_c}\right] \sqrt{\frac{2gH(\rho_p - \rho_f)}{\rho_f}} \tag{2.2}$$

The main difference between Equation (2.1) and Equation (2.2) is the exponent on the D_i/D_c term, its value being $\frac{1}{3}$ in the empirical equation as against unity in the theoretical. The term $\sqrt{\frac{2n}{3k}}$ is likely to be a function of D_i/D_c [29].

Both Equations (2.1) and (2.2) predict U_{ms} to be directly proportional to H^b, with b equal to 0.5, which was confirmed experimentally by other authors such as Thorley *et al.* [45] and Cowan *et al.* [37]. This value was justified theoretically by Madonna *et al.* [38]. Smith and Reddy [35] obtained $U_{ms} = aH^{0.50-1.76(D_i/D_c)}$, showing from their experiments that b was smaller than 0.5. Lim and Grace [27] found b in the range $1.0 - 1.4$ for a large diameter bed. Green and Bridgwater [30] also indicated that the exponent on H is greater in larger diameter vessels. These facts show that the value of b is not well established and probably depends on the geometry of the system.

The proportionality between U_{ms} and d_p has been verified by other authors working with beds of closely sized materials [45, 34] and with beds containing a wide spread of particle sizes [35]. Manurung [36], working with materials consisting of both close-fractions and mixed sizes, obtained $U_{ms}\ \alpha\ d_p^{0.62}$ for otherwise fixed conditions, using the reciprocal mean diameter for d_p.

As noted by Mathur and Epstein [1], Equation (2.1) underestimated the minimum spouting velocity by a factor of nearly 2 for a single measurment (on wheat) in a 0.91 m diameter vessel. Wu *et al.* [39], using a column of 156 *mm* I.D found that for air spouting at room temperature, Equation (2.1) underestimated U_{ms} with a deviation up to 30%, while at higher temperatures the equation actually worked better. Ottawa sand with a particle diameter range from 0.945 *mm* to 1.665 *mm* and orifices with diameters from 12.70 *mm* to 26.64 *mm* were used in Wu's work. The change of temperature was reflected in a change of both gas density and gas viscosity: when temperature increases, the gas density decreases and the gas viscosity increases. The effect of fluid density in Equation (2.1) is such that U_{ms} increases with increasing temperature. The absence of fluid viscosity in this equation has, however, been questioned by Charlton *et al.* [26]. Fane and Mitchell [25] proposed an empirical dimensional correction to Equation (2.1) based on experimental data in a 1.1 m diameter column and claimed that U_{ms} first falls and then begins to rise as bed diameter is increased, the latter being in a direction opposite to that suggested by Equation (2.1). This claim was supported by both Lim *et al.* [27] and He *et al.* [28]. Thus Equation(2.1) has not been very successful for large columns.

2.3.2 Correlation of Grbavcic *et al.*

Using the model of Mamuro and Hattori [31] at maximum spoutable bed height, Grbavcic *et al.* [32] proposed the following correlation for predicting U_{ms} for spherical particles:

$$\frac{\frac{U_{ms}}{U_{mf}} - a_s}{1 - a_s} = 1 - \left[1 - \frac{H}{H_m}\right]^3 \tag{2.3}$$

where a_s is defined as the ratio of the area of the spout to that of the column. Since a_s is much smaller than 1 in most cases, Equation (2.4) can be further simplified to

$$\frac{U_{ms}}{U_{mf}} = 1 - \left[1 - \frac{H}{H_m}\right]^3 \tag{2.4}$$

where U_{mf} is given by the Ergun (1952) equation:

$$-\left(\frac{dp}{dz}\right)_{mf} = (\rho_p - \rho_f)(1 - \epsilon_{mf})g = f_1 U_{mf} + f_2 U_{mf}^2 \tag{2.5}$$

with f_1 and f_2 given by

$$f_1 = 150\frac{\mu(1 - \epsilon_{mf})^2}{(\phi d_p)^2 \epsilon_{mf}^3}$$

$$f_2 = 1.75\frac{\rho_f(1 - \epsilon_{mf})}{\phi d_p \epsilon_{mf}^3}$$

Since the Grbavcic equation was verified only for water spouted beds at room temperature, its application to high temperature air spouted beds has yet to be examined.

2.3.3 Wu *et al.* Modification of Equation (2.1)

A modified form of the Mathur and Gishler [24] equation, with best fit values of the coefficient and of the exponents on the dimensionless groups for conditions including elevated temperature, was given by Wu *et al.* [39]:

$$\frac{U_{ms}}{\sqrt{2gH}} = 10.6 \left[\frac{d_p}{D_c}\right]^{1.05} \left[\frac{D_i}{D_c}\right]^{0.266} \left[\frac{H}{D_c}\right]^{-0.095} \left[\frac{\rho_p - \rho_f}{\rho_f}\right]^{0.256} \tag{2.6}$$

The most significant difference from the original Mathur and Gishler equation is that the exponent on $(\rho_P - \rho_f)/\rho_f$ is 0.256 instead of 0.5. Unlike Mathur and Gishler [24], $(\rho_P - \rho_f)/\rho_f$ and $2gH$ were not grouped as one parameter.

As pointed by Ye *et al.* [21], both the Mathur and Gishler equation and the Wu equation underpredicted U_{ms} at very high temperature, though the latter equation worked better than the former.

Ye *et al.* showed in his experimental data that U_{ms} decreases with increasing temperature for smaller particles and increases with increasing temperature for larger particles. The effects of d_p and temperature appeared to be much more complex than predicted. The problem encountered in spouted beds is inherently more complex than in fluidization, for which U_{mf} always increases with an increase in temperature [43].

Most of the existing equations mentioned above have not paid much attention to the change of viscosity due to the change of temperature. Gas viscosity increases with temperature [40]. Deficiencies in predictions may be due to inadequate knowledge of how to include d_p in the above equations, and the absence of fluid viscosity. A detailed study on the effects of different independent variables on minimum spouting velocity at high temperature is thus of some importance.

2.3.4 The Maximum Value of U_{ms}

The value of U_{ms} at the maximum spoutable bed height is termed U_m, the maximum value of the minimum spouting velocity [41]. For many materials, U_m is expected to coincide with the minimum fluidization velocity since beyond H_m a spouted bed transforms into a fluidized bed. Experimental data by previous workers show that U_m often exceeds U_{mf}. In the case of sand ($d_p = 0.42 - 0.83\ mm$) in a spouted bed of 152 mm I.D. at room temperature, U_m is approximately equal to U_{mf}, while it is 33% higher than U_{mf} for wheat ($d_p = 3.2 - 6.4\ mm$) and 45% for semicoke ($d_p = 1 - 5\ mm$) [1]. Values of U_m exceeding U_{mf} by 10-33% have been reported by Becker [41] for a variety of uniform size materials. Differences in the properties of the solid materials and in spouting vessel geometry might affect the ratio U_m/U_{mf}. For a fixed D_i/D_c ratio, U_m increases with increasing column diameter, while for a fixed value of D_c, it increases with increasing orifice diameter.

2.4 Maximum Spoutable Bed Height

The maximum spoutable bed height, H_m, is the maximum height at which steady stable spouting can be maintained. For bed heights above H_m, the bed will sometimes be partitioned into an internal spouting zone and an upper level fluidization region. Mathur and Epstein [1] suggested three distinct mechanisms for spout termination beyond H_m. i.e.,

1. Fluidization of Annular Solids
2. Choking of the Spout
3. Growth of Instability at the Spout-Annulus Interface

At the maximum spoutable bed height, Equation (2.1) becomes

$$U_m = \left[\frac{d_p}{D_c}\right]\left[\frac{D_i}{D_c}\right]^{1/3}\sqrt{\frac{2gH_m(\rho_p - \rho_f)}{\rho_f}} \tag{2.1a}$$

As mentioned above, U_m has a close relationship with U_{mf}. In general,

$$\frac{U_m}{U_{mf}} = b_1 = 1.0 \; - \; 1.5 \tag{2.7}$$

On the other hand, U_{mf} can be estimated from the Ergun [42] equation on substitution of the empirical approximations of Wen and Yu [43], i.e. $1/\phi\epsilon_{mf}^3 = 14$ and $(1-\epsilon_{mf})/\phi^2\epsilon_{mf}^3 = 11$, which yields

$$Re_{mf} = \frac{d_p U_{mf}\rho_f}{\mu} = 33.7(\sqrt{1 + 35.9 \times 10^{-6} Ar} - 1) \tag{2.8}$$

where

$$Ar = \frac{d_p^3(\rho_p - \rho_f)g\rho_f}{\mu^2} \tag{2.9}$$

Equations (2.1a), (2.7) and (2.8) are combined to eliminate U_m and U_{mf}, the result being

$$H_m = \left[\frac{D_c^2}{d_p}\right]\left[\frac{D_c}{D_i}\right]^{2/3}\left[\frac{568b_1^2}{Ar}\right](\sqrt{1 + 35.9 \times 10^{-6} Ar} - 1)^2 \tag{2.10}$$

McNab and Bridgwater [44] found that Equation (2.10) gave the best fit to existing experimental data for H_m in gas spouted beds with $b_1 = 1.11$.

Thorley *et al.* [45] were able to predict values of H_m, though only approximately, under a variety of conditions by simultaneously solving an equation for U_{ms} with an equation for U_{mf}. This approach was subsequently adopted by other workers with variations in the particular equations used for calculating spouting and fluidization velocities. The majority of the empirical and semi-empirical models for predicting H_m were listed by Mamuro and Hattori [31]. Mathur and Epstein [1] listed the empirical equations for predicting H_m and made a comparison to decide which of the various calculation methods proposed are suitable for predictive purposes. The Malek and Lu [46] equation is the most simple correlation based on a sufficiently wide range of variables to be of practical interest. It is given by

$$\frac{H_m}{D_c} = 0.105 \left[\frac{D_c}{d_p}\right]^{0.75} \left[\frac{D_c}{D_i}\right]^{0.4} \left[\frac{\lambda^2}{\rho_p^{1.2}}\right] \tag{2.11}$$

where λ is a shape factor with values ranging from 1.0 for millet, sand and timothy seed to 1.65 for gravel, while ρ_p is the particle density in g/cm^3.

Lefroy and Davidson [47] derived the following expression for H_m by extending their force balance equations on spouted beds:

$$\frac{\pi(D_c^2 - D_s^2)}{8D_sH_m} tan\gamma = 0.36 \tag{2.12}$$

Grbavcic *et al.* [32] proposed an empirical equation to calculate H_m in their correlation for U_{ms} based on data for water-spouted beds of spherical glass particles:

$$\frac{H_m}{D_c} = 0.347 \left(\frac{D_c}{D_i}\right)^{0.41} \left(\frac{D_c}{d_p}\right)^{0.31} \tag{2.13}$$

Littman *et al.* [48, 49] developed two models using monodispersed spherical particles. The first of these models states that

$$\frac{H_m D_i}{D_c^2} = 0.215 + \frac{0.005}{A} \quad for \;\; A > 0.02 \tag{2.14}$$

where A is defined by

$$A = \frac{\rho U_{mf} U_t}{(\rho_p - \rho_f) g D_i} \tag{2.15}$$

U_{mf} is calculated from Equation (2.8), and U_t is estimated from the following:

$$\begin{gathered} Ar = 18Re_t + 2.7Re_t^{1.687};\; Re_t \leq 1000 \\ Re_t = 1.745Ar^{0.5};\; Re_t > 1000 \end{gathered} \tag{2.16}$$

The second model states that

$$\frac{H_m D_s}{D_c^2 - D_s^2} = 0.345 \left(\frac{D_s}{D_c}\right)^{-0.384} \tag{2.17}$$

The first model was derived from momentum considerations. It was established that the A-parameter linked the maximum jet penetration to the momentum exiting the inlet orifice. The latter model ($H_m - D_s$ relationship) follows from a solution of the vectorial form of Ergun's equation for the annular flow field. In that analysis McNab's [50] relationship was used to predict the spout diameter, while the Lefroy and Davidson [47] pressure profile was assumed to hold at the spout-annulus interface.

Wu [22] compared some of the existing H_m correlations, such as the equation of McNab and Bridgwater, Littman's first model for H_m, and that of Malek and Lu, with his experimental data at temperatures up to $420°C$. The results showed that the McNab and Bridgwater relation, Equation (2.10), gave the best prediction.

Equation (2.10) does not take the temperature effect explicitly into consideration. The effect of temperature can be determined by differentiating Equation (2.10) with respect to Ar while other variables are kept constant (see Appendix B):

$$\begin{aligned} \frac{dH_m}{dAr} &= C_1 \left[\sqrt{\frac{1}{Ar} + 35.9 \times 10^{-6}} - \sqrt{\frac{1}{Ar}}\right] \\ &\times \left[\sqrt{\frac{1}{Ar^3}} - \sqrt{\frac{1}{Ar^3 + 35.9 \times 10^{-6} Ar^4}}\right] \\ &> 0 \quad for \;\; Ar > 0 \end{aligned} \tag{2.18}$$

The above equation shows that for all value of Ar, $dH_m/dAr > 0$, which indicates that H_m always increases with increasing Ar. For gas spouting, when temperature increases, fluid density decreases while viscosity increases, which results in decreasing the value of Ar if d_p is fixed. Therefore, H_m also decreases with increasing temperature. This phenomenon was verified in both Wu's [22] and Zhao's [20] experiments.

The effect of temperature was further investigated experimentally by Wu *et al.* [39] by looking at the effect of changing gas density at constant viscosity and vice versa. Wu *et al.* found that H_m increased with increasing ρ_f and with decreasing μ; in other words, H_m is higher if the spouting gas is more dense and less viscous. Thus correlations which contain the effect of both μ and ρ seem to work better than those which ignore μ.

The particle diameter effect on H_m can be examined by substituting Equation (2.9) into Equation (2.10) and then differentiating the latter with respect to d_p, setting $dH_m/d(d_p)$ equal to zero; then

$$(d_p)_{crit} = 60.6\left[\frac{\mu^2}{g(\rho_p - \rho_f)\rho_f}\right]^{1/3} \tag{2.19}$$

where $(d_p)_{crit}$ is the critical value of d_p, below which H_m increases with d_p and above which H_m decreases as d_p increases. This critical value changes with temperature. The qualitative effect of increasing d_p was observed by Wu at temperatures up to $420°C$.

2.5 Spout Diameter

The spout is the central core of the bed and is a region of high fluid velocity and low solids concentration. Knowledge of the spout diameter is necessary for an understanding of the dynamics of the bed and for design purposes. There are many equations available for estimating the average spout diameter [1, 53]. However, attempts to apply principles of solids flow mechanics to the determination of D_s have achieved only qualitative success.

Bridgwater and Mathur [51] developed a simplified theoretical model which was derived from a force balance analysis. Their theoretical equation is

$$\frac{32 f \rho_f Q_s^2}{\pi^2 \psi (D_c - D_s) D_s^4} = 1 \tag{2.20}$$

This dimensionless equation was reduced to a more manageable dimensional form based on a number of approximations; in SI units of kg, m and s,

$$D_s = 0.384 \left[\frac{G^{0.5} D_c^{0.75}}{\rho_b^{0.25}} \right] \tag{2.21}$$

This result is primarily restricted to air spouting, and it was later pointed out by McNab and Bridgwater [52] that the model of Bridgwater and Mathur was oversimplified.

The longitudinal average value of spout diameter, D_s, has been correlated empirically by a dimensional correlation over a wide range of experimental data by McNab [50], applying statistical analysis to the data. The following expression is the result:

$$D_s = 2.0 \left[\frac{G^{0.49} D_c^{0.68}}{\rho_b^{0.41}} \right] \tag{2.22}$$

in the same units as for Equation (2.21).

The McNab equation and that of Bridgwater and Mathur have the same variables and the exponent on each of the variables has the same order of magnitude. The main difference is in the modifying coefficient. McNab's equation was later found by Wu *et al.* [39] to be unsuitable for estimating D_s at elevated bed temperatures, because it overpredicted the effect of temperature on average spout diameter.

A more restrictive equation, which applies only to beds at their maximum spoutable height, but which has the virtue of being dimensionally consistent, is given by Littman and Morgan [49].

The most recent approach to determine the average spout diameter was carried out by Wu *et al.* [39], who developed the following expression for D_s by applying a least squares fit to their data using the theoretical model of Bridgwater and Mathur [51]:

$$D_s = 5.606 \left[\frac{G^{0.4333} D_c^{0.5832} \mu^{0.1334}}{(\rho_b \rho_f g)^{0.2834}} \right] \tag{2.23}$$

This equation showed relatively good agreement with Wu's experimental data. Besides, it was dimensionally consistent, which was another advantage over the McNab expression. Wu found that the effect of bed temperature on D_s was not very significant. At a constant bed height and a constant value of U_s/U_{ms}, D_s was observed to decrease slightly with increasing bed temperature.

Ye *et al.* [21] compared his expermental data with Equations (2.21), (2.22) and (2.23) and found that all three equations underpredicted D_s, but that Equation (2.23) of Wu *et al.* was the best of the three.

Krzywanski *et al.* [54] developed a relationship giving spout diameter as a function of bed level for both two dimensional and cylindrical spouted beds. This approach requires no prior knowledge of the pressure and particle/gas velocity fields in either the spout or the annulus. However, it does require input information about the average spout diameter, which can be obtained from standard correlations.

2.6 Pressure Drop and Pressure Distribution

Equations for the longitudinal pressure profile in the annulus and the overall bed pressure drop were put forward by Epstein and Levine [55] using the Ergun equation [42] and force balance analysis of Mamuro and Hattori [31]. This is the only model that has a theoretical basis and also fits the experimental data reasonably well. Other equations were developed by Manurung [36] and Lefroy and Davidson [47], as well as by Morgan and Littman [56]. Manurung's equation [36] for pressure drop was developed by considering ΔP_s, the absolute spouting pressure drop to approach the fluidised bed pressure drop as the bed depth increases to infinity. Lefroy and Davidson [47] presented an empirical correlation based on their pressure measurements at the spout-annulus interface. Morgan and Littman [56] developed general pressure drop correlations based on a number of experimental pressure measurements reported in the literature.

Wu *et al.* [39] showed that the bed temperature had no observable effect on the pressure drop and the shape of the longitudinal and radial pressure profiles. In general, the radial profiles in the cylindrical section were flat [1] and the longitudinal profiles could be described by the quarter cosine curve of Lefroy and Davidson [47]. It has also been shown [57] that the particle shape and voidage coefficients developed by Wen and Yu [43] for use in the Ergun equation [42], which is applied in some of the above spouted bed pressure drop relationships, remain unchanged even at high temperatures.

Chapter 3

Experimental Apparatus

3.1 Equipment

3.1.1 Choice and Description of Equipment

Experiments were carried out in a half column spouted bed. The use of a half column allows visual observation and direct measurement of such hydrodynamic parameters as maximum spoutable bed height and spout diameter. The validity of using a half column for the present measurements has been justified by Whiting and Geldart [58], Geldart *et al.* [59] and Lim [60].

The spouted bed column was constructed of 316 stainless steel and consists of two parts: (1) a half cylindrical section of 0.156 m I.D. and 1.06 m height with a wall of 6.4 mm thickness. This section was also furnished with solids input and discharge lines; (2) a truncated 60° included angle half conical section 0.13 m high with a semi-circular orifice as the spouting gas inlet. A flat stainless steel panel on which three 1/4 inch thick transparent fused quartz glass plates were mounted for direct observation served as the front. The quartz glass was able to withstand high temperature. On top of the column, a sand feed system was built which had a conical container and a ball valve. The feed line was then connected to the air exhaust pipe. When feeding the sand into the column, a low flow rate of spouting air was maintained so that sand could get into the spouted bed column by gravity. If no spouting air was maintained, the bed of solids was packed too tightly, which made the initial spouting very difficult. The feed control valve was then closed during the whole experiment period. There was one sand discharge line 0.2 m above the cylindrical base and eight measuring ports, one 0.38 mm above the orifice in the conical section and seven in the cylindrical section with vertical separations of 100 mm. These ports were all used for measuring pressure during the experiment. The fluid inlet section was a 26.64 mm I.D. half pipe with a straight vertical length of 0.300 m. This is shown in Figure 3.3.

Three different orifice diameters were used in the experiments, namely 12.7, 19.05 and 26.64 mm, respectively. In order to get a more stable spouting than otherwise, all orifices had a converging nozzle-type bottom and an extended collar 3.2 mm high at the top, as shown in Figure 3.4. A very fine stainless steel wire screen was placed underneath the orifice so as to prevent sand particles from falling down into the inlet pipe.

A high temperature insulating material (970-J paper supplied by Plibrico Limited of Canada) was used as the gasket material between the glass and the steel panel. The thickness of gasket material used was such that the internal surface between the quartz glasses and the steel panel was sufficiently smooth to avoid disturbing the flow pattern in the bed.

The spouted bed was externally insulated by ceramic fibre insulation of thickness 1 inch to prevent heat loss to the surroundings. The ceramic fibre was also used to cover the quartz glass windows, and these covers were only removed momentarily for visual observation.

3.1.2 Heaters

Three cylindrical electric heaters (Watlow Ceramic Fiber Heaters), each with a maximum power rating of 3.6 kw, were mounted on the outside of 2-inch 316 stainless steel pipes. These heaters may be operated up to 1100°C with suitable control. Ceramic rings were packed inside the pipes to enhance heat transfer. High temperature gaskets (supplied by

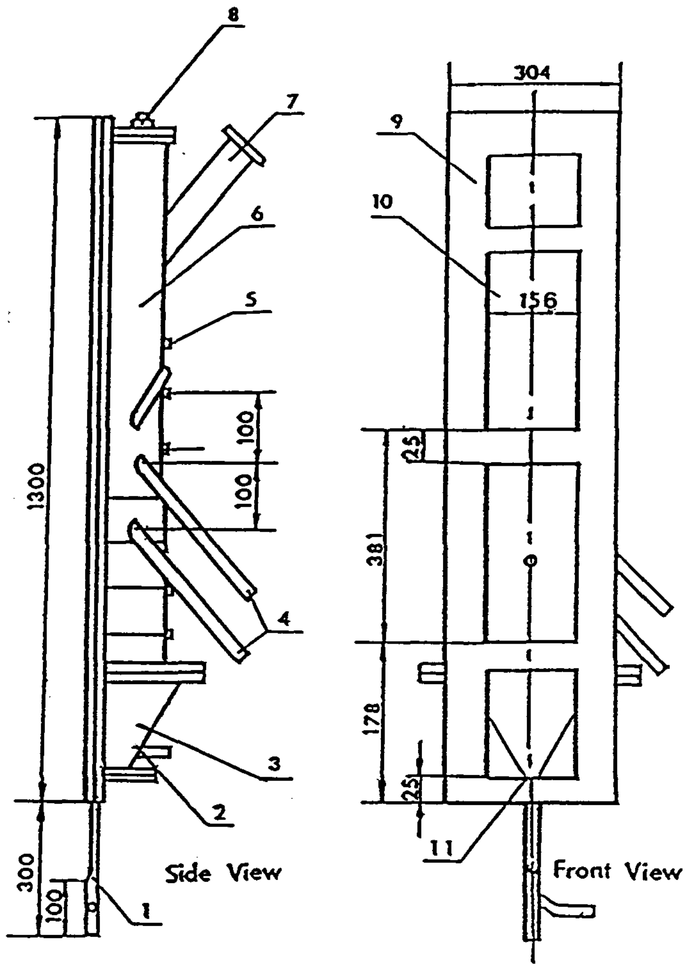

1. Spouting flow line. 2. Pressure port. 3. Conical base. 4. Solids discharge lines. 5. Measuring port. 6. Half-column. 7. Gas exhaust line. 8. Port for thermocouple. 9. Front panel. 10. Quartz glass window. 11. Orifice. (All dimensions are in mm.)

Figure 3.3: Details of the spouted bed column.

Size	*Dimension (mm)*						
	A	*B*	*C*	*D*	*E*	*F*	*G*
S	50.8	41.0	12.70	3.2	3.2	9.5	1.6
M	50.8	41.0	19.05	3.2	3.2	9.5	1.6
L	50.8	41.0	26.64	3.2	3.2	9.5	1.6

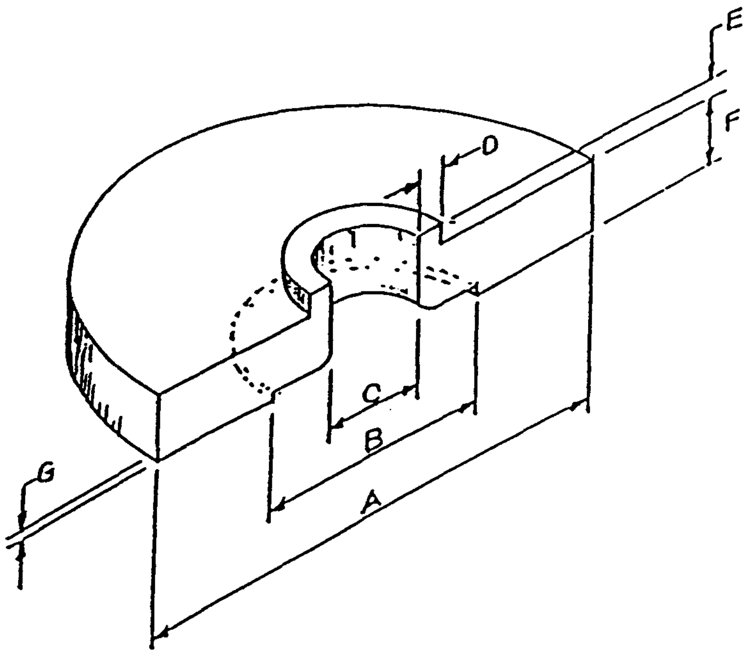

Figure 3.4: Dimensions of the orifice plates.

A.R. Thompson Ltd.) were used in the joint sections of the pipes. All three heaters were controlled by monitoring the temperature using thermocouples in the gap between the outside wall of the pipe and the inside wall of the heater. The heaters were housed in a metal box and blanketed by the ceramic glass fibre insulation.

Another small heater (supplied from Thermacraft Ltd.) with a power rating of 1.2 *kw* was mounted on the fluid inlet section to further heat the inlet air to the desired temperature.

3.2 Instrumentation

The schematic flow diameter of the experimental setup is shown in Figure 3.5. Air flow from the building compressor passed through one of the two rotameters, which were used to control and adjust the flow rate. Calibration curves for the rotameters at standard conditions are given in Appendix A. The measured flow rates are then converted to the actual conditions in the spouted bed. The detailed calculation of the volumetric flow rate through the spouted bed, V_S, and the minimum spouting velocity are presented in the next chapter.

From the rotameter, air flowed into the heating units and was raised to the desired temperature before it was admitted into the spouted bed. The high temperature air from the bed was discharged into the surrounding atmosphere outside the building through an exhaust hose.

Temperatures were measured and monitored by seven Chromel-Alumel type thermocouples, four of which showed their readings on the temperature controllers for the four heaters. The rest were connected to a digital display through a selecting switch. One was positioned in the outlet of the large heating unit and the other in the inlet section of the spouting air. A long thermocouple rod with a diameter of 1/4 inch was inserted into

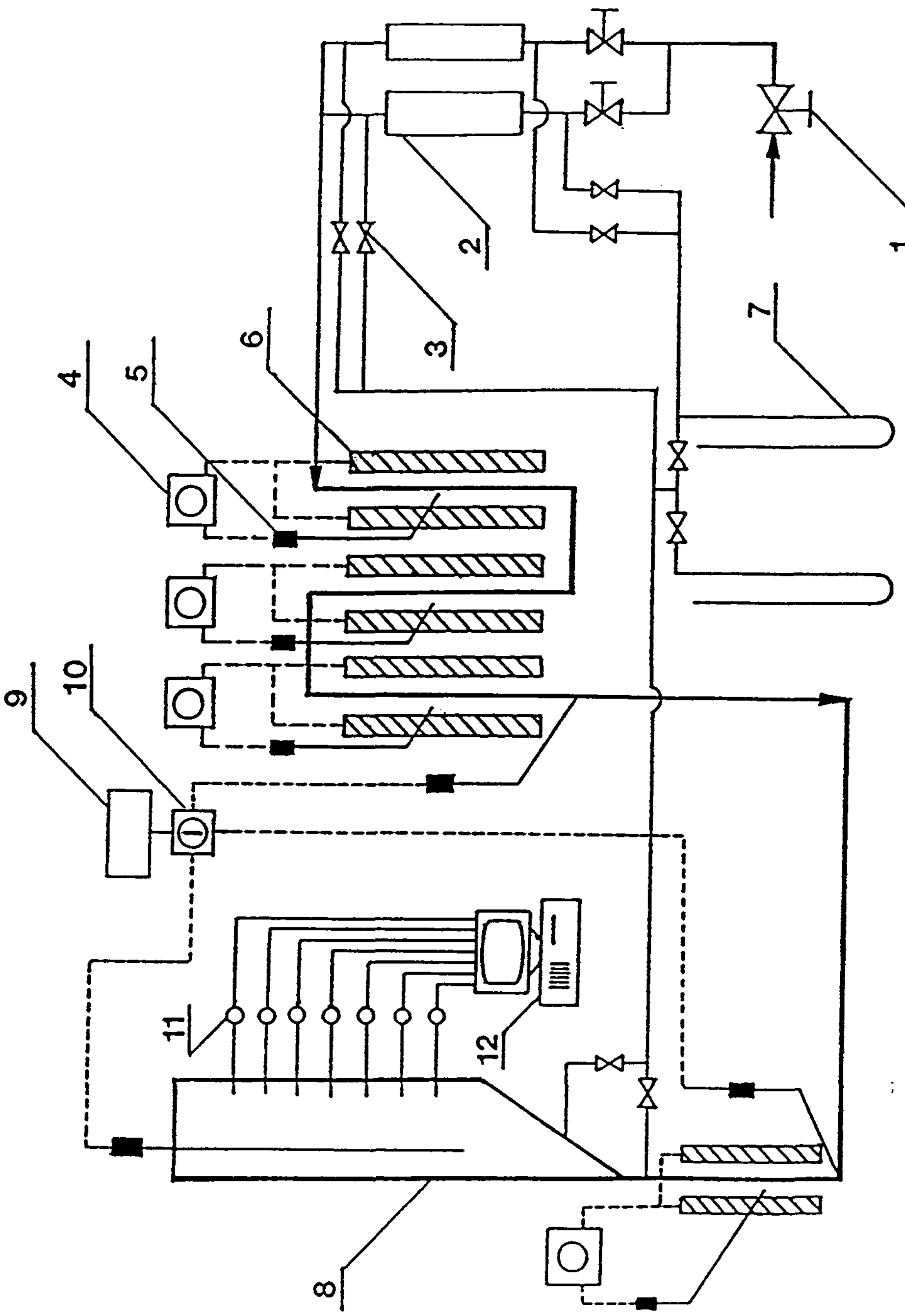

1. Valves 2. Rotameter. 3. Tube clamp. 4. Temperature controller. 5. Thermocouple. 6. Electric heater. 7. Manometer. 8. Spouted bed. 9. Digital display. 10. Temperature selecting switch. 11. Transducer. 12. Computer.

Figure 3.5: Schematic of the experimental equipment

the spouted bed from the top to measure the temperature at different vertical positions in the bed. The average value of the temperature measurement along the bed height was taken as the average bed temperature.

Two open U-tube manometers containing water were alternately connected to the two pressure taps before and after the rotameter and to the two ports below and above the inlet orifice to the spouted bed. They were used to determine the absolute pressure inside the rotameter and the absolute pressure in the spouted bed, respectively. These values were used for calculating the gas flowrate and the minimum spouting velocity at bed conditions. The absolute pressure inside the rotameter was obtained from the average of the two manometer readings at the ports before and after the rotameter. The pressure port below the orifice in the conical section was used to measure the overall pressure drop of the spouted bed, $-\Delta P_s$, from which the average absolute pressure in the bed was determined. A stainless steel screen was placed under the orifice to prevent sand particles from falling into the gas inlet tube. But the screen also caused blockage by the entrained small broken pieces of ceramic packing from the heating section and by the sand particles as well. This made measurement of the bed pressure drop unreproducible. To solve this problem, an alternative pressure tap was located 38 mm above the orifice in the actual experimental runs. A calibration was obtained by correlating $-\Delta P_s$ under no-screen conditions with the measured bed pressure drop, $-\Delta P_a$, using the pressure tap above the orifice, where the latter term was obtained from Equation (4.27) [22]. The equation in Figure 3.6, obtained by Wu [22], is

$$-\Delta P_s = 0.171 + 0.976(-\Delta P_a) \tag{3.24}$$

The pressure profile along the bed was measured using pressure transducers through the other seven pressure ports at the back of the column at intervals of 100 mm. A

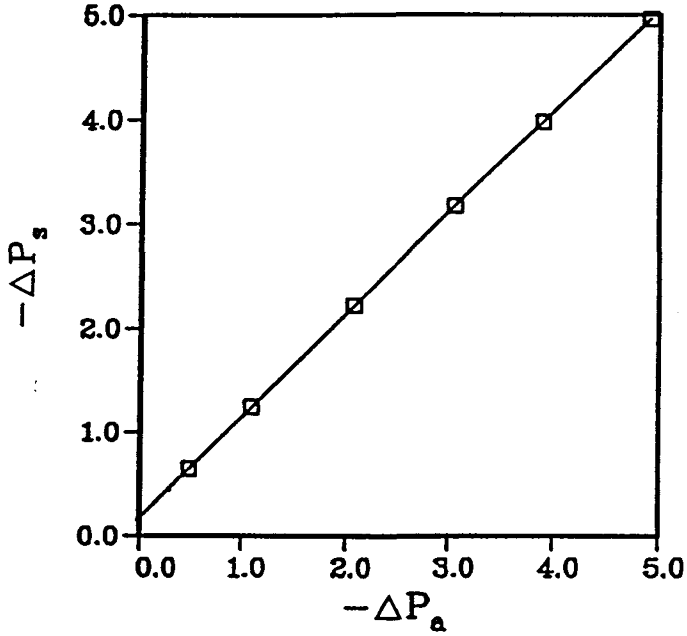

Figure 3.6: Calibration curve for $-\Delta P_s$ versus $-\Delta P_a$.

2 meter long stainless steel tube with a diameter of 1/4 inch was used to connect the transducers to the pressure ports to ensure that the transducers were not exposed to the high temperature air. The signals from the transducers were logged in to the computer through a cable with a 37-pin female connector. A dash-8 board interface and Labtech software were installed in the computer.

Photographic slides were taken using a camera to record each run, from which maximum spoutable bed height, spout diameter and spout shape could be determined.

3.3 Bed Material

Target sand, supplied by Target Products Ltd., was used as bed material in this study. The sand, with a sphericity only a little below unity, was screened to a relatively narrow size range before particle sizes and particle density were measured. Five different mean sizes were prepared in this study. The mean particle diameter of each size fraction was

Table 3.1: Typical measurement of sand particles.

mesh	$dia.(mm)$	$avg.dia., d_{p_i}(mm)$	$net\ weight(g)$	x_i	x_i/d_{p_i}
$-7+9$	2.80/2.00	2.40	0.2	0.00016	0.00007
$-9+12$	2.00/1.40	1.70	44.7	0.03498	0.02058
$-12+14$	1.40/1.18	1.29	905.6	0.70877	0.54944
$-14+16$	1.18/1.00	1.09	234.4	0.18345	0.16831
$-16+20$	1.00/0.85	0.925	69.0	0.05400	0.05838
$-20+24$	0.85/0.71	0.78	9.8	0.00767	0.00983
-24	0.71/0	0.355	14.0	0.01096	0.03087
Total			1277.7		0.83747
$d_{p_j} = \frac{1}{\Sigma(x_i/d_{p_i})} = 1.1942\ mm$					

determined from a U.S. sieve analysis using the following equation:

$$d_{p_j} = \frac{1}{\Sigma(x_i/d_{p_i})} \tag{3.25}$$

where x_i is the weight fraction of particles with an average adjacent screen aperture size of d_{p_i}. Several measurements were taken for each size to yield an average diameter. Table 3.1 is a typical measurement of sand particles.

In order to determine the difference in the particle diameter of cold and heated sand particles, the cold sand size was first measured at room temperature. Then, the sand was heated at 300 $°C$ for five hours so as to remove the moisture in the particles. It was found that at 300 $°C$, the color of the sand changed appreciably. After the heated sand was cooled down to room temperature, it was then screened to measure its mean particle diameter. The results are listed in Table 3.2. The heated sand values were the actual particle diameters used in the present experiments. All the sands were first heat-treated in this manner.

The density of heat-treated sand particles was obtained by measuring the volume of water displaced by a known weight of particles. Because the sand particles could be permeable to water, the particles were first coated with a water seal (Thomson's

Table 3.2: Mean diameters of sand particles

Cold sand avg. dia. (mm)	Heated sand avg. dia. (mm)	% diff.
2.216	2.025	9.43
1.646	1.630	0.98
1.216	1.200	1.33
1.027	1.010	1.68
0.919	0.915	0.44

Seal) before the measurement. In the density measurement, a 100 cm^3 volumetric flask and a high accuracy (0.05 mg) balance were used. The volume occupied by the sand was calculated from volume difference, from which the density of the sand particles was determined. It was found that the density of the uncoated sand was higher than that of the coated sand by about 10 %. The latter value was 2547 kg/m^3 for all particle sizes.

The bulk density of loosely packed sand was measured using the procedure of Oman and Watson [61]. First, a 250 cm^3 graduate cylinder was partially filled with a known weight of sand. Then this cylinder was inverted with its open end covered and quickly reinverted to its original position. The volume of sand was then recorded and the bulk density thus determined. The loosely packed solids voidage was determined from the particle density and the bulk density.

Chapter 4

Experimental Procedures and Conditions

4.1 Operating procedure

4.1.1 Operation

Before running the experiment, the large heating unit with three electric heaters was turned on for about 20 minutes to preheat the heating section and the ceramic packings inside them. The air flow was not turned on during this heating period. Then the heater controllers were set to the appropriate temperature level so as to reach the first desired temperature in the spouted bed. With a small flow rate of air, sand was added to the bed from the top of the column through the sand input system, which consisted of a funnel and a ball valve. The valve could control the amount of sand being put into the system. After the column was fed with a certain amount of sand, the valve was closed and the funnel still contained some sand for later use. The height of the bed was adjusted either by adding more sand from the hopper or by releasing some sand through the discharge line. The air flow rate was increased and adjusted to maintain a steady spouting condition. The long thermocouple was inserted from the top of the column to different levels of the bed for measuring the bed temperature. When the bed reached the desired temperature within $\pm 5°C$, measurements were taken as described in the next subsection. When all the measurements were completed, the heaters were turned off and the outlet valve was opened to discharge the hot sand particles into a container. The sands were drained either by gravity or by maintaining a high flowrate, which yielded a spout fountain to accelerate the discharge of the sands. The column could be emptied in about 20 minutes. Air flow was kept on for an additional 60 minutes to cool off the whole apparatus.

4.1.2 Measurement

H_m was determined by increasing the bed height until stable spouting could not be obtained for any gas flowrate. The corresponding loosely-packed bed height was then taken as H_m.

The minimum spouting velocity was measured by observing the bed through the transparent front panel. The gas flowrate was first increased to a value above the minimum spouting condition and then decreased slowly until spouting ceased. The gas flowrate at which the fountain just collapsed was taken as the minimum spouting flowrate. The calculation of the minimum spouting velocity is given in the next subsection.

Measurement of spout diameter was performed in two steps. The first step was effected during an experimental run by holding a stainless steel rule horizontally against the transparent front panel and measuring the local spout diameter at several bed levels to yield a full spout shape. The more accurate second step involved making a photographic slide of the spouted bed for each run and, after the experiment, projecting the slide and measuring the spout diameter at 10 cm intervals along the bed height. The area-average spout diameter was calculated as follows, always at $U_s/U_{ms} = 1.05$:

$$D_s = \left[\frac{1}{H_a}\int_0^{H_a}\{D_s(z)\}^2 dz\right]^{\frac{1}{2}} \tag{4.26}$$

where $D_s(z)$ was the measured spout diameter at bed level, z. The numerical integration was done with "QINT4P", a routine described by Tom Nicol [63]. The routine is shown in Appendix E.2.

The pressure drop due to the bed according to Mathur and Epstein [1] should be determined as follows:

$$-\Delta P_a = \sqrt{P_B^2 - P_E^2 + P_{ATM}^2} - P_{ATM} \tag{4.27}$$

where P_B is the measured absolute upstream pressure for the bed and P_E is the corresponding value at the same flowrate for an empty column. The calibration of P_E versus rotameter reading was obtained in the form of a polynomial equation as follows:

$$P_E = 3.50 \times 10^{-3} + 1.73 \times 10^{-3} R + 2.35 \times 10^{-4} R^2 - 3.63 \times 10^{-6} R^3 + 3.21 \times 10^{-8} R^4 \tag{4.28}$$

where R is the large rotameter reading.

The pressure profile was measured by connecting a set of manometers to the corresponding ports along the bed height. A set of pressure transducers was also installed and connected to a data-logging computer.

4.1.3 Calculation of U_{ms}

Flowrate in the Spouted Bed

Figure (4.7) is a simplified flow diagram of the experimental apparatus. Applying the ideal gas law,

$$V_S = V_R \left[\frac{P_R T_S}{P_S T_R} \right] \tag{4.29}$$

From the rotameter reading, V_{STD} was determined from one of the two calibration curves in Appendix A. This value is not equal to the actual volumetric flowrate V_R through the rotameter. However, it has been shown via Equations (A.85) and (A.87) in Appendix A that for a rotameter,

$$V_R = \frac{B_1}{\sqrt{\rho_R}} \tag{4.30}$$

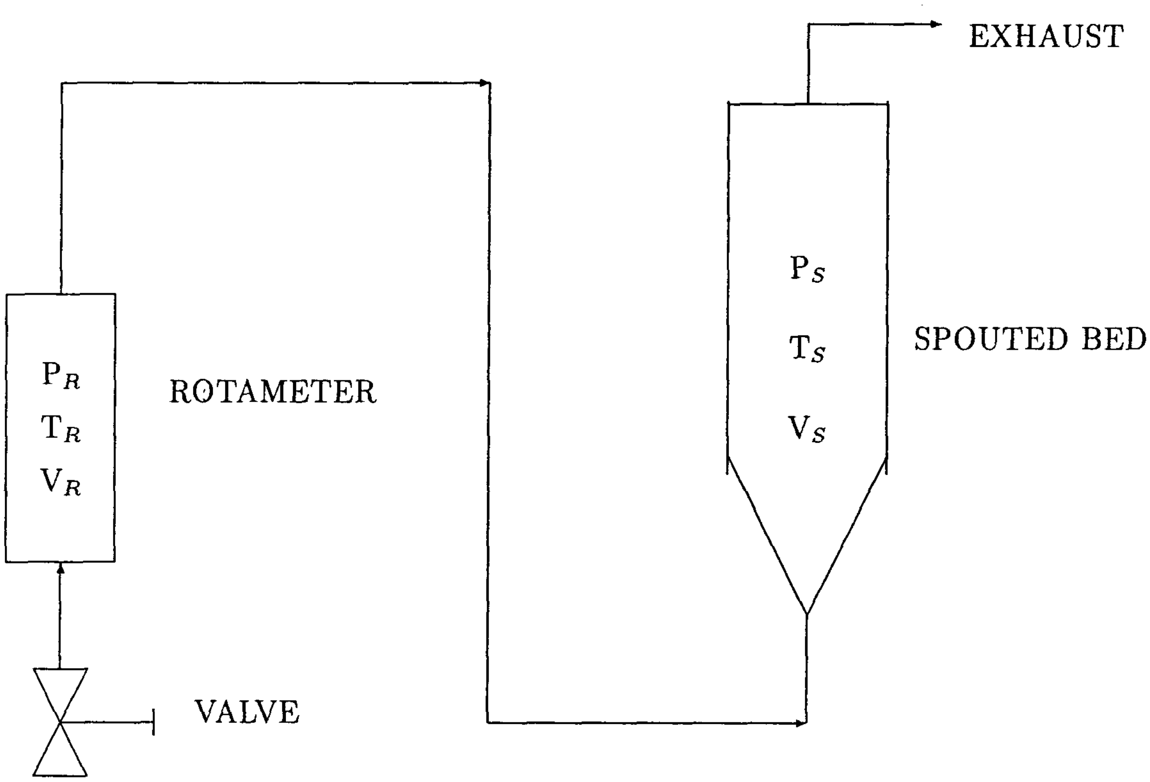

Figure 4.7: Simplified flow diagram of the apparatus.

Therefore

$$\frac{V_R}{V_{STD}} = \sqrt{\frac{\rho_{STD}}{\rho_R}} \tag{4.31}$$

and

$$V_R = V_{STD}\sqrt{\frac{\rho_{STD}}{\rho_R}} = V_{STD}\sqrt{\frac{P_{STD}}{P_R}} \tag{4.32}$$

Substituting Equation (4.32) into Equation (4.29) gives the flowrate in the spouted bed,

$$V_S = V_{STD}\sqrt{\frac{P_{STD}}{P_R}}\left[\frac{P_R T_S}{P_S T_R}\right] = V_{STD}\left[\frac{T_S}{T_R}\right]\frac{\sqrt{P_{STD}P_R}}{P_S} \tag{4.33}$$

Minimum Spouting Velocity

From Equation (4.33), we can proceed with the detailed calculation of U_{ms} as follows:

(1) Determine the temperature both in the rotameter, T_R, and in the spouted bed, T_S. Note that T_S is an average value of all the temperature values along the bed height.

(2) Determine the flowrate of the air, V_{STD}.

$$V_{STD} = 0.4800 + 0.2945 \times R \qquad (large\ rotameter) \tag{4.34}$$

$$V_{STD} = 0.2693 + 0.0212 \times R \qquad (small\ rotameter) \tag{4.35}$$

where R is the rotameter reading.

(3) Determine the average absolute pressure of the rotameter, P_R.

$$P_R = P_g + \frac{\Delta R_1}{2} + P_{atm} \tag{4.36}$$

where P_g is the gauge pressure upstream of the rotameter and ΔR_1 is the pressure difference across the rotameter.

(4) Determine the average absolute pressure of the spouted bed, P_S.

a. Calculate absolute pressure at the port above the orifice, P_B.

$$P_B = P_{atm} + \Delta R_2 \tag{4.37}$$

where ΔR_2 is the gauge pressure at the port above the orifice.

b. From Equation (4.28), calculate the corresponding value at the same flow rate for an empty column, P_E.

c. From Equation (4.27), calculate $-\Delta P_a$.

d. From Equation (3.24), calculate $-\Delta P_s$.

e. Then

$$P_S = P_{atm} + \frac{(-\Delta P_s)}{2} \tag{4.38}$$

(5) From Equation (4.33), calculate the volumetric flow rate through the spouted bed, V_S.

(6) Calculate U_{ms}:

$$U_{ms} = \frac{V_S}{\frac{\pi}{8} D_c^2} \tag{4.39}$$

4.2 Experimental Conditions

4.2.1 Range

For the experimental work, three orifice diameters, five particles sizes and six temperature settings were used. The scheduled number of runs for the experimental program thus came to $3 \times 5 \times 6 = 90$. The operating conditions of the experiments are listed in Appendix C. The range encompassed was

U_s/U_{ms}	1.0 - 1.1
$d_p(mm)$	0.915 - 2.025
$D_i(mm)$	12.70 - 26.64
$H(m)$	0.10 - 1.00
$T(°C)$	$20°C$ - $580°C$

4.2.2 Experimental Error Calculation

In this thesis, the following definitions are used for the comparison of the experimental values with predicted values:

$$\%\ dev = \frac{CAL - EXP}{EXP} \times 100\% \tag{4.40}$$

$$RMS\ \%\ ERROR = \sqrt{[\sum(\%\ dev)^2]/M} \tag{4.41}$$

$$AVG\ \ ERROR = [\sum \mid \%\ dev \mid]/M \tag{4.42}$$

where

EXP = experimental value

CAL = predicted value

M = number of data points

Chapter 5

Results: Minimum Spouting Velocity

5.1 Measurement difficulties

The minimum spouting velocity, U_{ms}, was calculated using the procedure described in Section 4.1.3. Generally the U_{ms} value was more difficult to obtain at high temperature than at room temperature, partly because spouting became less stable at high temperature but mainly because of the spouting equipment itself. At high temperature, the fluid density is low and thus a very small change in the flowmeter setting could result in a large flowrate change. The smaller flowmeter was occasionally used when required air flowrates at high temperature were relatively low. The ceramic rings inside the heaters easily broke into small pieces because of high bed temperatures, thus blocking the screen under the orifice and thereby changing the measured value of U_{ms}. The screen was therefore cleaned before each run and measurement of U_{ms} usually performed several times to ensure a certain level of reproducibility. Another factor which made the measurement of U_{ms} at high temperature more difficult was that to reach the required high temperature, the rate of heating affected the approach to the set point value of the temperature controller. It was relatively difficult to maintain a high temperature at the desired value in the bed because the signal to which the controller responded was not from a point inside the spouted bed, but rather, from a point at the heater outlet. In these experimental runs, all the elevated bed temperatures could therefore only be maintained within $\pm 5°C$ of their desired values.

5.2 Effect of Particle Diameter

Although the Target sand employed in this work was almost spherical, its exact particle shape factor remained uncertain. The mean particle size was narrowed down by screening and the average particle diameter calculated using Equation (3.25).

The effect of particle diameter is shown in Figures 5.8 and 5.9. In all case, minimum spouting velocity U_{ms} increases with particle diameter for a fixed orifice diameter, at any given bed height. This observation is consistent with the empirical equation of Mathur and Gishler, Equation (2.1). Only four particle sizes are shown in Figure 5.8, because the smallest size could not be spouted with this intermediate size orifice. The effect of temperature can also been seen in the two graphs. Generally, U_{ms} increases with increasing temperature. For the intermediate size orifice this temperature effect is consistent, but for the small size orifice this generalization only applies unambiguously to the largest particles.

5.3 Effect of Orifice Diameter

According to the Mathur - Gishler equation, when other conditions are fixed, U_{ms} increases with orifice diameter. Figure 5.10 and 5.11 show the effect of orifice diameter on U_{ms}. In Figure 5.10 at room temperature, U_{ms} of the middle orifice has the smallest value at the given bed height of 0.3 m when $d_p = 2.025$ mm; while at the temperature of $300°C$, the same orifice shows the largest value. At the high temperature of $580°C$, when orifice diameter becomes larger, the U_{ms} value also increases. For $d_p = 1.010$ mm at the lower bed height of 0.2 m, maxima are observed in Figure 5.11 at both elevated temperatures but not at room temperature. At $580°C$, U_{ms} became smaller than at $300°C$ for the large orifice. In both figures, there was no consistent trend of U_{ms} with orifice diameter. The difference between the two figures could be attributed to the differences in particle

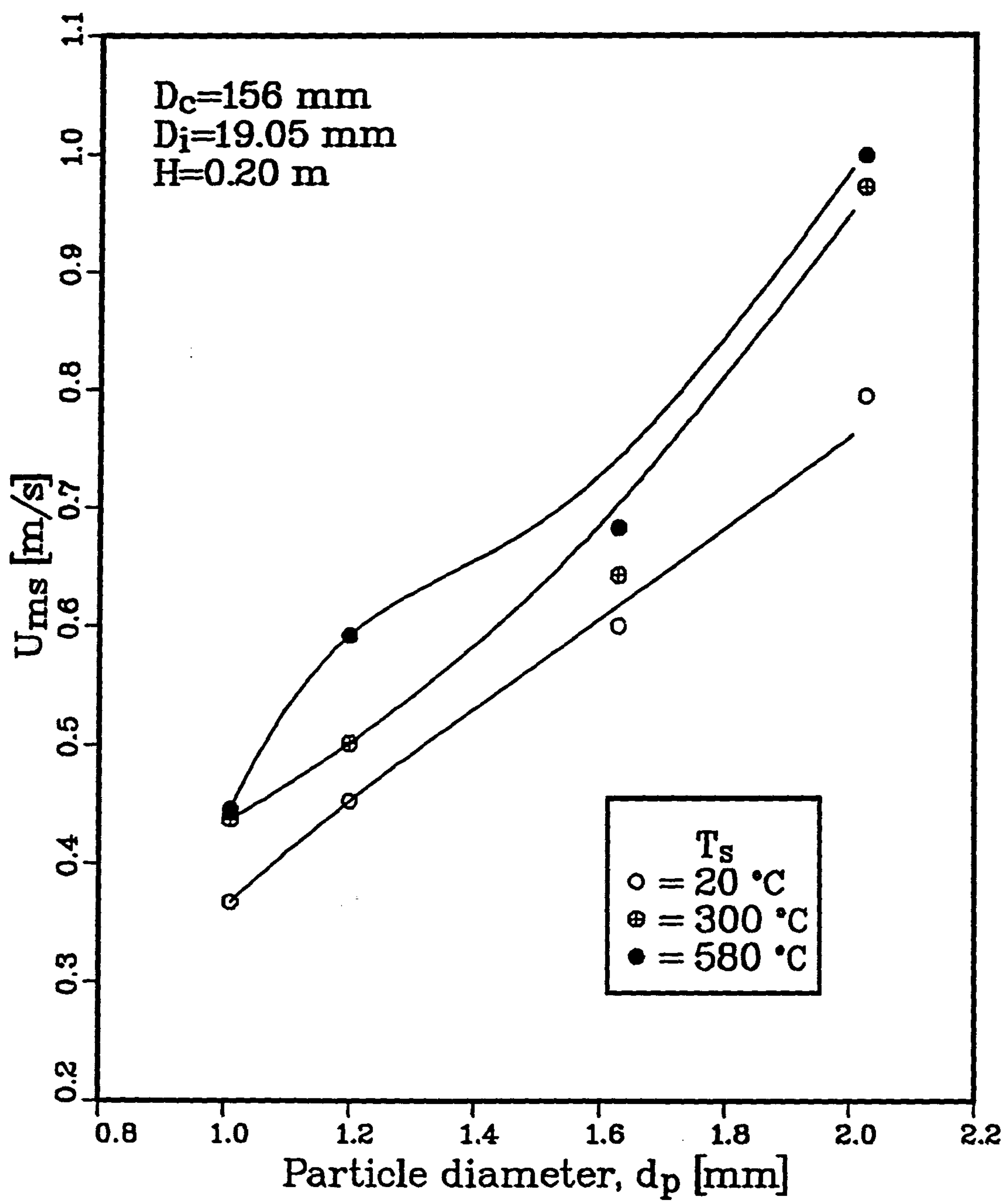

Figure 5.8: Effect of particle diameter on U_{ms}. (D_c=156 mm, D_i=19.05 mm, H=0.2 m)

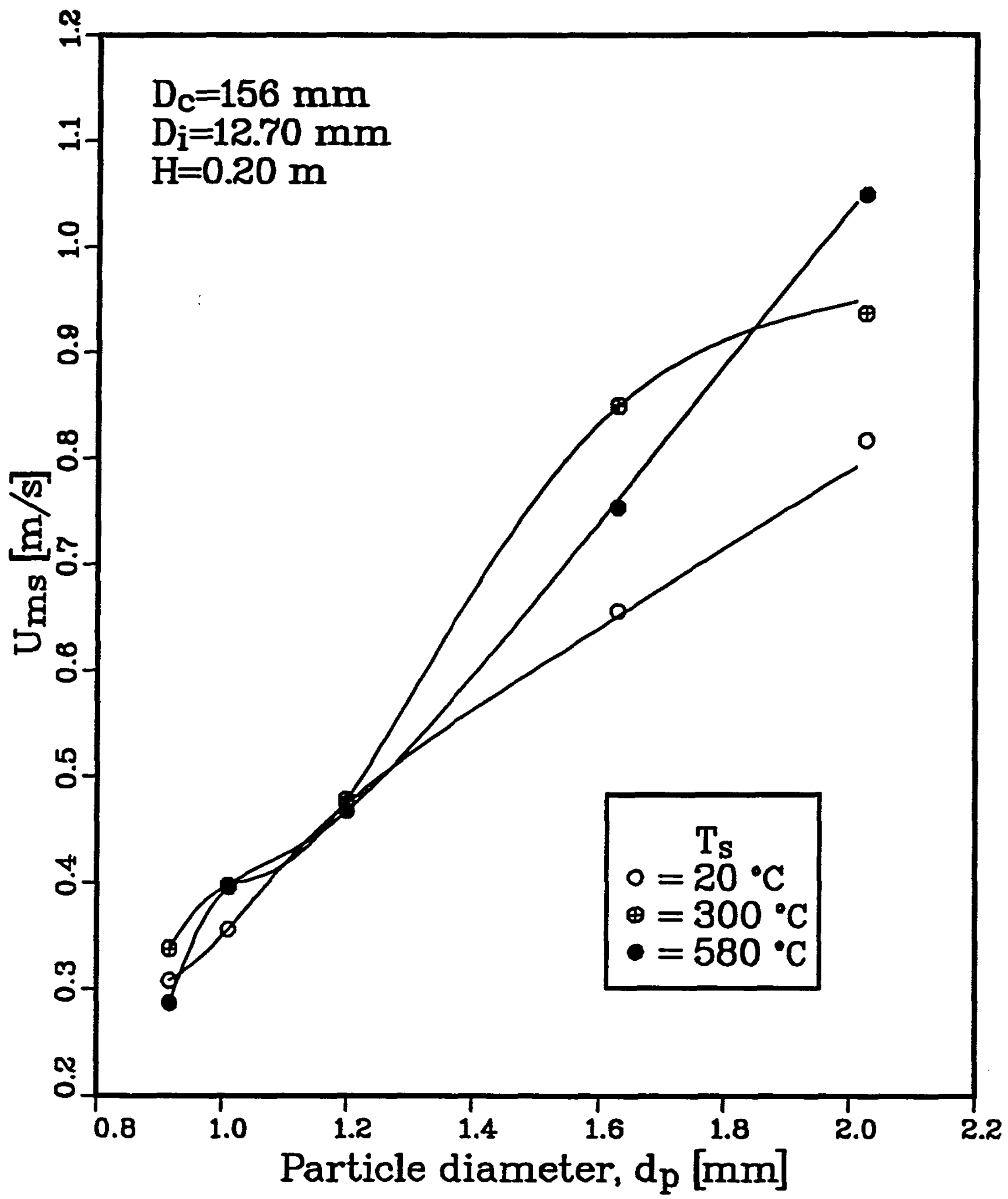

Figure 5.9: Effect of particle diameter on U_{ms}. (D_c=156 mm, D_i=12.70 mm, H=0.2 m)

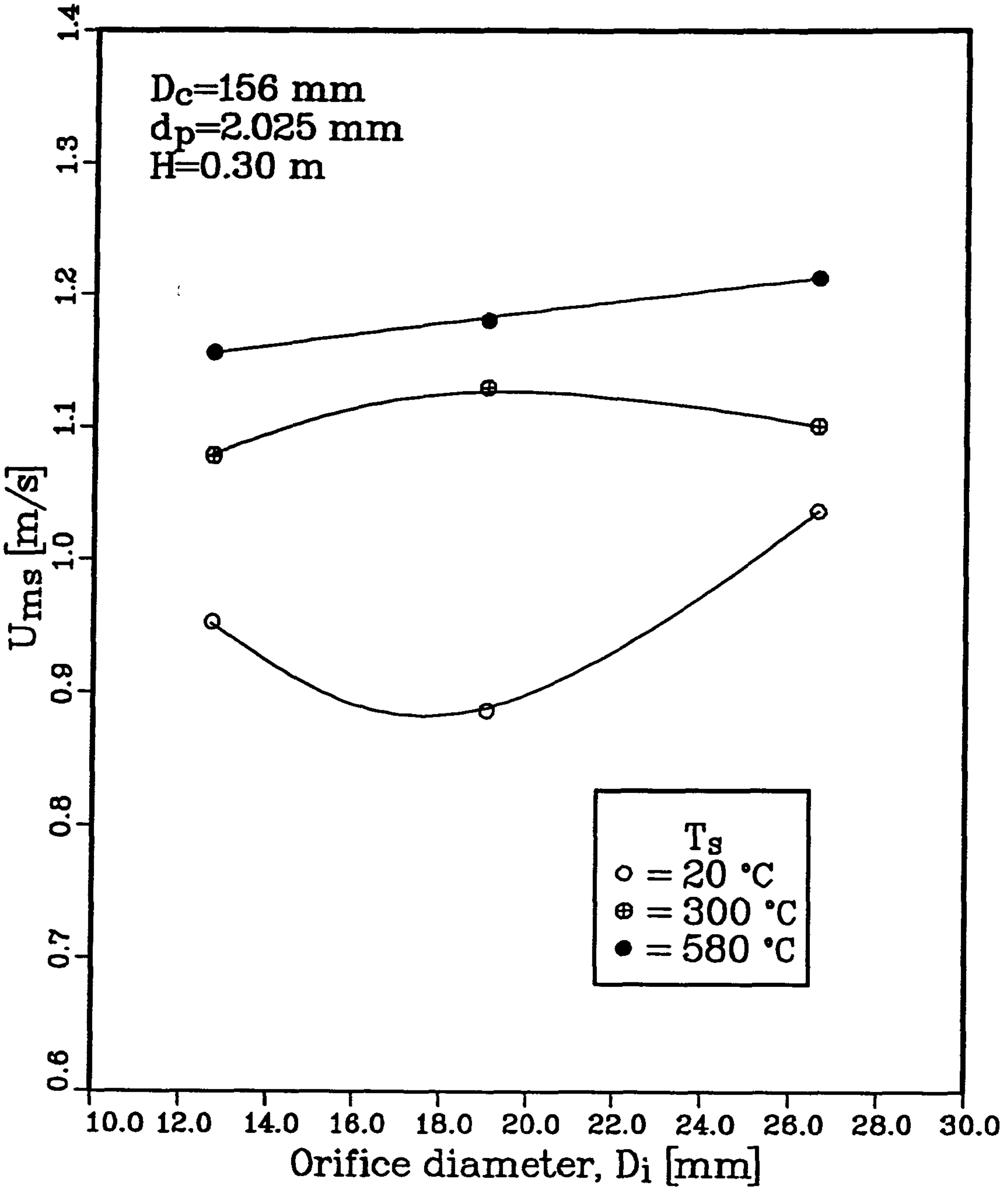

Figure 5.10: Effect of orifice diameter on U_{ms}. (D_c=156 mm, d_p=2.025 mm, H=0.3 m)

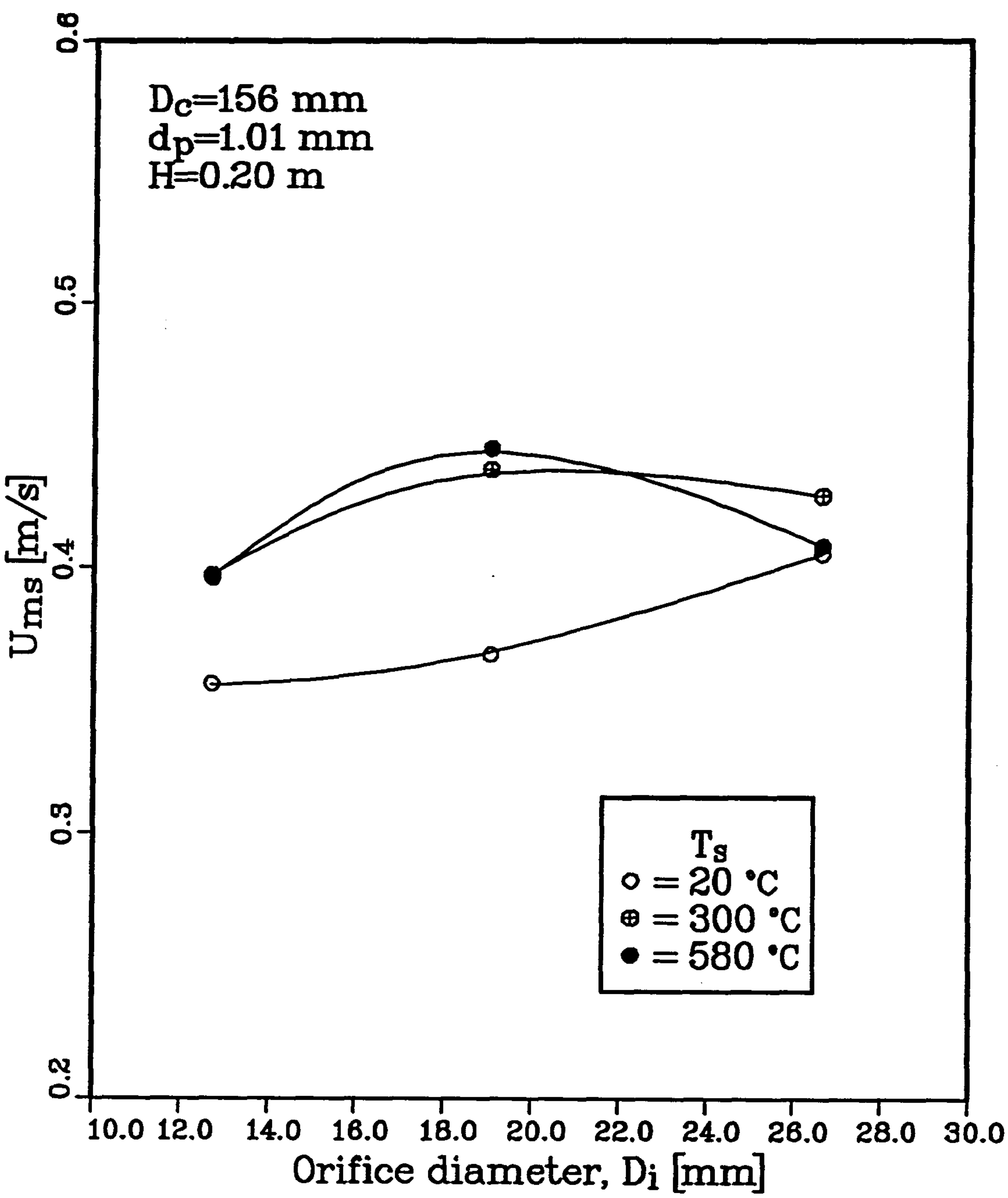

Figure 5.11: Effect of orifice diameter on U_{ms}. (D_c=156 mm, d_p=1.010 mm, H=0.2 m)

size and bed height. This result shows that the Mathur - Gishler equation might not be suitable for predicting U_{ms} at all temperature levels for different particles. The increase of U_{ms} with temperature is again illustrated for most cases plotted in Figures 5.10 and 5.11.

5.4 Effect of Bed Height

Figure 5.12 shows the effect of bed height H on U_{ms} at different temperatures. It is seen that U_{ms} always increases with H and that the previously mentioned temperature effect on U_{ms} increases as H increases.

5.5 Effect of Temperature

The effect of temperature and particle size for a given bed height at three different orifice diameters, is illustrated in Figures 5.13 – 5.15. The curves in these figures, as well as in Figures 5.8 – 5.12, were fitted to the data by the method of cubic splines assuming in most cases that U_{ms} was reproducible to $\pm 5\%$.

In Figure 5.13 for the intermediate size orifice, it is observed that the higher the temperature, the larger the value of U_{ms}. This trend is consistent with Equation (2.1) of Mathur and Gishler. Thus, when the temperature of the air is high, the air density becomes smaller, which results in a higher value of U_{ms}. A similar effect of temperature is shown in Figures 5.14 and 5.15, but mainly for the larger particles. The data for the 1.63 mm particles in Figure 5.15 display more erratic behaviour than the rest. As already illustrated by Figures 5.8 and 5.9, U_{ms} in Figures 5.13 – 5.15 always increases with d_p.

It is basically known that for small particles at high temperature, viscous forces are dominant. For large particles especially at low temperature, kinetic forces are dominant. Considerations such as these, which might explain some of the apparent anomalies or

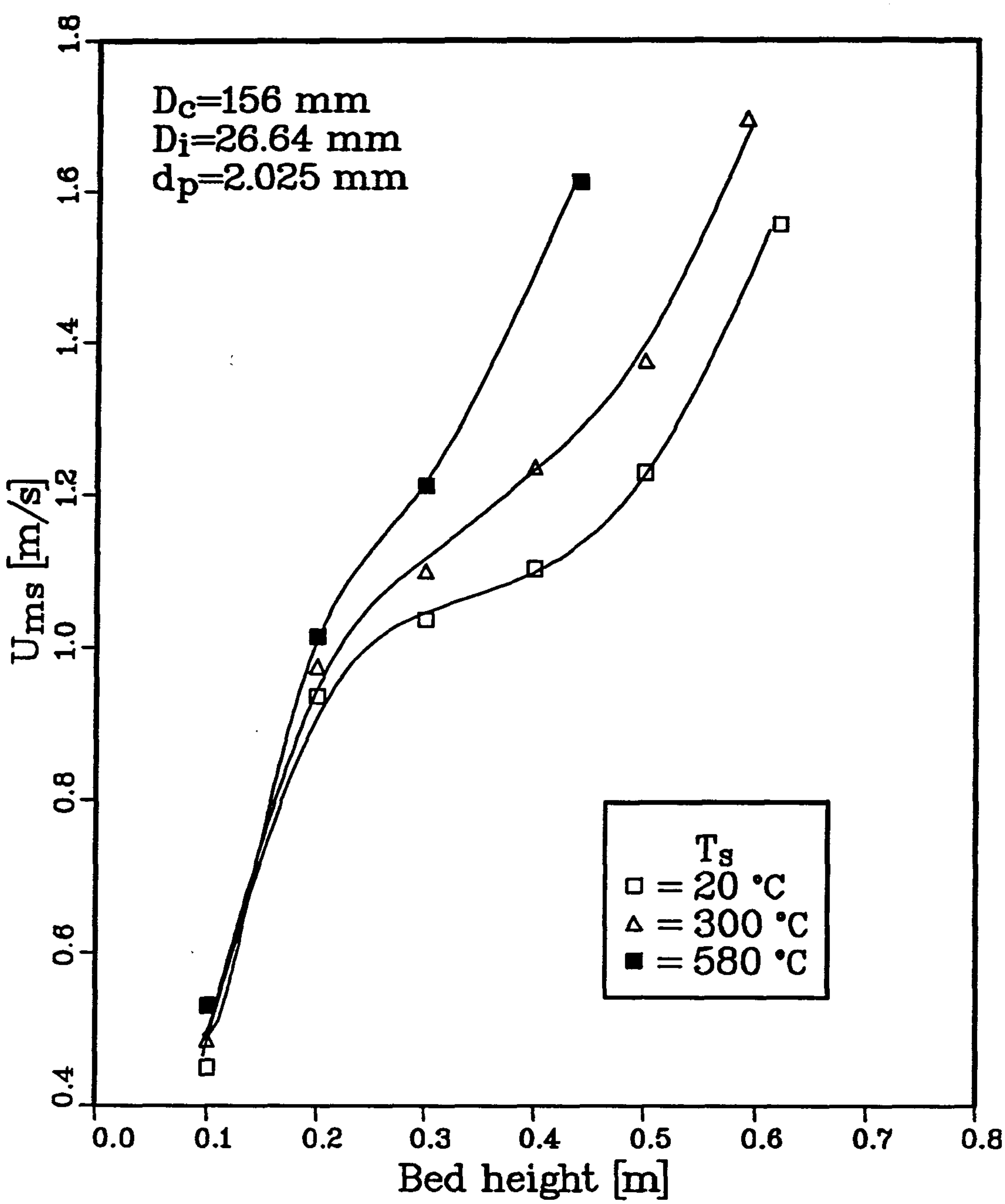

Figure 5.12: Effect of bed height on U_{ms}. (D_c=156 mm, D_i=26.64 mm, d_p=2.025 mm)

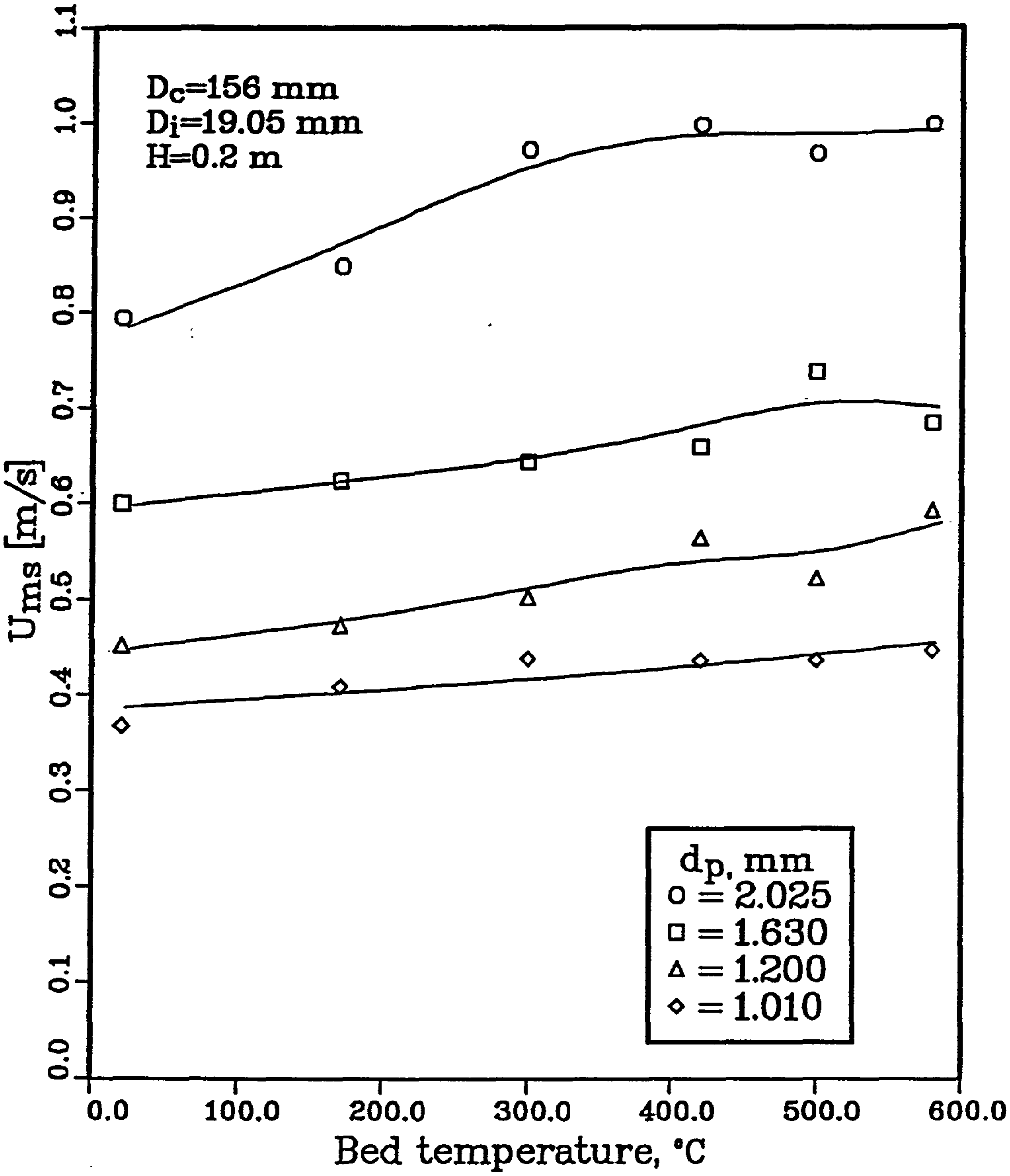

Figure 5.13: Effect of temperature on U_{ms}. (D_c=156 mm, D_i=19.05 mm)

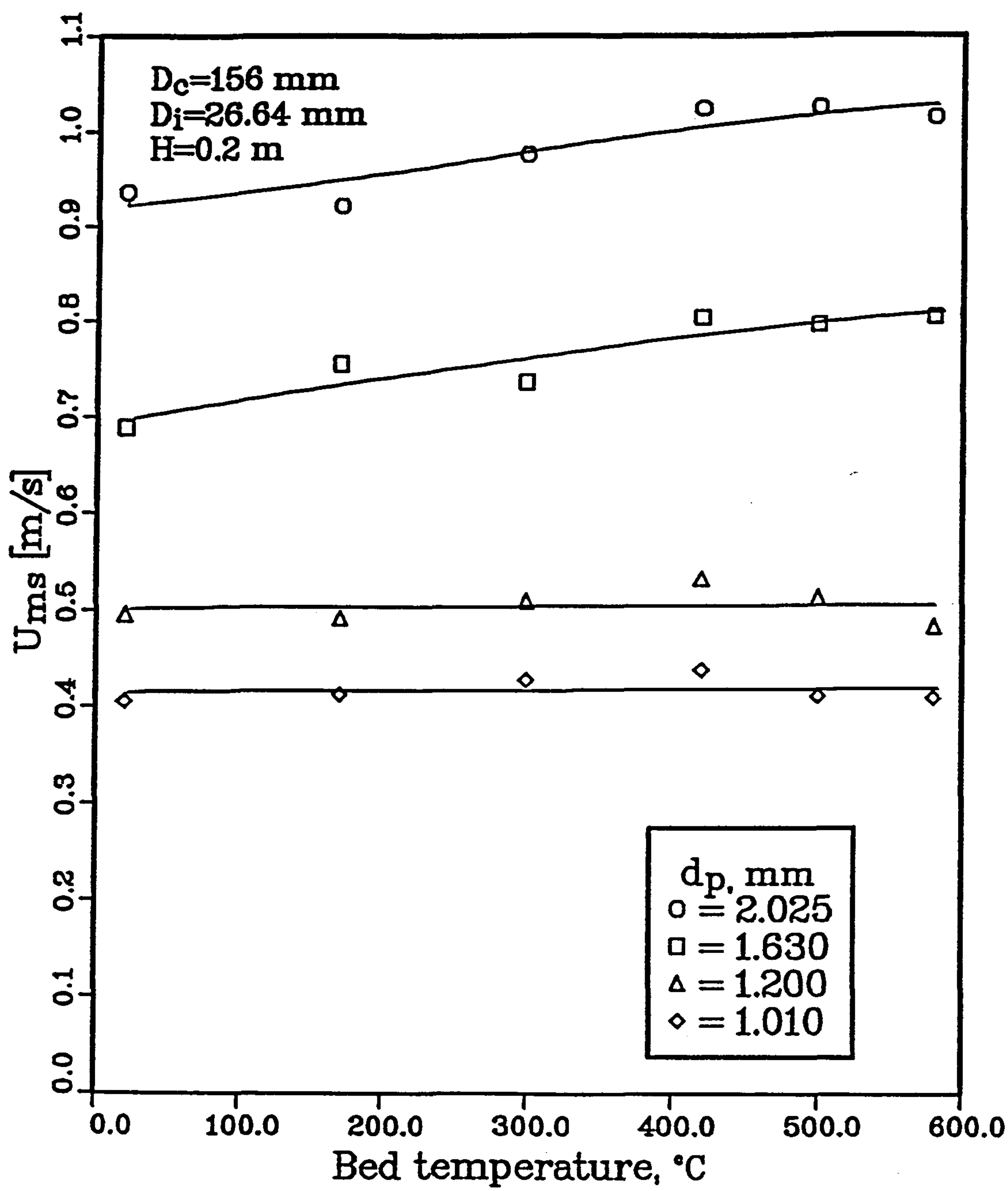

Figure 5.14: Effect of temperature on U_{ms}. (D_c=156 mm, D_i=26.64 mm)

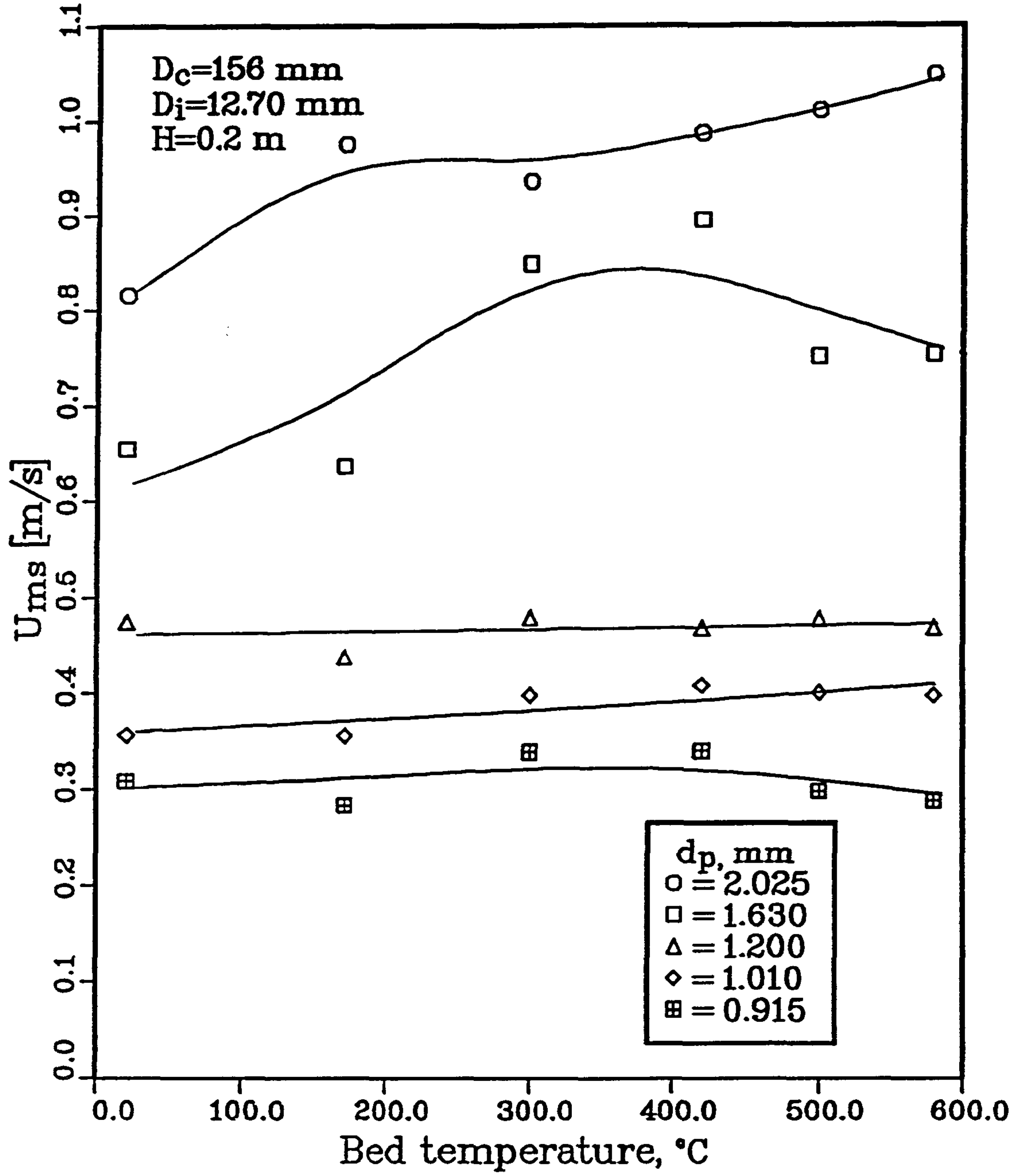

Figure 5.15: Effect of temperature on U_{ms}. (D_c=156 mm, D_i=12.70 mm)

irregularities in Figures 5.8 and 5.15, are best approached by dimensional analysis.

5.6 Data Correlation

5.6.1 First Option

Ignoring μ and particle shape, after Mathur and Gishler [24] and Wu *et al.* [39],

$$U_{ms} = \boldsymbol{f}(d_p, \rho_p - \rho_f, \rho_f, D_c, D_i, H, g) \tag{5.43}$$

By dimensional analysis,

$$\frac{U_{ms}}{\sqrt{gH}} = \psi\left(\frac{d_p}{D_c}, \frac{D_i}{D_c}, \frac{H}{D_c}, \frac{\rho_p - \rho_f}{\rho_f}\right) \tag{5.44}$$

The Mathur - Gishler relation, Equation (2.1), can be expressed as follows:

$$\frac{U_{ms}}{\sqrt{2gH}} = \left(\frac{d_p}{D_c}\right)\left(\frac{D_i}{D_c}\right)^{\frac{1}{3}}\left(\frac{H}{D_c}\right)^{0}\left(\frac{\rho_p - \rho_f}{\rho_f}\right)^{\frac{1}{2}} \tag{5.45}$$

The equation of Wu *et al.* is

$$\frac{U_{ms}}{\sqrt{2gH}} = 10.6\left(\frac{d_p}{D_c}\right)^{1.05}\left(\frac{D_i}{D_c}\right)^{0.266}\left(\frac{H}{D_c}\right)^{-0.095}\left(\frac{\rho_p - \rho_f}{\rho_f}\right)^{0.256} \tag{5.46}$$

The simple power relation based on Equation (5.44), of which Equation (5.45) and (5.46) are particular examples, is

$$\frac{U_{ms}}{\sqrt{2gH}} = \boldsymbol{K}\left(\frac{d_p}{D_c}\right)^{\sigma}\left(\frac{D_i}{D_c}\right)^{\tau}\left(\frac{H}{D_c}\right)^{\omega}\left(\frac{\rho_p - \rho_f}{\rho_f}\right)^{\xi} \tag{5.47}$$

with d_p in the present study evaluated as the reciprocal mean diameter by screen analysis. The five constants based on a least squares correlation of all the present data, K, σ, τ, ω and ξ, were 28.4, 1.17, 0.127, -0.0452 and 0.151, respectively. These constants, together with those of Mathur and Gishler and of Wu *et al.* are summarized in Table 5.3, which also contains the corresponding RMS errors on U_{ms} when applying the corresponding

Table 5.3: Constants in Equation (5.47) and root mean square errors for three correlations

parameter	K	σ	τ	ω	ξ	RMS, %
Mathur-Gishler eq.	1.0	1.0	0.333	0	0.5	17.4* 18.7**
Wu et al. eq.	10.6	1.05	0.266	-0.095	0.256	16.5* 7.82**
This work	28.4	1.17	0.127	-0.0452	0.151	8.10* 13.1**

* — — — RMS using present data

** — — — RMS using Wu's data

empirical equations both to the present data and to the data of Wu [22]. It is seen in the table that the RMS error for the present equation applied to the present data is less than half that of the other two equations, and that even for Wu's data, the present equation does significantly better than the Mathur - Gishler equation.

5.6.2 Second Option

Ignoring particle shape but including μ,

$$U_{ms} = f(d_p, (\rho_p - \rho_f), \rho_f, \mu, D_c, D_i, H, g) \tag{5.48}$$

By dimensional analysis,

$$\frac{d_p U_{ms} \rho_f}{\mu} = \psi \left(\frac{d_p^3(\rho_p - \rho_f)\rho_f g}{\mu^2}, \frac{D_i}{D_c}, \frac{H}{D_c}, \frac{D_i}{d_p}, \frac{\rho_p - \rho_f}{\rho_f} \right) \tag{5.49}$$

i.e.

$$Re_{ms} = \psi \left(Ar, \frac{D_i}{D_c}, \frac{H}{D_c}, \frac{D_i}{d_p}, \frac{\rho_p - \rho_f}{\rho_f} \right) \tag{5.50}$$

If one ignores the last group on the assumption that particle and fluid densities are adequately accounted for by the Archimedes number, then

$$Re_{ms} = \psi' \left(Ar, \frac{D_i}{D_c}, \frac{H}{D_c}, \frac{D_i}{d_p} \right) \tag{5.51}$$

By forcing a direct proportionality between Re_{ms} and Ar in Equation (5.50), thereby effectively eliminating μ as a variable and therefore making the result just another form of Equation (5.44),

$$Re_{ms} = Ar^{1/2}\psi''\left(\frac{D_i}{D_c}, \frac{H}{D_c}, \frac{D_i}{d_p}, \frac{\rho_p - \rho_f}{\rho_f}\right) \tag{5.52}$$

Correlating the present data by simple power relationships based on Equation (5.50), (5.51) and (5.52), the resulting empirical equations were

$$Re_{ms} = 4.95 \times 10^{-4} Ar^{0.753}\left(\frac{D_i}{D_c}\right)^{0.0364}\left(\frac{H}{D_c}\right)^{0.464}\left(\frac{D_i}{d_p}\right)^{0.0943}\left(\frac{\rho_p - \rho_f}{\rho_f}\right)^{0.258} \tag{5.53}$$

$$Re_{ms} = 40.05 Ar^{0.647}\left(\frac{D_i}{D_c}\right)^{0.346}\left(\frac{H}{D_c}\right)^{0.459}\left(\frac{D_i}{d_p}\right)^{-0.2178} \tag{5.54}$$

and

$$Re_{ms} = 38.07 Ar^{1/2}\left(\frac{D_i}{D_c}\right)^{0.795}\left(\frac{H}{D_c}\right)^{0.457}\left(\frac{D_i}{d_p}\right)^{-0.665}\left(\frac{\rho_p - \rho_f}{\rho_f}\right)^{-0.346} \tag{5.55}$$

respectively. Note that Equation (5.55) is equivalent to

$$\frac{U_{ms}}{\sqrt{2gH}} = 26.92\left(\frac{d_p}{D_c}\right)^{1.165}\left(\frac{D_i}{D_c}\right)^{0.130}\left(\frac{H}{D_c}\right)^{-0.043}\left(\frac{\rho_p - \rho_f}{\rho_f}\right)^{0.154} \tag{5.56}$$

which is very similar to Equation (5.47) with the empirical constants as listed previously. The RMS errors were 8.22%, 8.17% and 8.10% for Equation (5.53), (5.54) and (5.55), respectively. The differences between these values are insignificant, and the absolute match between the RMS errors obtained by Equations (5.55) and (5.47) is attributable to correlating the same variables by different but inter-convertible dimensionless groups.

5.6.3 Third Option

If we assume that the effects of fluid and particle properties are fully accounted for in the minimum fluidization velocity, U_{mf}, for the given fluid-particle system, then

$$U_{ms} = fctn(U_{mf}, d_p, D_i, D_c, H) \tag{5.57}$$

By dimensional analysis,

$$\frac{U_{ms}}{U_{mf}} = \frac{Re_{ms}}{Re_{mf}} = \psi\left(\frac{D_i}{D_c}, \frac{H}{D_c}, \frac{D_i}{d_p}\right) \tag{5.58}$$

i.e.

$$\frac{Re_{ms}}{f(Ar)} = \psi\left(\frac{D_i}{D_c}, \frac{H}{D_c}, \frac{D_i}{d_p}\right) \tag{5.59}$$

or

$$Re_{ms} = f(Ar)\psi\left(\frac{D_i}{D_c}, \frac{H}{D_c}, \frac{D_i}{d_p}\right) \tag{5.60}$$

If one includes the additional ratio $(\rho_p - \rho_f)/\rho_f$ in the correlation, then

$$Re_{ms} = f(Ar)\psi'\left(\frac{D_i}{D_c}, \frac{H}{D_c}, \frac{D_i}{d_p}, \frac{\rho_p - \rho_f}{\rho_f}\right) \tag{5.61}$$

Two well tested functional relationships, $f(Ar)$, from the literature are that of Wen and Yu [43],

$$Re_{mf} = f(Ar) = \sqrt{(33.7)^2 + 0.0408\,Ar} - 33.7 = 33.7[\sqrt{1 + 3.59 \times 10^{-5} Ar} - 1] \tag{5.62}$$

and that of Grace [64],

$$Re_{mf} = f(Ar) = \sqrt{(27.2)^2 + 0.0408\,Ar} - 27.2 = 27.2[\sqrt{1 + 5.51 \times 10^{-5} Ar} - 1] \tag{5.63}$$

Simple power relationships based on Equations (5.60) and (5.61), each combined with either Equation (5.62) or (5.63), were used to correlate the present data. The resulting equations and their root mean square errors are:

From Equation (5.60) plus (5.62),

$$Re_{ms} = 24.6[\sqrt{1 + 3.59 \times 10^{-5} Ar} - 1]\left(\frac{D_i}{D_c}\right)^{0.0296}\left(\frac{H}{D_c}\right)^{0.311}\left(\frac{D_i}{d_p}\right)^{0.0604} \quad \pm\ 12.6\% \tag{5.64}$$

From Equation (5.60) plus (5.63),

$$Re_{ms} = 25.7[\sqrt{1 + 5.51 \times 10^{-5} Ar} - 1]\left(\frac{D_i}{D_c}\right)^{0.118}\left(\frac{H}{D_c}\right)^{0.350}\left(\frac{D_i}{d_p}\right)^{-0.0201} \quad \pm\ 10.5\% \tag{5.65}$$

From Equation (5.61) plus (5.62),

$$Re_{ms} = 1.83[\sqrt{1 + 3.59 \times 10^{-5} Ar} - 1] \left(\frac{D_i}{D_c}\right)^{-0.0177} \left(\frac{H}{D_c}\right)^{0.438} \left(\frac{D_i}{d_p}\right)^{0.132} \left(\frac{\rho_p - \rho_f)}{\rho_f}\right)^{0.272} \pm 8.28\% \tag{5.66}$$

From Equation (5.61) plus (5.63),

$$Re_{ms} = 4.19[\sqrt{1 + 5.51 \times 10^{-5} Ar} - 1] \left(\frac{D_i}{D_c}\right)^{0.0847} \left(\frac{H}{D_c}\right)^{0.439} \left(\frac{D_i}{d_p}\right)^{0.0302} \left(\frac{\rho_p - \rho_f)}{\rho_f}\right)^{0.1897} \pm 8.17\% \tag{5.67}$$

The inclusion of $(\rho_p - \rho_f)/\rho_f$ thus gives better correlation than its exclusion, and the use of the Grace $f(Ar)$ is then marginally better than that of Wen and Yu.

5.6.4 Fourth Option

Alternately, if we assume that fluid and particle properties are best accounted for by the free setting velocity, U_t, of the particles, which is related to the minimum inlet jet velocity, U_{mi}, then

$$U_{mi} = \left(\frac{D_c}{D_i}\right)^2 U_{ms} = fctn(U_t, D_c, D_i, H, d_p) \tag{5.68}$$

By dimensional analysis,

$$\frac{U_{ms}}{U_t} = \frac{Re_{ms}}{Re_t} = \psi \left(\frac{D_i}{D_c}, \frac{H}{D_c}, \frac{D_i}{d_p}\right) \tag{5.69}$$

But

$$Re_t = \frac{d_p U_t \rho_f}{\mu} = \phi\,(Ar) \tag{5.70}$$

Therefore

$$Re_{ms} = \phi\,(Ar) \psi \left(\frac{D_i}{D_c}, \frac{H}{D_c}, \frac{D_i}{d_p}\right) \tag{5.71}$$

If, as before, one includes the additional ratio $(\rho_p - \rho_f)/\rho_f$ in the correlation, then

$$Re_{ms} = \phi\,(Ar) \psi' \left(\frac{D_i}{D_c}, \frac{H}{D_c}, \frac{D_i}{d_p}, \frac{\rho_p - \rho_f}{\rho_f}\right) \tag{5.72}$$

A correlation for Re_t as a function of Ar, i.e. $\phi\ (Ar)$, over a wide range of Re_t was ontained from Table (5.3) of Clift *et al.* [62]:

$$log_{10}\ Re_t = -1.81391 + 1.34671W - 0.1242W^2 + 0.006344W^3 \qquad (5.73)$$

$$12.2 < Re_t \leq 6.35 \times 10^3$$

where $W = log_{10}N_D$ and $N_D = 4Ar/3$.

Based on simple power relationships amongst the remaining non-dimensional ratios in Equations (5.71) and (5.72), the resulting empirical correlations and their root mean square errors are:

$$Re_{ms} = \phi(Ar) \times 0.391 \left(\frac{D_i}{D_c}\right)^{0.515} \left(\frac{H}{D_c}\right)^{0.521} \left(\frac{D_i}{d_p}\right)^{-0.374} \qquad \pm\ 9.01\% \qquad (5.74)$$

and

$$Re_{ms} = \phi(Ar) \times 1.63 \left(\frac{D_i}{D_c}\right)^{0.541} \left(\frac{H}{D_c}\right)^{0.452} \left(\frac{D_i}{d_p}\right)^{-0.414} \left(\frac{\rho_p - \rho_f}{\rho_f}\right)^{-0.149} \qquad \pm\ 7.43\% \qquad (5.75)$$

Note that in the correlations all the data were used which satisfied the condition $H \geq 0.2\ m$. The Fortran program for the U_{ms} correlations is listed in Appendix E. A parity plot for Equation (5.75), the best fit correlation of all those generated in the present work, is presented in Figure 5.16.

The goodness of fit of all the present data for Equation (5.75) is compared in Table 5.4 with that of Mathur and Gishler [24], Equation (2.1); Wu *et al.* [39], Equation (2.6); and Grbavcic *et al.* [32], Equation (2.4). It is seen that, while Equation (5.75) shows considerably smaller average and RMS errors than the others, the Grbavcic equation gives a better overall fit than that of Wu *et al.*, which in turn is slightly better than that of Mathur and Gishler. Percentage deviations for individual runs are listed in Appendix F.

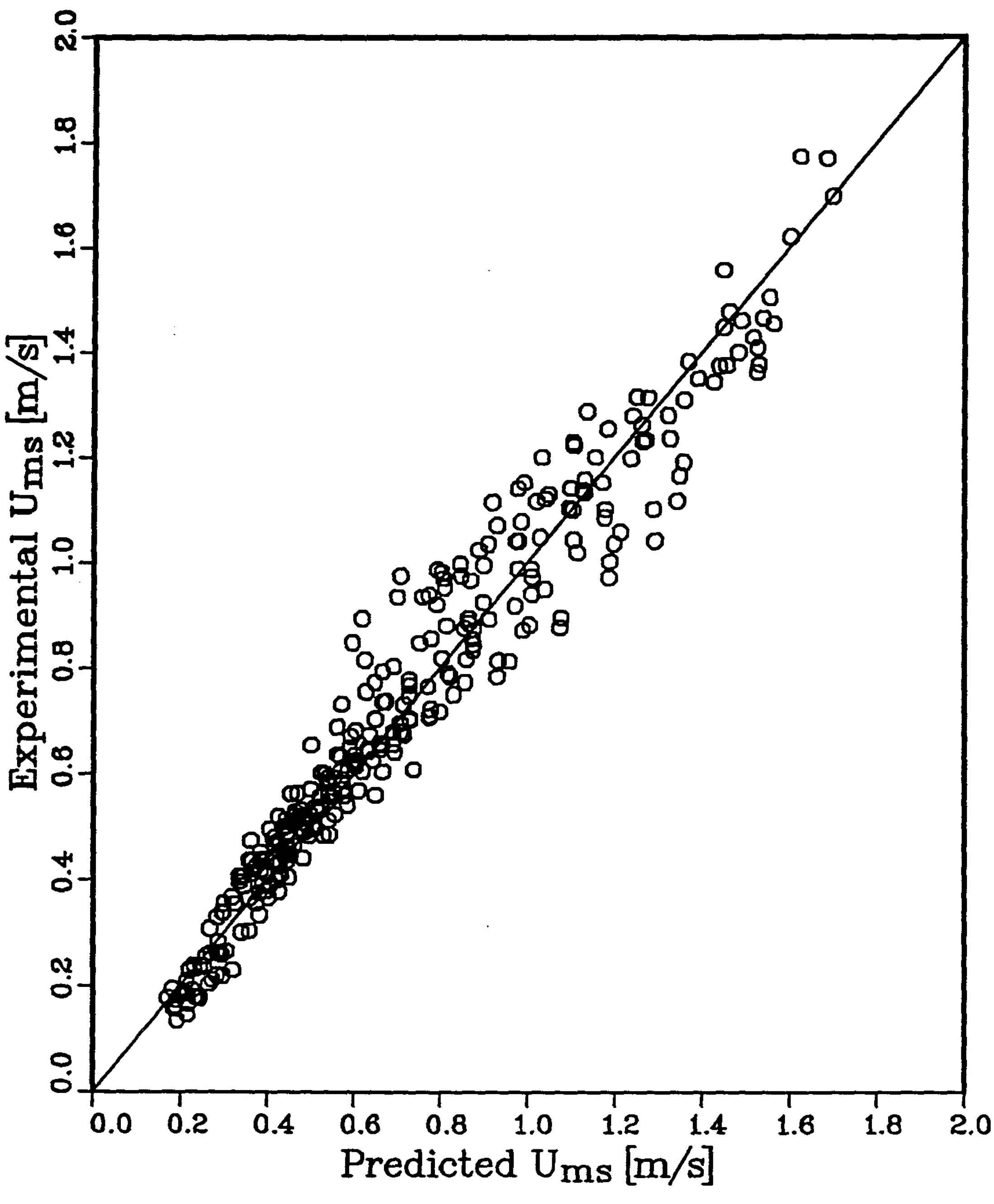

Figure 5.16: Experimental values of U_{ms} vs. values predicted by Equation (5.75).

Table 5.4: Comparison of average and root mean square errors of U_{ms} by equations of Mathur and Gishler, Wu *et al.*, Grbavcic *et al.* and best fit by present work

	M - G Eq.	*Wu Eq.*	*Grbavcic Eq.*	*This work*
AVG ERR, %	14.2	13.3	11.2	5.82
RMS ERR, %	17.4	16.5	13.6	7.43

A comparison of the experimental data with the above four correlations for the two largest particle sizes is shown in Figures 5.17 and 5.18 for the two smaller orifice sizes, at both room temperature and $580°C$. For these particular particles it appears that the Mathur - Gishler equation actually gives better predictability than the equation of Wu *et al.* at high temperature and vice versa at room temperature, while the equation of Grbavcic *et al.* gives its best agreement for both temperatures at low bed height. Equation (5.75) gives somewhat more consistent agreement with the experimental data than the others, irrespective of temperature or bed height. Although data for $H = 0.1\ m$ were ignored in arriving at this empirical equation (as well as at all the others generated in this thesis), data points for $H = 0.1\ m$ are shown in Figures 5.17 and 5.18 for comparison purposes.

Applied to the experimental data of Wu [22], Equation (5.75) shows an RMS error of 10.38 %. The same method of correlating Wu's data yields the empirical equation

$$Re_{ms} = \phi(Ar) \times 2.03 \left(\frac{D_i}{D_c}\right)^{0.632} \left(\frac{H}{D_c}\right)^{0.381} \left(\frac{D_i}{d_p}\right)^{-0.377} \left(\frac{\rho_p - \rho_f}{\rho_f}\right)^{-0.145} \tag{5.76}$$

with an RMS error of 6.62 %. This value is smaller than 7.82 %, the RMS error obtained for the same data by Equation (2.6) of Wu *et al.* [39], which ignores viscosity as a parameter, and supports the choice of free-settling terminal velocity of the particles is a key parameter in the correlation of U_{ms}. Correlating the 305 data points of the present study along with the 112 data points of Wu [22] by the same scheme yields

$$Re_{ms} = \phi(Ar) \times 1.31 \left(\frac{D_i}{D_c}\right)^{0.555} \left(\frac{H}{D_c}\right)^{0.467} \left(\frac{D_i}{d_p}\right)^{-0.388} \left(\frac{\rho_p - \rho_f}{\rho_f}\right)^{-0.126} \tag{5.77}$$

with an RMS error of 8.21 %. That this value exceeds the RMS error for both Equation (5.75) and (5.76) could be due to a global difference in the way the respective data sets are clustered.

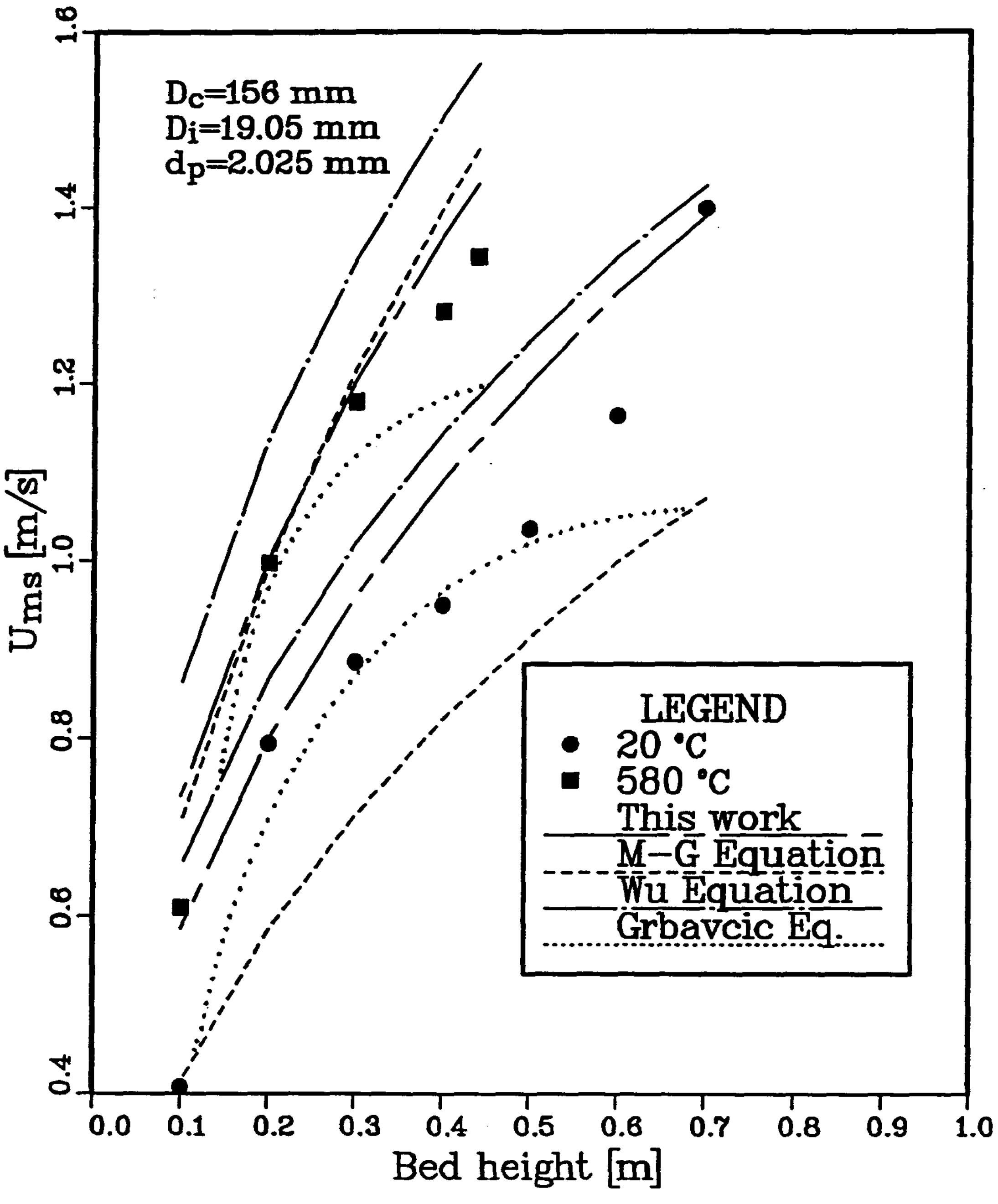

Figure 5.17: Comparison of correlations for U_{ms} with experimental data. (D_c=156 mm, D_i=19.05 mm, d_p=2.025 mm)

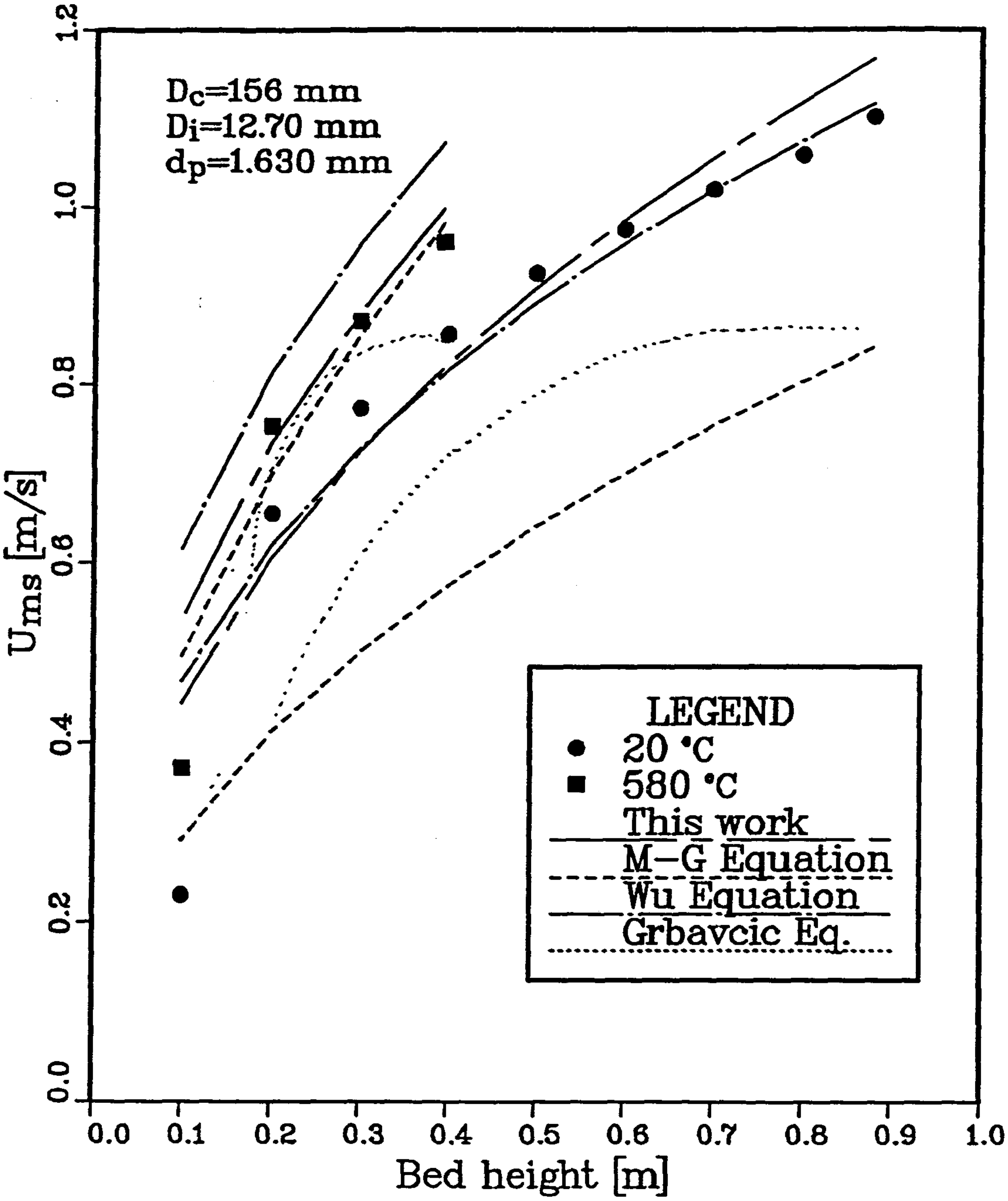

Figure 5.18: Comparison of correlations for U_{ms} with experimental data. (D_c=156 mm, D_i=12.70 mm, d_p=1.630 mm)

Chapter 6

Results: Maximum Spoutable Bed Height

The maximum spoutable bed height , H_m, is the maximum bed height at which steady or stable spouting can be obtained. Above such a height, spouting can not be effected for any gas flow, so it is a transition point on a regime map. The measurement of H_m was approached from bed heights above H_m, so that solids were intermittently discharged from the column until stable spouting could just be achieved, for which H was taken as H_m. Further measurements were then made for values of H below H_m by progressively discharging more solids.

6.1 Spoutability

In the present study, four of the five particle sizes could spout at all temperatures. The smallest particles, with a mean diameter of 0.915 mm, could only spout when the smallest orifice was used at both room temperature and high temperature and when the intermediate size orifice was used at room temperature. Table 6.5 lists all the spoutability trials for the sand particles. Chandnani [23] developed a criterion, based on experiments at room temperature, which states that stable spouting can only occur if $D_i/d_p < 25.4$. However, this criterion failed for two situations. For the intermediate size orifice with $D_i/d_p = 20.82$, spouting only occurred at room temperature. For the large size orifice with $D_i/d_p = 26.38$, spouting was obtainable for all temperature levels. These results suggest that temperature has some effect on the criterion. Similar results were obtained by Wu *et al.* [39].

Table 6.5: Spoutability of sand particles

Run	D_i (mm)	d_p (mm)	D_i/d_p	*Spoutability*					
				$20°C$	$170°C$	$300°C$	$420°C$	$500°C$	$580°C$
$1-6$	19.05	2.025	9.407	$\surd$	$\surd$	$\surd$	$\surd$	$\surd$	$\surd$
$7-12$	19.05	1.630	11.69	$\surd$	$\surd$	$\surd$	$\surd$	$\surd$	$\surd$
$13-18$	19.05	1.200	15.88	$\surd$	$\surd$	$\surd$	$\surd$	$\surd$	$\surd$
$19-24$	19.05	1.010	18.86	$\surd$	$\surd$	$\surd$	$\surd$	$\surd$	$\surd$
$25-30$	19.05	0.915	20.82	$\surd$	$\times$	$\times$	$\times$	$\times$	$\times$
$31-36$	26.64	2.025	13.16	$\surd$	$\surd$	$\surd$	$\surd$	$\surd$	$\surd$
$37-42$	26.64	1.630	16.34	$\surd$	$\surd$	$\surd$	$\surd$	$\surd$	$\surd$
$43-48$	26.64	1.200	22.20	$\surd$	$\surd$	$\surd$	$\surd$	$\surd$	$\surd$
$49-54$	26.64	1.010	26.38	$\surd$	$\surd$	$\surd$	$\surd$	$\surd$	$\surd$
$55-60$	26.64	0.915	29.11	$\times$	$\times$	$\times$	$\times$	$\times$	$\times$
$61-66$	12.70	2.025	6.272	$\surd$	$\surd$	$\surd$	$\surd$	$\surd$	$\surd$
$67-72$	12.70	1.630	7.791	$\surd$	$\surd$	$\surd$	$\surd$	$\surd$	$\surd$
$73-78$	12.70	1.200	10.58	$\surd$	$\surd$	$\surd$	$\surd$	$\surd$	$\surd$
$79-84$	12.70	1.010	12.57	$\surd$	$\surd$	$\surd$	$\surd$	$\surd$	$\surd$
$85-90$	12.70	0.915	13.88	$\surd$	$\surd$	$\surd$	$\surd$	$\surd$	$\surd$

6.2 Maximum Spoutable Bed Height

A frequently used equation in predicting H_m is that of McNab and Bridgwater [44], Equation (2.10). With $b_1 = 1.11$ to best fit their existing experimental data, it becomes

$$H_m = \left[\frac{D_c^2}{d_p}\right]\left[\frac{D_c}{D_i}\right]^{2/3}\left[\frac{700}{Ar}\right](\sqrt{1+35.9\times10^{-6}Ar}-1)^2 \qquad (2.10a)$$

In the present study, using the experimental data obtained, two graphs were composed based on the McNab - Bridgwater equation. In Figure 6.19, H_m/D_c was plotted against $[D_c/d_p]\,[D_c/D_i]^{2/3}\,[700/Ar]\,(\sqrt{1+35.9\times10^{-6}Ar}-1)^2$. The predicted values show fair agreement with the experimental values (RMS=24.7 %). However, with $b_1 = 1.11$, Equation (2.10a) is not the best fit. By applying a least squares analysis, a best fit straight line through the origin for the experimental data in the present work has a slope 0.881 (RMS=22.1%). Therefore a new value of b_1, 1.04, was obtained. This suggested value predicts a lower bed height than the McNab - Bridgwater equation. Both equations are plotted in Figure 6.19. Another graph, which plots $[H_m d_p/D_c^2]\,[D_i/D_c]^{2/3}$ against Ar, is presented in Figure 6.20. Along with the experimental data, it also shows the McNab - Bridgwater equation plotted with both the old and the new value of b_1. In both graphs, solid lines represent the McNab - Bridgwater equation and dashed lines represent the newly fitted equation.

6.2.1 Effect of Particle diameter on H_m

If the expression for Ar is substituted into Equation (2.10a), the latter becomes

$$\begin{aligned} H_m &= \frac{C_2}{d_p^4}\left[\sqrt{1+C_3 d_p^3}-1\right]^2 \\ &= C_2\left[\sqrt{\frac{1}{d_p^4}+\frac{C_3}{d_p}}-\frac{1}{d_p^2}\right]^2 \end{aligned} \qquad (6.78)$$

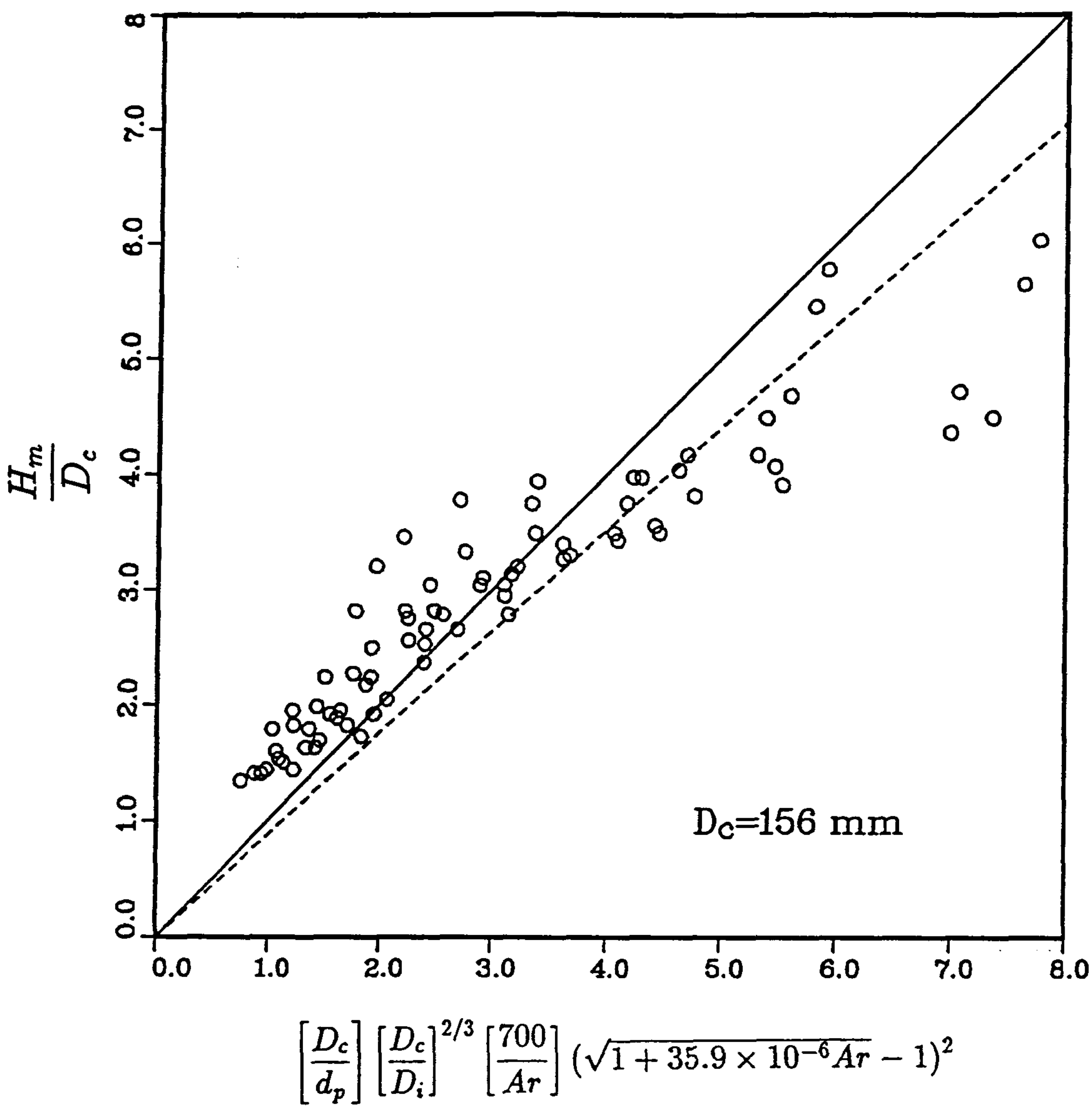

Figure 6.19: Comparison between experimental data (points), prediction by Equation 2.10a (solid line) and prediction by modified equation (broken line).

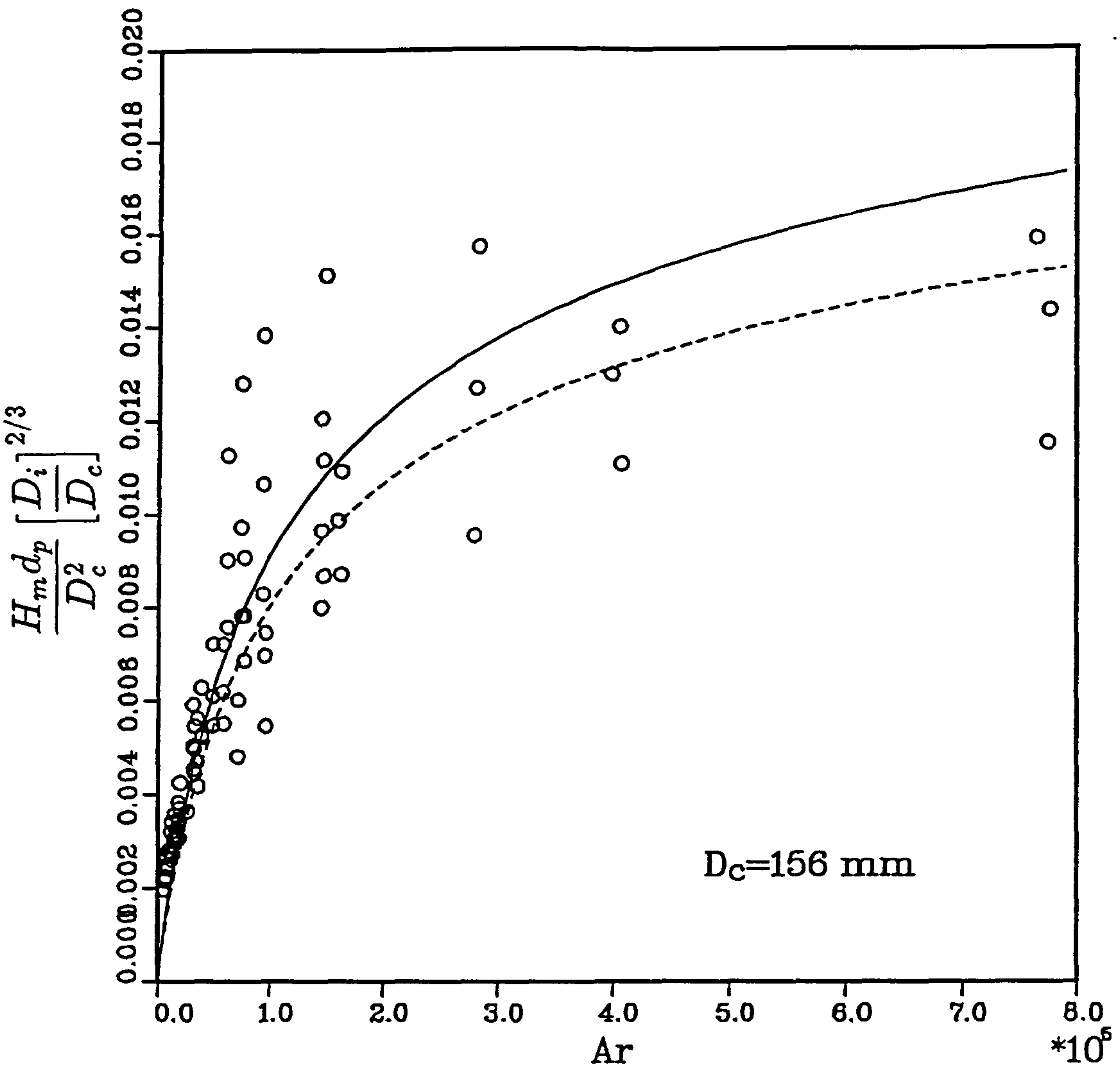

Figure 6.20: Comparison between experimental data (points), prediction by Equation 2.10a (solid line) and prediction by modified equation (broken line).

where $C_2 = 700 D_c^{8/3} D_i^{2/3} \mu^2 / (\rho_p - \rho_f)\rho_f g$ and $C_3 = 35.9 \times 10^{-6} (\rho_p - \rho_f)\rho_f g / \mu^2$. $(d_p)_{crit}$ is found by setting $d(H_m)/d(d_p)$ equal to zero. The solution is

$$(d_p)^3_{crit} = 8/C_3 \tag{6.79}$$

or

$$(d_p)_{crit} = 60.6 \left[\frac{\mu^2}{(\rho_p - \rho_f) g \rho_f} \right]^{1/3} \tag{6.80}$$

Because $d^2 H_m / d(d_p)^2$ from Equation (6.78) is negative at $d_p = (d_p)_{crit}$, this critical value of d_p represents the particle diameter at which H_m achieves a maximum as d_p is increased for a fixed column geometry and fixed fluid and particle properties.

Equation (6.80) states that the critical value of d_p depends on particle density, gas density and gas viscosity. In this thesis, the particle density in all the experiments is the same, so only the gas properties, which depend on temperature, could change the value of $(d_p)_{crit}$. For air spouting of sand particles at atmospheric pressure, the critical values of d_p as given by Equation (6.80) are listed in Table 6.6.

Table 6.6: Change of critical value of d_p with temperature

temperature T, $(°C)$	20	170	300	420	500	580
density ρ_f, (kg/m^3)	1.205	0.797	0.616	0.509	0.457	0.414
viscosity $\mu \times 10^5$, $(kg/m{\cdot}s)$	1.84	2.48	3.00	3.43	3.65	3.79
critical value d_p, (mm)	1.358	1.902	2.353	2.741	2.962	3.139

The experimental data showing the effect of particle diameter for different orifice sizes and temperatures, and the same effect calculated by the McNab - Bridgwater relation, Equation (2.10a), are plotted in Figures 6.21, 6.22 and 6.23. Generally, Equation (2.10a) overpredicted H_m substantially at room temperatures and underpredicted H_m slightly at high temperatures. Considering the fact that the least squares fitted equation whereby b_1 equals 1.04 instead of 1.11 gives lower bed height prediction over all temperature levels, the modified McNab - Bridgwater equation with $b_1 = 1.04$ would strike a better balance between its predictions at low and high temperatures.

From Table 6.6 and the discussion above about the critical value of particle diameter for H_m, it is noted that H_m increases with increasing d_p below the critical value and decreases with increasing d_p above it. This trend is demonstrated in figures 6.21 - 6.23 at room temperature. The trend towards a maximum is also exhibited at the two higher temperatures, but since the values of $(d_p)_{crit}$ listed for these two temperatures in Table 6.6 exceed the largest particle size studied, the corresponding maxima are not achieved within the range of the plots. It should also be noted that the use of the approximate Wen - Yu [43] constant, 35.9×10^{-6}, in the derivation of Equation (2.10) may be a source of error in the prediction of $(d_p)_{crit}$ by that equation.

6.2.2 Effect of Orifice Diameter on H_m

The effect of orifice diameter on H_m for three different temperatures, both experimentally and by the McNab - Bridgwater Equation (2.10a), are shown in Figures 6.24, 6.25, 6.26 and 6.27 for the four sand diameters of 2.025 mm, 1.630 mm, 1.200 mm and 1.010 mm, respectively. If all other conditions are fixed, then H_m decreases with increasing value of the orifice diameter. The observed trends were pretty much consistent with that predicted by Equation (2.10a).

6.2.3 Effect of Temperature on H_m

Equation (2.10) shows that H_m is a function of Ar, which incorporates the entire effect of fluid properties. Therefore, provided that other conditions remain the same, the effect of temperature on H_m is given by the effect of Ar on H_m. When temperature increases, air density decreases while air viscosity increases, which results in a lower value of Ar. If the McNab - Bridgwater Equation (2.10) is written as a relation between H_m and Ar, it

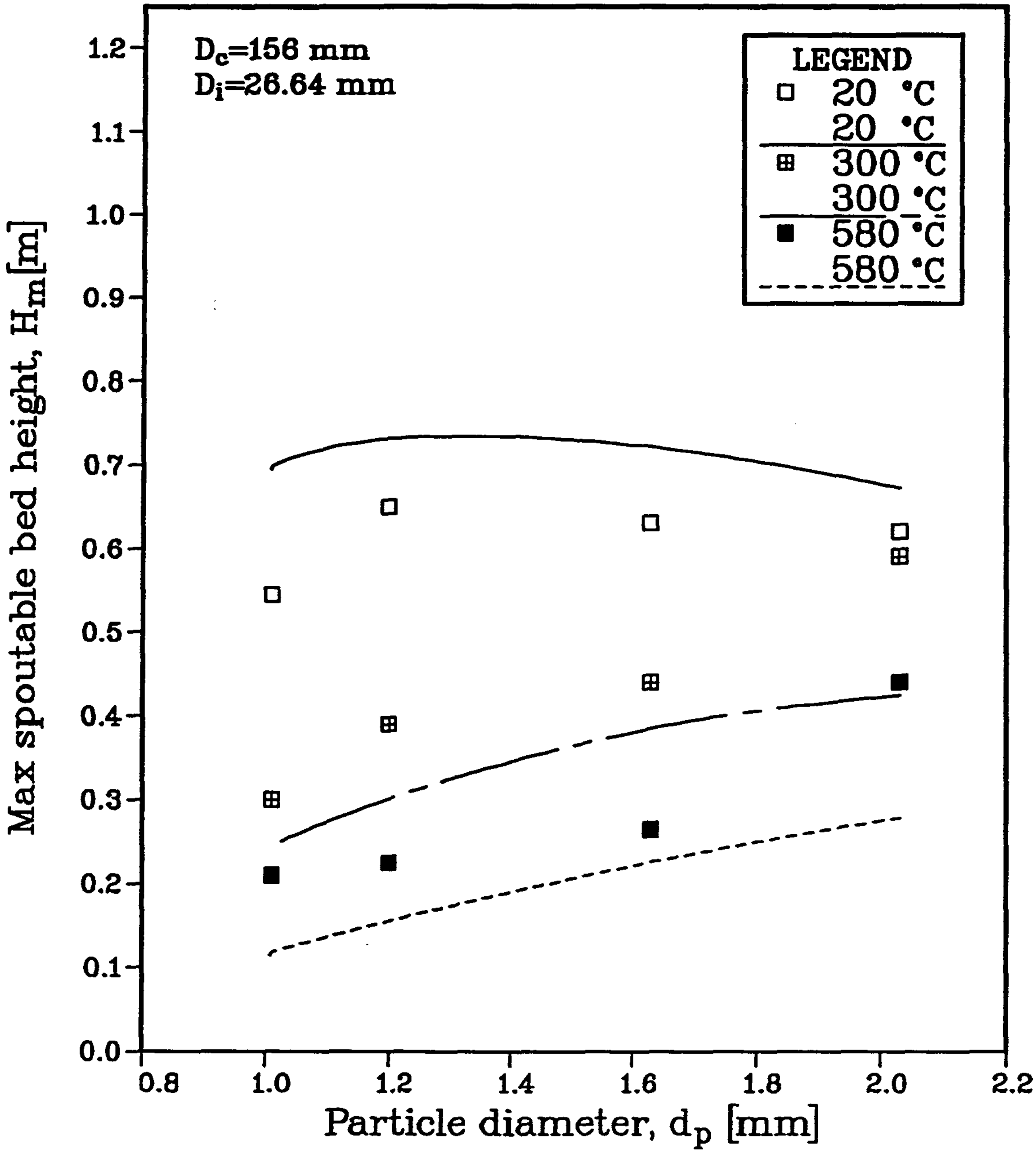

Figure 6.21: Effect of particle diameter on H_m. Points represent experimental data, lines represent McNab - Bridgwater equation. ($D_c = 156\ mm,\ D_i = 26.64\ mm$)

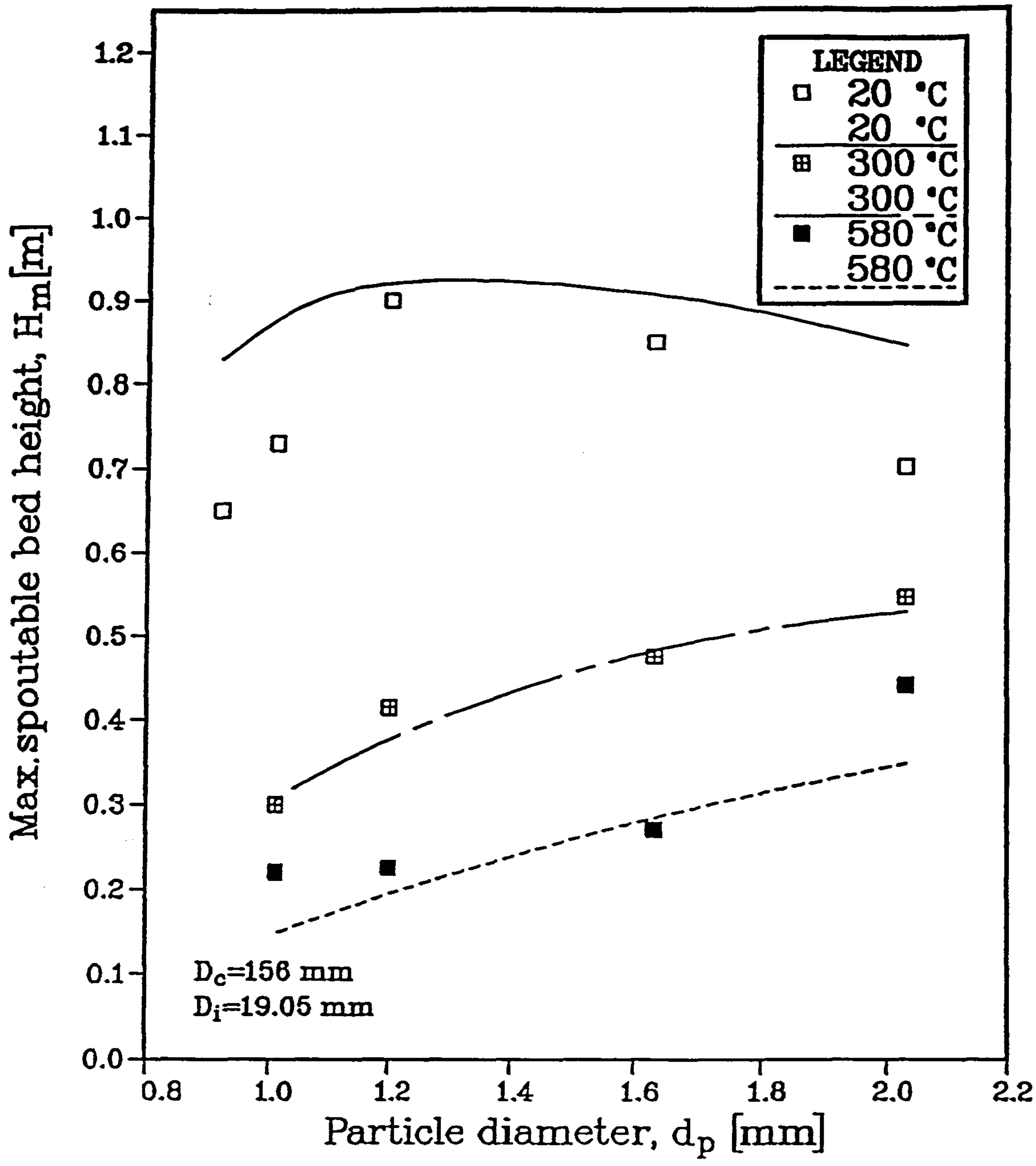

Figure 6.22: Effect of particle diameter on H_m. Points represent experimental data, lines represent McNab - Bridgwater equation. ($D_c = 156\ mm,\ D_i = 19.05\ mm$)

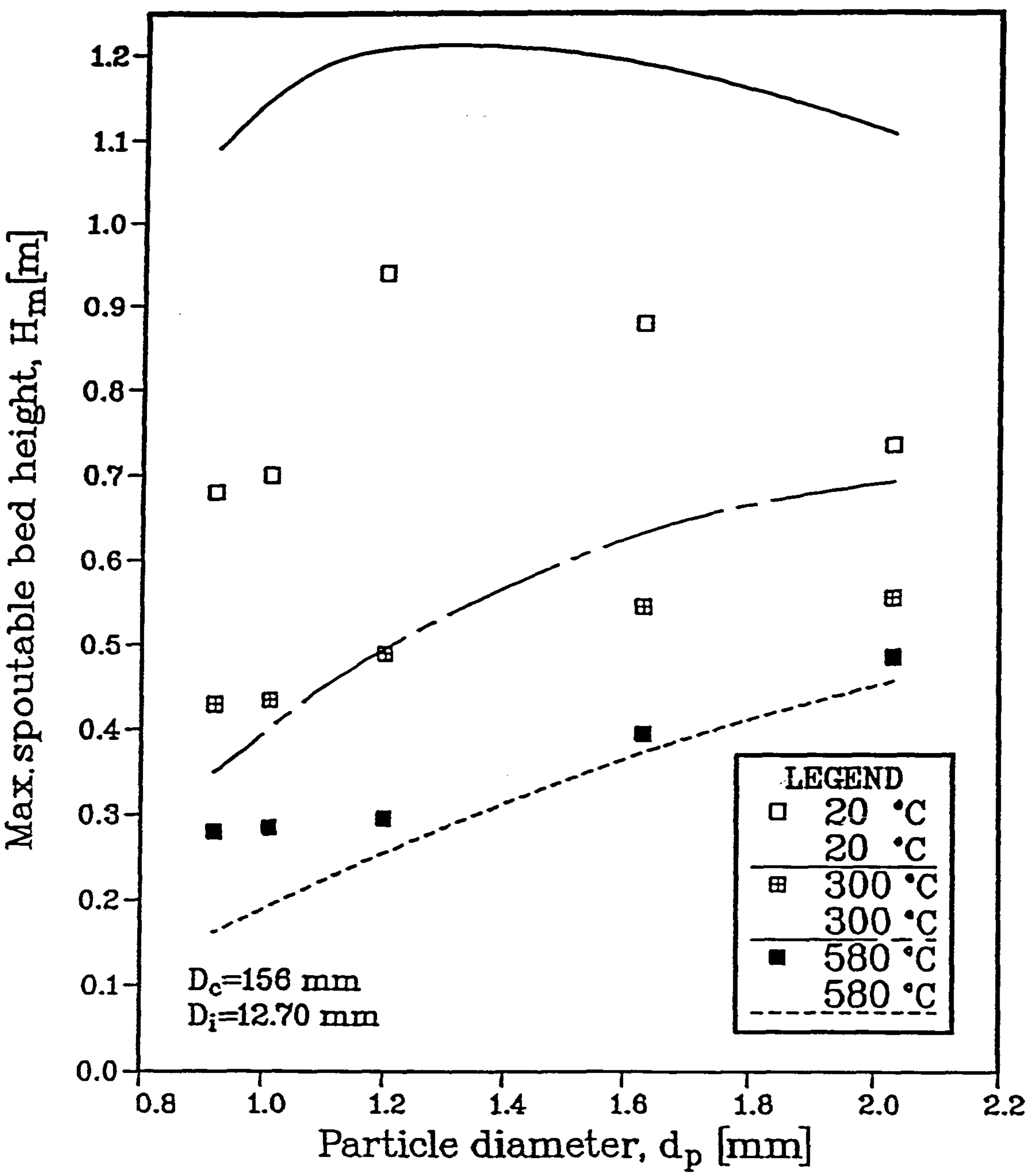

Figure 6.23: Effect of particle diameter on H_m. Points represent experimental data, lines represent McNab - Bridgwater equation. ($D_c = 156\ mm$, $D_i = 12.70\ mm$)

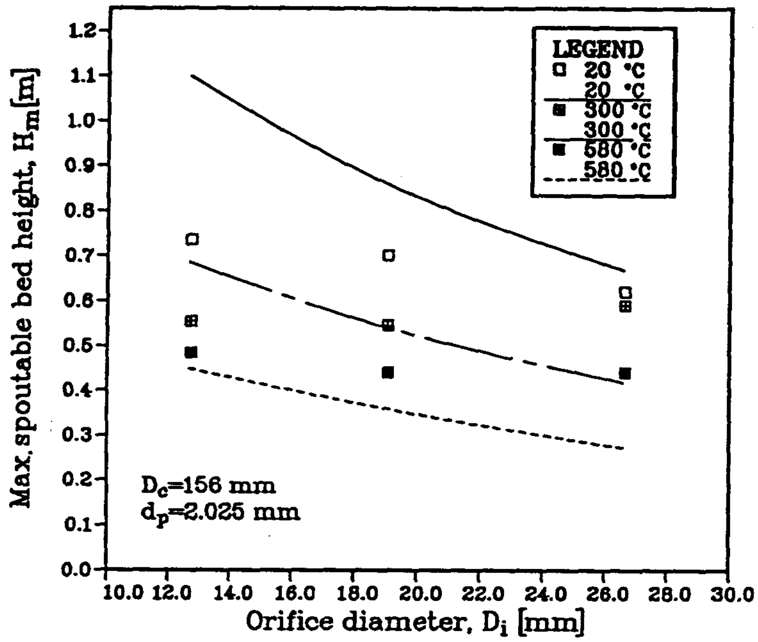

Figure 6.24: Effect of orifice diameter on H_m. Points represent experimental data, lines represent McNab - Bridgwater equation. (D_c=156 mm, d_p=2.025 mm)

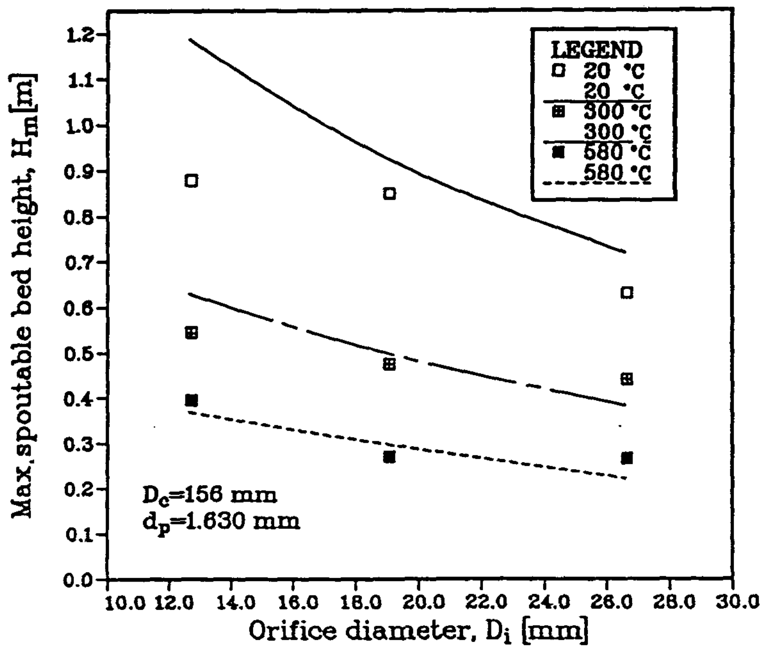

Figure 6.25: Effect of orifice diameter on H_m. Points represent experimental data, lines represent McNab - Bridgwater equation. (D_c=156 mm, d_p=1.630 mm)

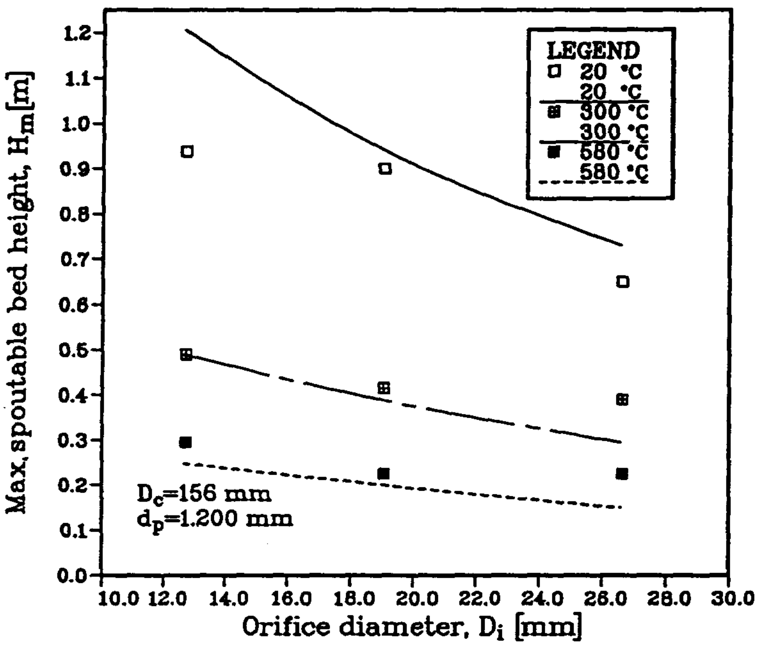

Figure 6.26: Effect of orifice diameter on H_m. Points represent experimental data, lines represent McNab - Bridgwater equation. (D_c=156 mm, d_p=1.200 mm)

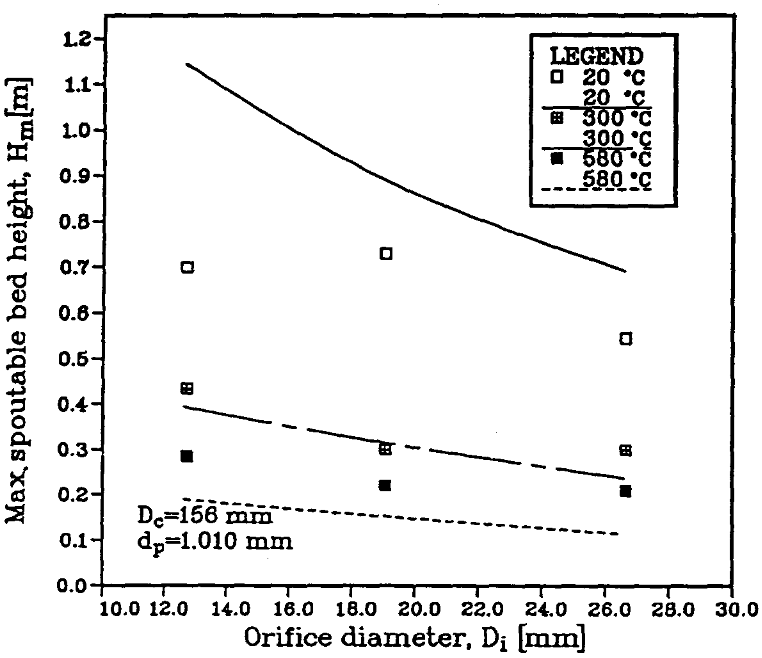

Figure 6.27: Effect of orifice diameter on H_m. Points represent experimental data, lines represent McNab - Bridgwater equation. (D_c=156 mm, d_p=1.010 mm)

has the form

$$H_m = C_1 \left(\sqrt{\frac{1}{Ar} + 35.9 \times 10^{-6} Ar} - \sqrt{\frac{1}{Ar}} \right)^2 \tag{6.81}$$

Differentiating both sides of Equation (6.81) with respect to Ar, while other variables included in C_1 are kept constant, leads to (see Appendix B):

$$\frac{dH_m}{dAr} > 0 \;\; for \;\; Ar > 0 \tag{6.82}$$

A derivative greater than zero for all values of Ar implies that H_m increases with increasing Ar. Thus, H_m should increase with decreasing temperature. The prediction was well supported by the experimental results plotted in Figures 6.28, 6.29 and 6.30 for two particle sizes. The H_m data using the intermediate size orifice (Figure 6.29) are reasonably well predicted by Equation (2.10a); and data from the other two orifices (Figure 6.28 and Figure 6.30) were qualitatively in agreement with this equation. The existence of a critical diameter, as discussed in Section 6.2.1 and illustrated in Figures 6.21 – 6.23, helps to explain why the smaller particles, for which H_m always fall to the left of the maximum (i.e. on the H_m - rising side of the curve) on these figures, show a greater temperature effect in Figures 6.28 – 6.30 than the larger particles, which fall to the left of the maximum at the high temperatures but to the right of the maximum (i.e. on the H_m - falling side of the curve) at room temperature.

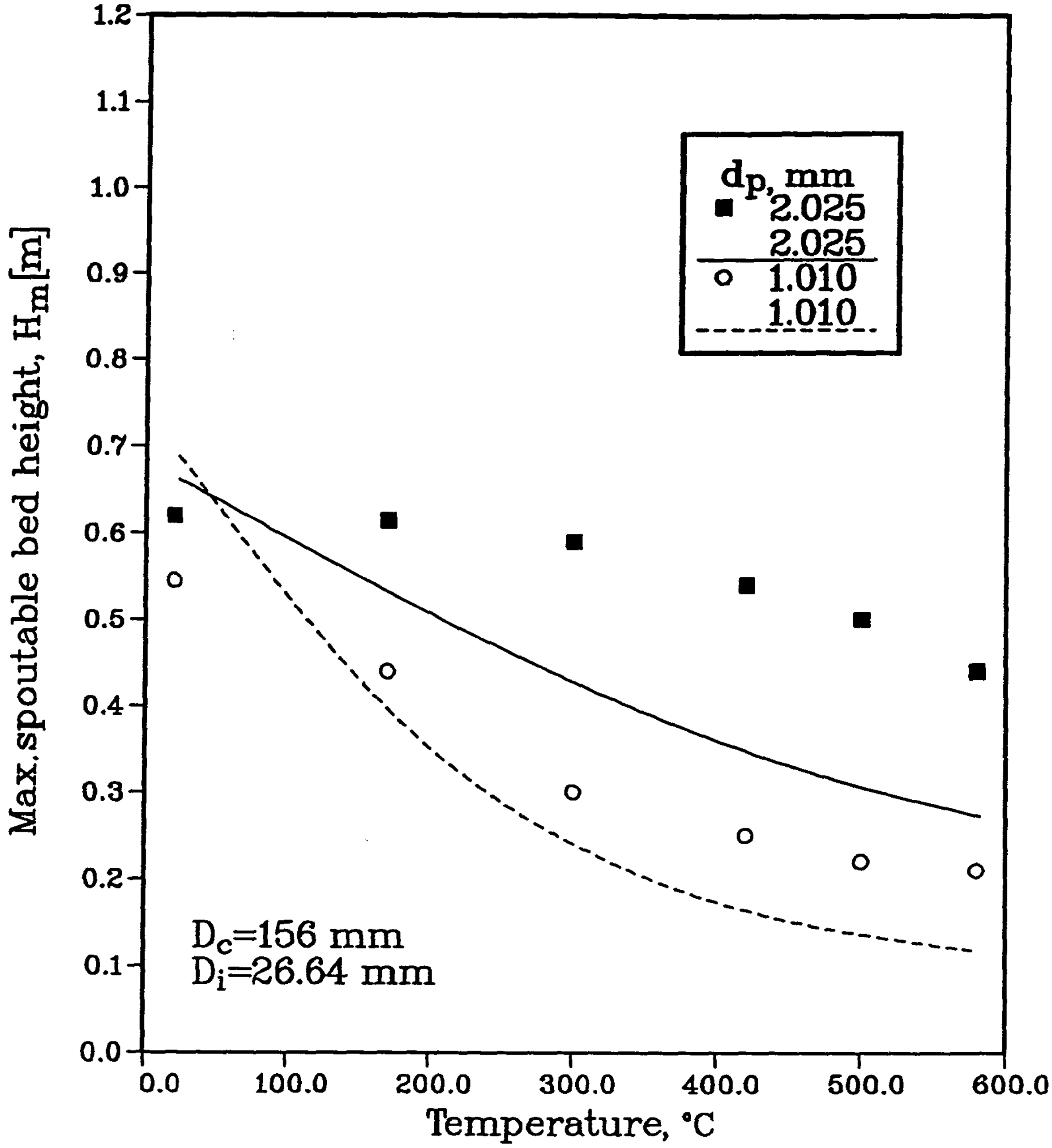

Figure 6.28: Effect of temperature on H_m. Points represent experimental data, lines represent McNab - Bridgwater equation. (D_c=156 mm, D_i=26.64 mm)

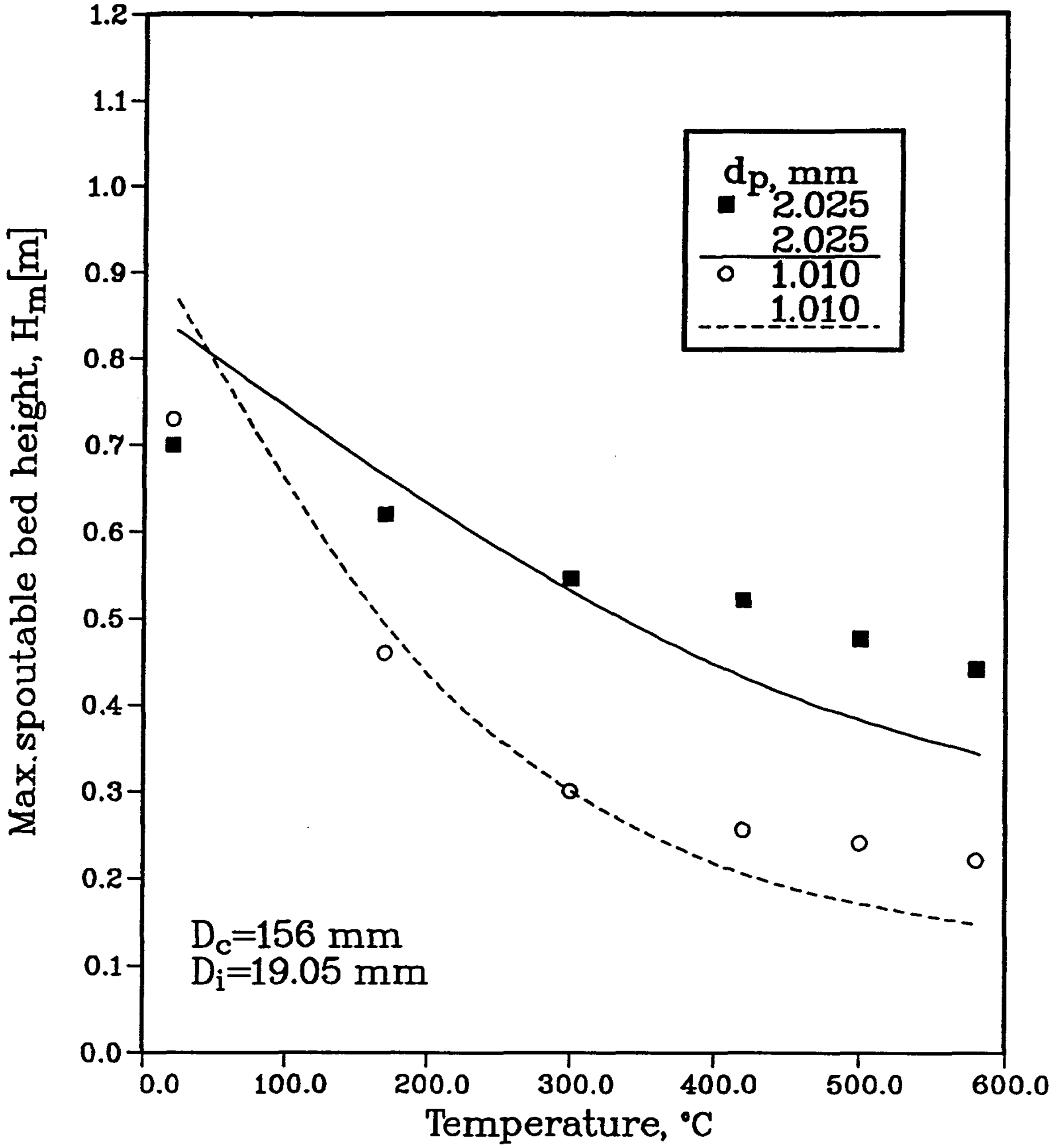

Figure 6.29: Effect of temperature on H_m. Points represent experimental data, lines represent McNab - Bridgwater equation. (D_c=156 mm, D_i=19.05 mm)

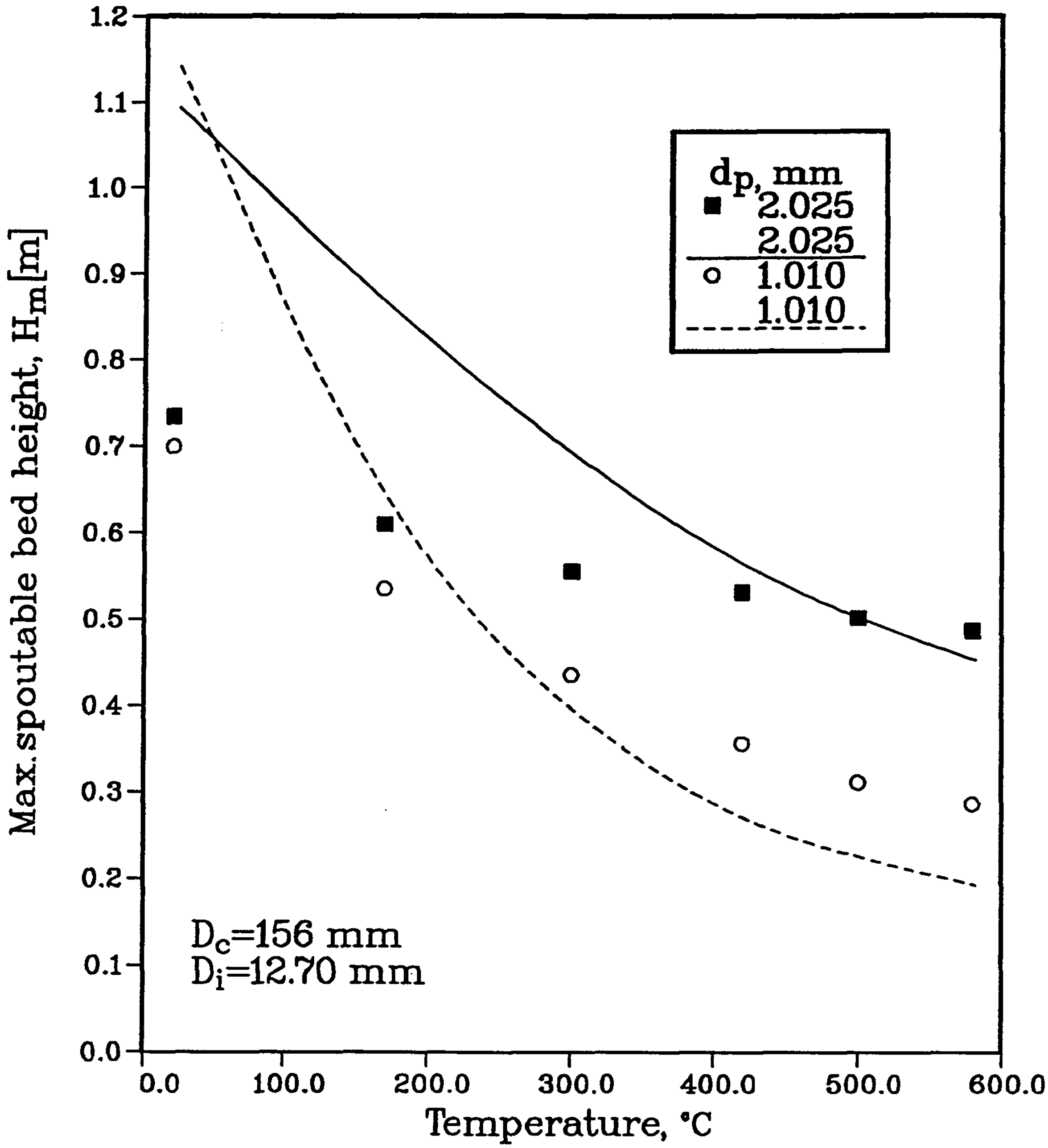

Figure 6.30: Effect of temperature on H_m. Points represent experimental data, lines represent McNab - Bridgwater equation. (D_c=156 mm, D_i=12.70 mm)

Chapter 7

Results: Average Spout Diameter

From visual observations in the experiments, the spout diameter expanded and then converged slightly in the conical region . Above the conical region, the spout diameter remained constant but diverged near the bed surface. The average spout diameter was determined using Eq.(4.26). As mentioned earlier, all D_s values were obtained at the condition $U/U_{ms} = 1.05$.

7.1 Effect of Bed Temperature on D_s

Basically the temperature had an almost negligible effect on the average spout diameter, as shown in Figures 7.31 and 7.32. This result was generally in agreement with the prediction of Wu *et al.* [39], Equation (2.23), but contradicted that of McNab [50], Equation (2.22), which predicts that D_s decreases with increasing temperature. The Wu *et al.* equation also gave better absolute prediction than the McNab equation, especially at elevated bed temperatures, where the latter consistently underpredicted D_s.

7.2 Effect of Bed Height on D_s

Average spout diameter was found to change with bed height. As shown in Figure 7.33, bed height had a large effect on the value of D_s. At the high bed temperatures, the spout diameter increased with increase of bed level, while at some of the lower temperatures, the spout diameter first decreased slightly with increasing bed level and then increased.

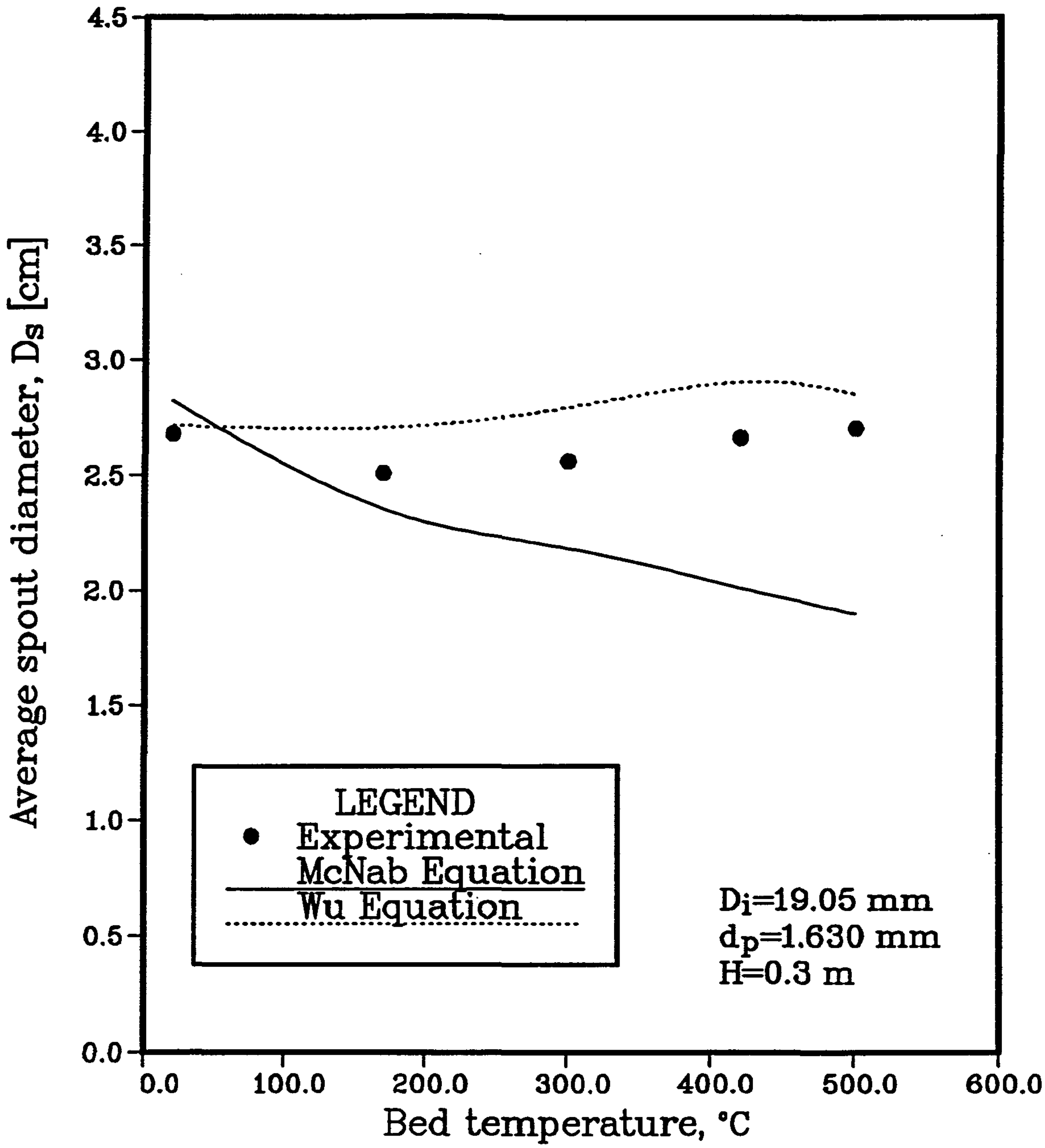

Figure 7.31: Effect of temperature on D_s. (D_c=156 mm, D_i=19.05 mm, d_p=1.630 mm)

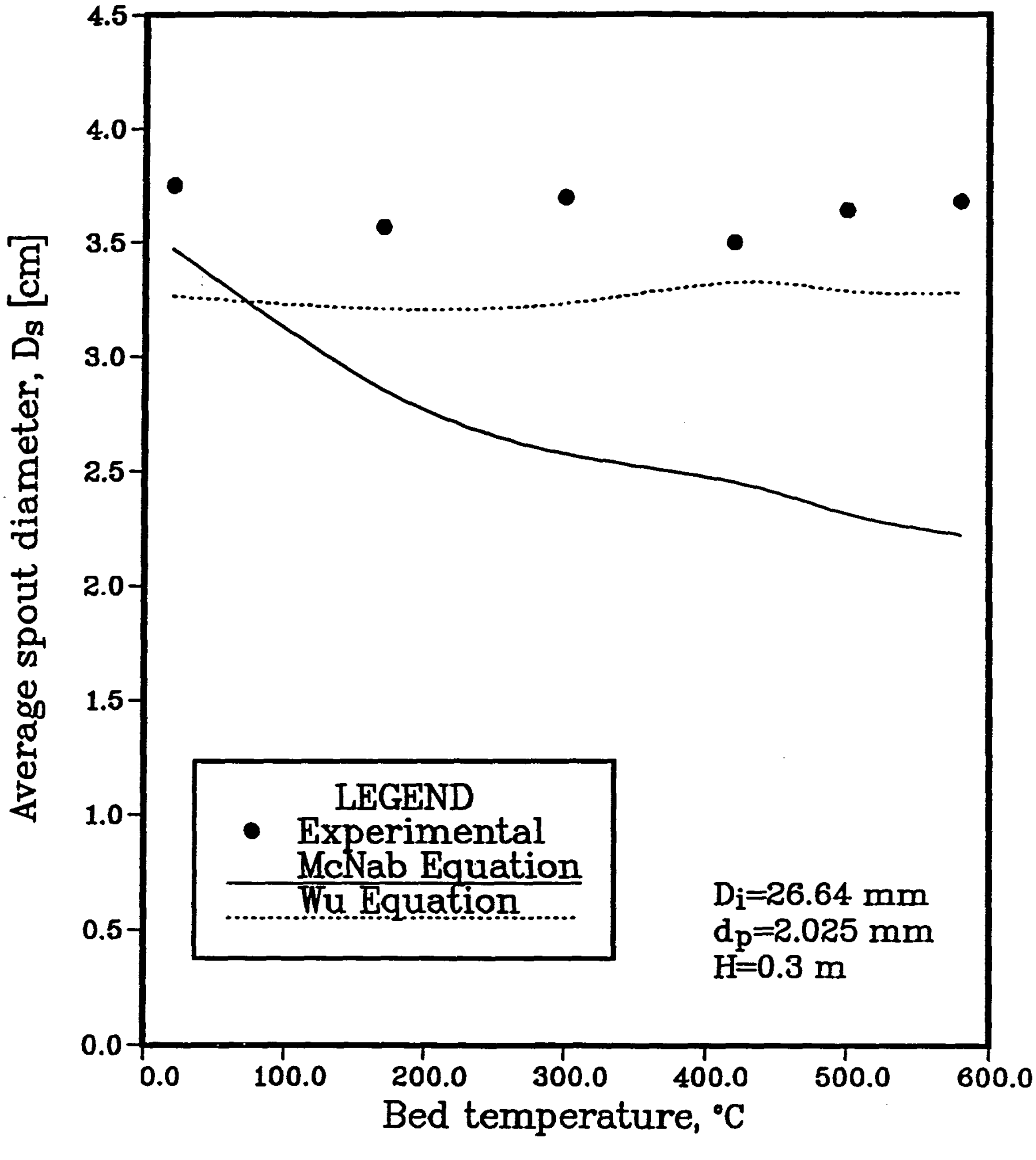

Figure 7.32: Effect of temperature on D_s. (D_c=156 mm, D_i=26.64 mm, d_p=2.025 mm)

At the high bed temperatures the spout diameter diverged continuously, as per spout shape (a) of Mathur and Epstein [1], while at the lower temperatures the spout diameter followed their undulating spout shape (e), except that it necked only once rather than twice. The spout shape and change of spout diameter in the vicinity of the gas inlet is a matter of importance since it directly affects the longitudinal profile of gas velocity in the spout, and consequently also influences particle velocity and voidage profiles.

7.3 Comparison with Existing Correlations

Two empirical equations for D_s were compared with all the experimental data. One was that of McNab [50], Equation (2.22), while the other was that of Wu *et al.* [39], Equation (2.23). Parity plots comparing the experimental values with the calculated values are given in Figures 7.34 and 7.35. In Figure 7.34, the predicted values by the McNab equation almost matched the experimental values in the temperature range $20 - 170°C$, but at the higher temperatures, the experimental values were consistently underpredicted by this equation (overall $RMS = 24.4\%$). Figure 7.35, in contrast, shows that calculated spout diameters using the Wu equation were very close to the experimental values at all temperature levels ($RMS = 10.4\%$). Both the experimental values and the calculated values, together with their percentage errors, are listed in Appendix G. The superiority of the Wu *et al.* equation over that of McNab apparently arises from the fact that the former, unlike the latter, explicitly includes the effect of gas density and gas viscosity, hence of gas temperature.

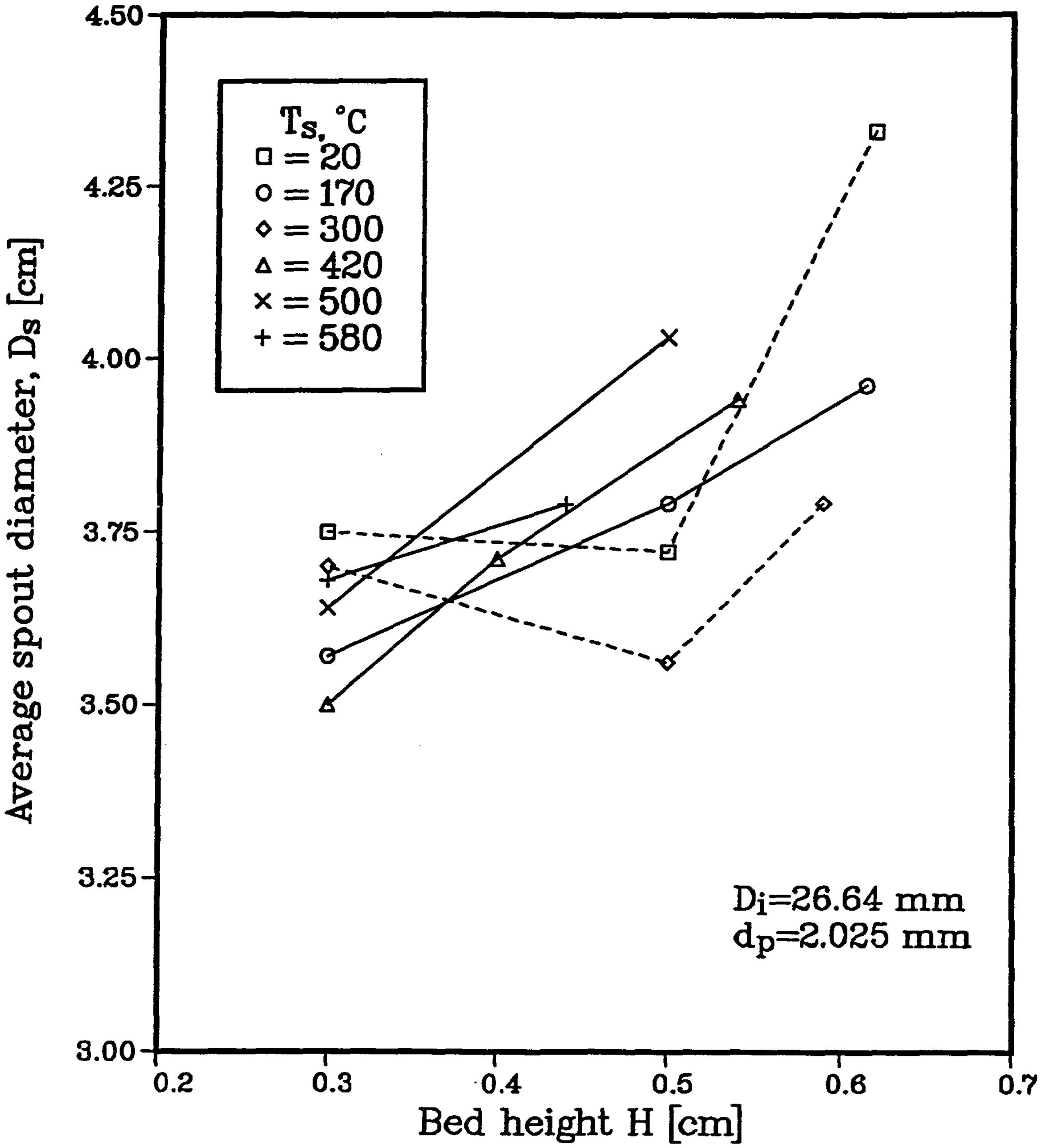

Figure 7.33: Effect of bed height on D_s. (D_c=156 mm, D_i=26.64 mm, d_p=2.025 mm)

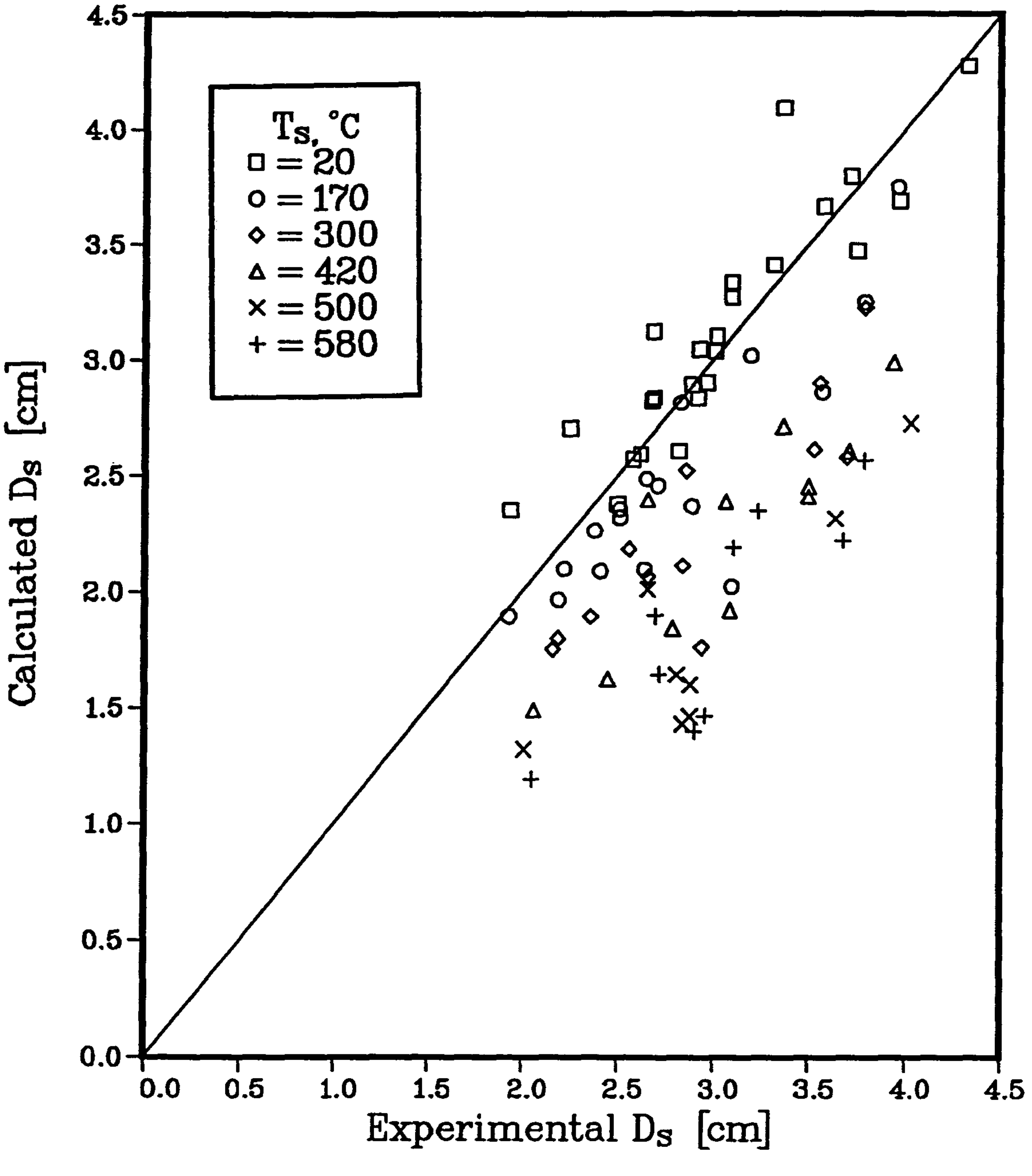

Figure 7.34: Comparison of D_s measured experimentally with D_s predicted by McNab equation. (D_c=156 mm)

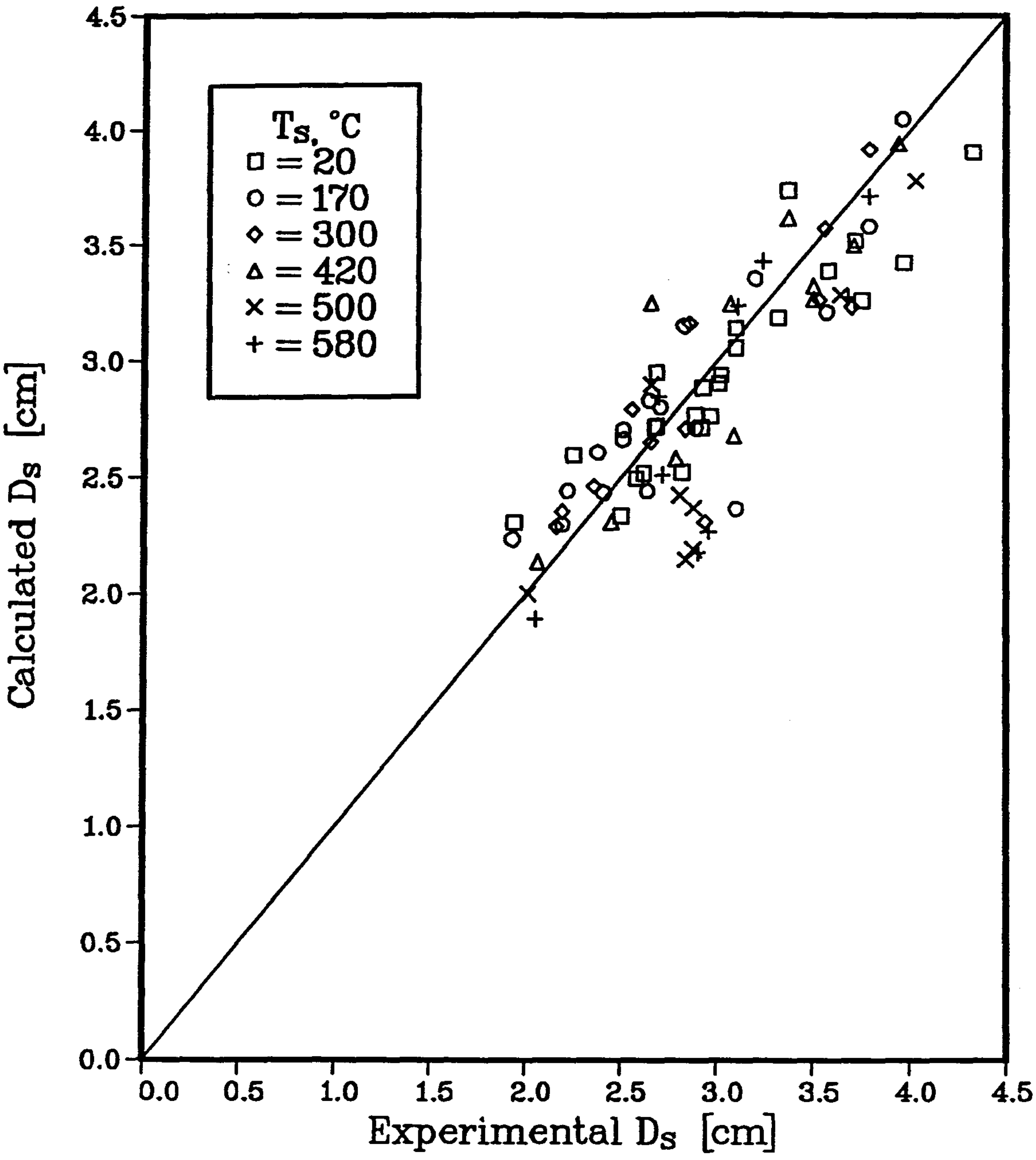

Figure 7.35: Comparison of D_s measured experimentally with D_s predicted by Wu *et al.* equation. (D_c=156 mm)

Chapter 8

Conclusions

1. Generally the value of U_{ms} is more difficult to obtain at high temperature than at room temperature, partly because spouting becomes less stable at high temperature but also because of increased measurement difficulties at elevated temperatures.

2. Minimum spouting velocity U_{ms} increases with particle diameter for a fixed orifice diameter, at any given bed height. This observation is consistent with the empirical equation of Mathur and Gishler, Equation (2.1).

3. There is no consistent trend of U_{ms} with orifice diameter, showing that the Mathur - Gishler equation might not be suitable for predicting U_{ms} at all temperature levels for different particles.

4. When the bed temperature is raised, U_{ms} increases, primarily because of the corresponding decrease in spouting gas density. Temperature has a larger effect on the U_{ms} of large particles than on that of small particles, possibly because viscous as opposed to inertial forces become more dominant for the latter.

5. U_{ms} always increases with H and the temperature effect on U_{ms} increases as H increases.

6. A best fit U_{ms} correlation is obtained by including the free settling velocity, U_t, of the particles, which largely accounts for fluid and particle properties. U_t is found to be better than U_{mf} as a correlating parameter for U_{ms}.

7. The best fit equation for U_{ms} and its root mean square error is:

$$Re_{ms} = \phi(Ar) \times 1.63 \left(\frac{D_i}{D_c}\right)^{0.541} \left(\frac{H}{D_c}\right)^{0.452} \left(\frac{D_i}{d_p}\right)^{-0.414} \left(\frac{\rho_p - \rho_f}{\rho_f}\right)^{-0.149} \quad \pm\ 7.43\% \qquad (5.75)$$

where $\phi(Ar) = Re_t$. Equation (5.75) shows considerably smaller average and RMS errors than the Grbavcic equation, which gives a better overall fit than that of Wu *et al.*, which in turn is slightly better than that of Mathur and Gishler.

8. The McNab - Bridgwater equation with $b_1 = 1.11$ overpredicts H_m significantly at room temperatures and underpredicts H_m slightly at high temperatures. The same equation with $b_1 = 1.04$ gives better overall agreement with the experimental data.

9. There exists a critical value of d_p at which H_m achieves a maximum as d_p is increased for a fixed column geometry and fixed fluid and particle properties. The higher the temperature, the larger this value is.

10. Temperature has an almost negligible effect on the average spout diameter. At high bed temperatures, the spout diameter increases with increase of bed height, while at lower temperatures, the spout diameter sometimes first decreases slightly with increasing bed height before it increases.

11. The Wu *et al.* equation gives better absolute prediction of D_s than does the McNab equation, especially at elevated bed temperatures, where the latter consistently underpredicts D_s. This is attributed to the fact that the Wu *et al.* equation explicitly includes the effect of gas density and gas viscosity, hence of gas temperature.

Notation

A	Ratio given by Equation (2.15)	(–)
A_1	Cross-sectional area of the rotameter tube	(m^2)
A_2	Area of annulus between the float and tube	(m^2)
A_c	Cross-sectional area of the column	(m^2)
A_F	Maximum cross-sectional area of the float	(m^2)
Ar	Archimedes number, $\frac{d_p^3(\rho_p-\rho_f)\rho_f g}{\mu^2}$	(–)
a_s	Ratio of spout area to column area	(–)
b	Value of exponent on H_m in equation for U_{ms}	(–)
b_1	U_m/U_{mf}	(–)
C_D	Drag coefficient	(–)
CAL	Predicted value	(–)
D_c	Inside diameter of column	(m)
D_i	Diameter of inlet orifice	(m)
D_s	Mean spout diameter	(m)
$D_s(z)$	Local spout diameter	(m)
d_p	Reciprocal mean diameter of particles	(m)
$(d_p)_{crit}$	Value of d_p at which H_m is a maximum	(m)
EXP	Experimental value	(–)
f	Friction factor	(–)
f_1	$150(1-\epsilon_a)^2\mu/d_p^2\epsilon_a^3$	(kg/m^3s)
f_2	$1.75(1-\epsilon_a)\rho_f/d_p\epsilon_a^3$	(kg/m^4)
G	Mass flowrate of gas	(kg/s)
g	Acceleration due to gravity	(m/s^2)

H	Static bed height	(m)
H_m	Maximum spoutable bed depth	(m)
h	H/H_m	(–)
k	Constant in Equation (2.2)	(–)
M	Number of data points	(–)
N_D	Best number, $\frac{4}{3}\ Ar$	(–)
n	Number of particles accelerated per unit time	(–)
P_{atm}	Atmospheric pressure	(Pa)
P_B	Absolute pressure measured just below inlet orifice with solids in the bed	(Pa)
P_E	Absolute pressure measured just below inlet orifice without solids in the bed	(Pa)
P_g	Gauge pressure upstream of rotameter	(Pa)
P_M	Absolute pressure of the gas meter	(Pa)
P_R	Absolute pressure of the rotameter	(Pa)
P_S	Absolute pressure in the bed	(Pa)
P_{STD}	1 *atm*	(Pa)
Q_s	Volumetric flowrate in the spout	(m^3/s)
R	Rotameter reading	(–)
T_R	Temperature of the rotameter	(° C)
T_S	Temperature of the spouted bed	(° C)
U_a	Superficial gas velocity in the annulus	(m/s)
U_m	Minimum superficial spouting velocity at H_m	(m/s)
U_{mf}	Minimum superficial fluidization velocity	(m/s)
U_{mi}	Minimum gas inlet velocity for spouting	(m/s)

U_{ms}	Minimum superficial spouting velocity	(m/s)
U_s	Superficial gas velocity	(m/s)
U_t	Free settling terminal velocity of the particles	(m/s)
V_F	Volume of the float	(m^3)
V_M	Measurement volumetric flowrate of the gas meter	(m^3/s)
V_S	Volumetric flowrate through the spouted bed	(m^3/s)
V_{STD}	Volumetric flowrate taken from the calibration curves	(m^3/s)
W	$log_{10}\ N_D$	(–)
x_i	Weight fraction of particles	(–)
z	Vertical distance from inlet orifice	(m)

$\triangle P_a$	Measured pressure drop above the orifice	(Pa)
$\triangle P_f$	Pressure drop across bed of particles at minimum fluidization	(Pa)
$\triangle P_{ms}$	Overall pressure drop at minimum spouting condition	(Pa)
$\triangle P_s$	Overall spouting pressure drop	(Pa)
γ	Angle of repose of solids	(–)
ϵ	Overall voidage of the bed	(–)
ϵ_{mf}	Voidage at minimum fluidization	(–)
λ	Reciprocal of sphericity	(–)
μ	Fluid viscosity	(kg/m·s)
ρ_b	Bulk density of particles	(kg/m^3)
ρ_F	Density of the rotameter float	(kg/m^3)
ρ_f	Fluid density	(kg/m^3)

ρ_p	Particle density	(kg/m^3)
ϕ	Particle sphericity	(–)
ψ	Net downward force of solids per unit volume	$(kg/m^2 \cdot s^2)$

Bibliography

[1] Mathur, K. B. and Epstein, N., "Spouted Beds", Academic Press, N.Y. (1974).

[2] Epstein, N. and Grace, J. R., "Spouting of Particulate Solids", Chapter 11 in 'Handbook of Powder Science and Technology', Fayed, M. E. and Otten, L., eds., Van Nostrand Reinhold Co., New York (1984).

[3] Bridgwater, J., "Fluidization", 2nd ed., Chapter 6, ed. J. F. Davidson, R. Clift and D. Harrison, London (1985).

[4] Barton, R. K. , Rigby, G. R. and Ratcliffe, J. S., "The Use of a Spouted Bed for the Low Temperature Carbonization of Coal", *Mechanical and Chemical Eng. Trans.*, **4**, 105 (May 1968).

[5] Barton, R. K. and Ratcliffe, J. S., "The Rates of Devolatilation of Coal under Spouted Bed Conditions", *Mechanical and Chemical Eng. Trans.*, **5**, 35 (May 1969).

[6] Ratcliffe, J. S. and Rigby, G. R., "Low Temperature Carbonization of Coal in a Spouted Bed – Prediction of Exit Char Volatile Matter", *Mechanical and Chemical Eng. Trans.*, **5**, 1 (May 1969).

[7] Foong, S. K., Lim, C. J. and Watkinson, A. P., "Coal Gasification in a Spouted Bed", *Can. J. Chem. Eng.*, **58**, 84 (1980).

[8] Foong, S. K., Cheng, G. and Watkinson, A. P., "Spouted Bed Gasification of Western Canadian Coals", *Can. J. Chem. Eng.*, **59**, 625 (1981).

[9] Foong, S. K., Barton, R. K. and Ratcliffe, J. S., "Characteristics of Multiple Spouted Beds", *Mechanical and Chemical Eng. Trans., Instn. Engrs. Australia*, MCII (1, 2), 7 (1975).

[10] Watkinson, A. P., Cheng, G. and Prakash, C. B., "Comparison of Coal Gasification in Fluidized and Spouted Beds", *Can. J. Chem. Eng.*, **61**, 468 (1983).

[11] Lim, C. J., Barua, S. K., Epstein, N., Grace, J. R. and Watkinson, A. P., "Spouted Bed and Spout-Fluid Bed Combustion of Solid Fuels", *Proc. Inst. Energy Symp. on Fluidized Combustion*, **1**, DISC/10/72, London, U. K., 72 (1984).

[12] Ingle, A. N. and Sarkar, S., "Gasification of Coal in Spouted-Bed", *Indian J. Technol.*, **14**, 515 (1976).

[13] Ray, T.B. and Sarkar, S., "Kinetics of Coal Pyrolysis in Spouted Bed", *Indian Chemical Engineer*, **18(2)**, 11 (1976).

[14] Jarallah, A., and Watkinson, A. P., "Pyrolysis of Western Canadian Coals in a Spouted-Bed", *Can. J. Chem. Eng.*, **63**, 227 (1985).

[15] Khoshnoodi, M. and Weinberg, F. J., "Combustion in Spouted Beds", *Combustion and Flame*, The Combustion Inst., **33**, 11 (1978).

[16] Arbib, H. A., Sawyer, R. F. and Weinberg, F. J., "The Combustion Characteristics of Spouted Beds", *Proc. 18th Internation Symp. on Combustion*, The Combustion Institute, 233 (1981).

[17] Arbib, H. A. and Levy, A., "Combustion of Low Heating Value Fuels and Wastes in the Spouted Bed", *Can. J. Chem. Eng.*, **60**, 528 (1982a)

[18] Arbib, H. A. and Levy, A., "The Reverse-Flow Spouted Bed Combustor", *Combustion Science and Technology*, **29**, 83 (1982b).

[19] Khoe, G. K., and Weve, D., "Visual Observations of Spouted Bed Gas Combustion Models and Their Flow Regimes", *Can. J. Chem. Eng.*, **61**, 460 (1983).

[20] Zhao, J., "Coal Combustion in Spouted and Spout-fluid Beds", M. A. Sc. Thesis, University of British Columbia, Vancouver, Canada (1986).

[21] Ye, Bogang, "Combustion Performance and High Temperature Hydrodynamics in a Spouted and Spout-fluid Bed", M. A. Sc. Thesis, University of British Columbia, Vancouver, Canada (1988).

[22] Wu, Stanley, "Hydrodynamics of Gas Spouting at High Temperature", M. A. Sc. Thesis, University of British Columbia, Vancouver, Canada (1986).

[23] Chandnani, P. P., "Gas Spouting of Fine Particles", M. A. Sc. Thesis, University of British Columbia, Vancouver, Canada (1984).

[24] Mathur, K. B. and Gishler, P. E., "A Technique for Contacting Gases with Solid Particles", *AIChE J.*, **1**, 157 (1955).

[25] Fane, A. G. and Mitchell, R. A. , "Minimum Spouting Velocity of Scaled–up Beds", *Can. J. Chem. Eng.*, **62**, 437 (1984).

[26] Charlton, B. G., Morris, J. B., and Williams, G. H., " An Experimental Study of Spouting Beds of Spheres", Rep. Mo. AERE-R4852, U. K. Atomic Energy Authority, Harwell (1965).

[27] Lim, C. J. and Grace, J. R., "Spouted Bed Hydrodynamics in a 0.91 m Diameter Vessel", *Can. J. Chem. Eng.*, **65**, 366 (1987).

[28] He, Yanlong, "Spouted Bed and Spout-fluid Bed Hydrodynamics in a 0.91 m Diameter Vessel", M. A. Sc. Thesis, University of British Columbia, Vancouver, Canada (1990).

[29] Ghosh, B., "A Study on the Spouted Bed, Part I: A Theoretical Analysis", *Indian Chem. Eng.*, **56**, 353 (1978).

[30] Green, M. C. and Bridgwater, J., "An Experimental Study of Spouting in Large Sector Beds", *Can. J. Chem. Eng.*, **61**, 281 (1983).

[31] Mamuro, T. and Hattori, H., "Flow Pattern of Fluid in Spouted Beds", *J. Chem. Eng. Japan*, **1**, 1 (1968); correction, *J. Chem. Eng. Japan*, **3**, 119 (1970).

[32] Grbavčić, Z. B., Vuković D. V., Zdanski, F. K. and Littman, H., "Fluid Flow Pattern, Minimum Spouting Velocity and Pressure Drop in Spouted Beds", *Can. J. Chem. Eng.*, **54**, 33 (1976).

[33] Thorley, B., Saunby, J. B., Mathur, K. B. and Osberg, G. L., "An Analysis of Air and Solid Flow in A Spouted Wheat Bed", *Can. J. Chem. Eng.*, **37**, 184 (1959).

[34] Buchanan, R. H. and Manurung, F., "Spouted Bed Low-temperature Carbonization of Coal", *Brit. Chem. Eng.*, **6**, 402 (1961).

[35] Smith, J. W. and Reddy, K. V. S., "Spouting of Mixed Particle-size Beds", *Can. J. Chem. Eng.*, **42**, 206 (1964).

[36] Manurung, F., "Studies in the Spouted Bed Technique with Particular Reference to Low Temperture Coal Carbonization", Ph.D. Thesis, University of New South Wales, Kensington, Australia (1964).

[37] Cowan, C. B., Peterson, W. S. and Osberg, G. L., "Spouting of Large Particles", *Eng. Journal (Canada)*, **41**, 60 (1958).

[38] Madonna, L. A., Lama, R. F. and Brisson, W. L., "Solids-air Jets", *Brit. Chem. Eng.*, **6**, 524 (1961).

[39] Wu, S. W. M., Lim, C. J. and Epstein, N., "Hydrodynamics of Spouted Beds at Elevated Temperatures", *Chem. Eng. Comm.*, **62**, 251 (1987).

[40] Nakamura, M., Hamada, Y. and Toyama, S., "An Experimental Investigation of Minimum Fluidization Velocity at Elevated Temperatures and Pressures", *Can.J.Chem.Eng*, **63**, 8 (1985).

[41] Becker, H. A., "An Investigation of Laws Governing the Spouting of Coarse Particles", *Chem. Eng. Sci.*, **13**, 245 (1961).

[42] Ergun, S., "Fluid Flow Through Packed Columns", *Chem. Eng. Progr.*, **48**, No.2, 89 (1952).

[43] Wen, C. Y. and Yu, Y. H., "A General Method for Predicting the Minimum Fluidization Velocity", *AIChE J.*, **12**, 610 (1966).

[44] McNab, G. S. and Bridgwater, J., "Spouted Beds—Estimation of Spouting Pressure Drop and the Particle Size for Deepest Bed", *Proc. European Congress on Particle Technology*, Nuremberg (1977).

[45] Thorley, B., Saunby, J. B., Mathur, K. B. and Osberg, G. L.,"An Analysis of Air and Solid Flow in a Spouted Wheat Bed", *Can. J. Chem. Eng.*, **37**, 184 (1959).

[46] Malek, M. A. and Lu, B. C. Y., "Pressure Drop and Spouted Bed Height in Spouted Beds", *Ind. Eng. Chem. Process Des. Develop*, **4**, 123 (1965).

[47] Lefroy, G. A. and Davidson, J. F., "The Mechanics of Spouted Beds", *Trans. Inst. Chem. Eng.*, **47**, T120 (1969).

[48] Littman, H., Morgan III, M. H., Vukovic, D. V., Zdanski, F. K. and Grbavcic, Z. B., "A Theory for Predicting the Maximum Spouting Height in a Spouted Bed", *Can. J. Chem. Eng.*, **55**, 497 (1977).

[49] Littman, H., Morgan III, M. H., Vukovic, D. V., Zdanski, F. K. and Grbavcic, Z. B., "Prediction of the Maximum Spoutable Height and the Average Spout to Inlet Tube Diameter Ratio in Spouted Beds of Spherical Particles", *Can. J. Chem. Eng.*, **57**, 684 (1979).

[50] McNab, G. S.,"Prediction of Spout Diameter", *Brit. Chem. Eng. and Proc. Technol.*, **17**, 532 (1972).

[51] Bridgwater, J. and Mathur, K. B., "Prediction of Spout Diameter in a Spouted Bed—A Theoretical Model", *Powder Technol.*, **6**, 183 (1972).

[52] McNab, G. S. and Bridgwater, J., "The Application of Soil Mechanics to Spouted Bed Design", *Can. J. Chem. Eng.*, **52**, 162 (1974).

[53] Littman, H., "The Measurement and Prediction of the Maximum Spoutable Height, Spout Diameter, Minimum Spouting Velocity and Pressure Drop at Minimum Spouting In Spouted Beds", Lecture Notes for C.S.Ch.E. Continuing Education Course on Spouted Beds, Vancouver, 1982.

[54] Krzywanski, R. S., Epstein, N. and Bowen, B. D., "Spout Diameter Variation in Two-dimensional and Cylindrical Spouted Beds: A Theoretical Model and its Verification", *Chem. Eng. Sci.*, **44**, 1617 (1989).

[55] Epstein, N. and Levine, S., "Non-Darcy Flow and Pressure Distribution in a Spouted Bed", Fluidization, *Proc. Second Engineering Foundation Conference on Fluidization*, Davidson, J. F. and Keairns, D. L., eds., p.98, Cambridge Univ. Press (April 1978).

[56] Morgan, M. H. and Littman, H., "General Relationships for the Minimum Spouting Pressure Drop Ratio, $\Delta P_{ms}/\Delta P_{mF}$, and the Spout-Annular Interfacial Condition in a Spouted Bed", in 'Fluidization', *Proc. 3rd Engng. Found. Conf.*, Henniker, Grace, J. R. and Matsen, J. M., eds., p.287, Plenum Press, New York (1980).

[57] Pattipati, R. R. and Wen, C. Y., "Minimum Fluidization Velocity at High Temperatures", *Ind. Eng. Chem. Process Des. Dev.*, **20**, 705 (1981).

[58] Whiting, K. J. and Geldart, D., "A Comparison of Cylindrical and Semi-cylindrical Spouted Beds of Coarse Particles", *Chem. Eng. Sci.*, **35**, 1499 (1980).

[59] Geldart, D., Hemsworth, A., Sundavadra, R. and Whiting, K. J., "A Comparison of Spouting and Jetting in Round and Half-round Fluidized Beds", *Can. J. Chem. Eng.*, **59**, 638 (1981).

[60] Lim, C. J., "Gas Residence Time Distribution and Related Flow Patterns in Spouted Beds", Ph.D. Thesis, University of British Columbia, Vancouver, Canada (1975).

[61] Oman, A. O. and Watson, K. M., "Pressure Drop in Granular Beds", *Refinery Management and Petroleum Chem. Tech.*, **36**, R-795 (November 1, 1944).

[62] Clift, R., Grace, J. R. and Weber, W. E., "Bubbles, Drops, and Particles", Academic Press, N.Y. (1978).

[63] Nicol, T., "Integration of Unequally Spaced Data Points", *UBC QINT4P*, University of British Columbia, Vancouver, Canada (1976).

[64] Grace, J. R., "Fluidized-bed Hydrodynamics", Chapter 8.1 in 'Handbook of Multiphase Systems', Hetsroni, M., ed., Hemisphere - McGraw - Hill, New York (1982).

Appendix A

Calibration of Rotameters

For a rotameter, the governing equation is:

$$G = C_D A_2 \left[\frac{2gV_F(\rho_F - \rho_f)\rho_f}{A_F[1-(A_2/A_1)^2]} \right]^{\frac{1}{2}} \tag{A.83}$$

The coefficient C_D depends on the shape of the float and the Reynolds number for flow through the annular space of area A_2. If the float is kept at a fixed vertical position, C_D can be assumed constant. For a specific rotameter, the only independent variable is then the fluid density. Equation (A.83) then becomes in the case of a gas flow,

$$G = B_1 \sqrt{\rho_f} \tag{A.84}$$

Figure A.36 is a simple flow sheet of the rotameter calibration set-up. If the ideal gas law is assumed, and $T_M = T_R = 20°C$, then

$$V_R = V_M \left[\frac{P_M}{P_R} \right] \tag{A.85}$$

and

$$G = G_R = \rho_R V_R = \rho_R V_M \left[\frac{P_M}{P_R} \right] \tag{A.86}$$

where the subscripts M and R refers to gas meter and rotameter, respectively, and $\rho_R = \rho_f$, the fluid density in the rotameter. Combining Equations (A.84) and (A.86) yields

$$B_1 = V_M \left[\frac{P_M}{P_R} \right] \sqrt{\rho_R} \tag{A.87}$$

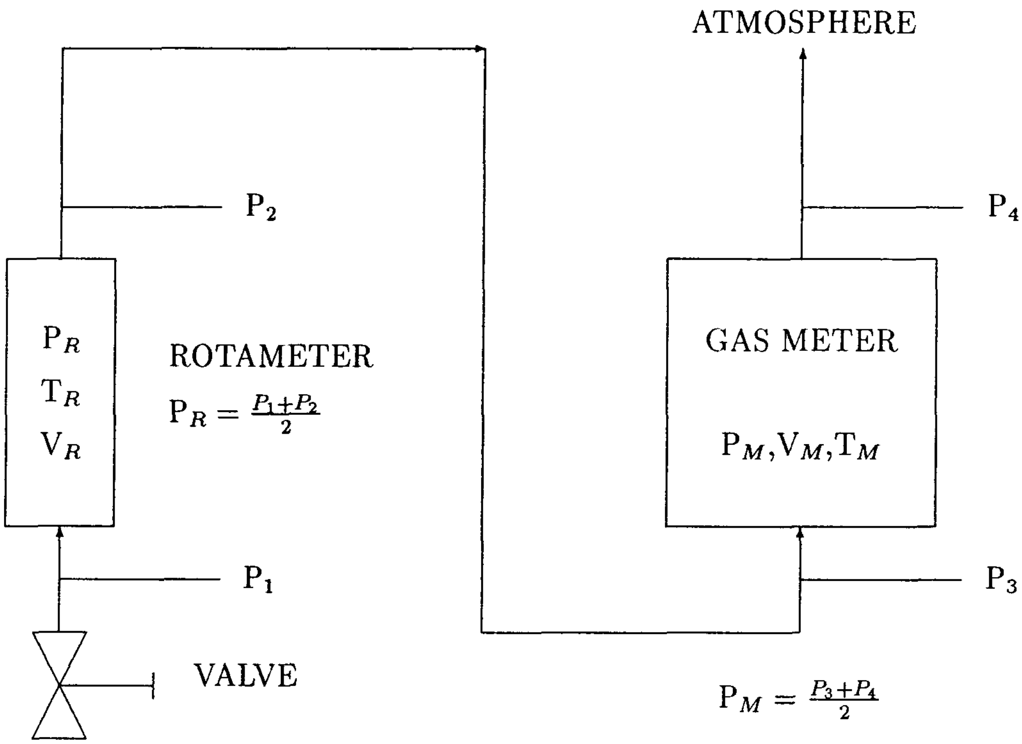

Figure A.36: Schematic set-up for rotameter calibration.

A standard condition of $P = 1\ atm$ and $T = 20°C$ was chosen. Substituting Eq. (A.87) into Eq. (A.84) gives

$$G_{STD} = \left[V_M \left[\frac{P_M}{P_R}\right] \sqrt{\rho_R}\right] \sqrt{\rho_{STD}} \tag{A.88}$$

and

$$V_{STD} = \frac{G_{STD}}{\rho_{STD}} = V_M \left[\frac{P_M}{P_R}\right] \sqrt{\frac{\rho_R}{\rho_{STD}}} \tag{A.89}$$

For an ideal gas,

$$\frac{\rho_R}{\rho_{STD}} = \frac{P_R}{P_{STD}} \tag{A.90}$$

Substituting this relation into Eq. (A.89) gives

$$V_{STD} = V_M \left[\frac{P_M}{\sqrt{P_R P_{STD}}}\right] \tag{A.91}$$

Using Equation (A.91), the two calibration curves which follow were produced by Wu [22]. These curves were checked against a gas meter and found to be accurate.

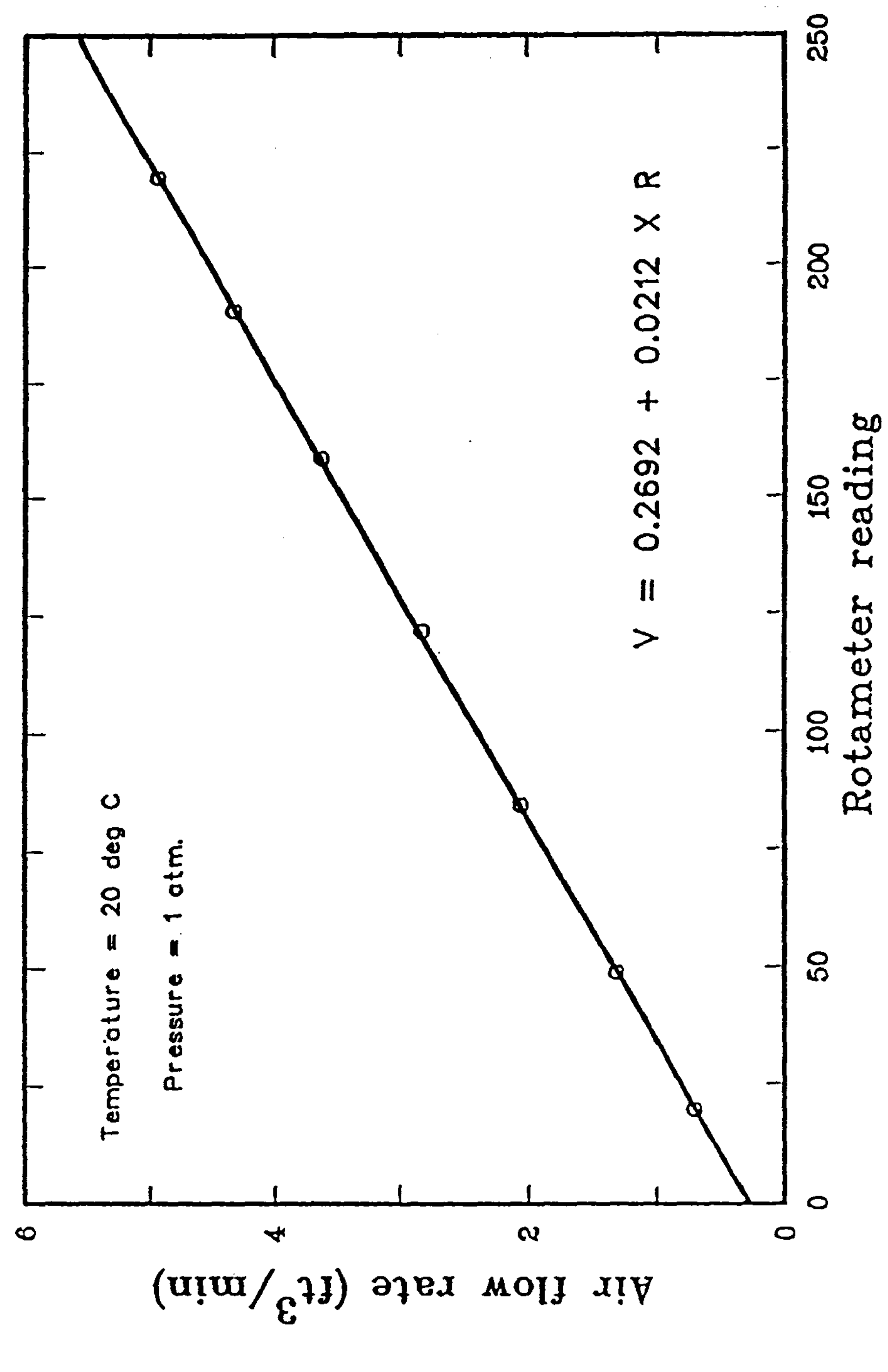

Figure A.37: Calibration curve (small rotameter).

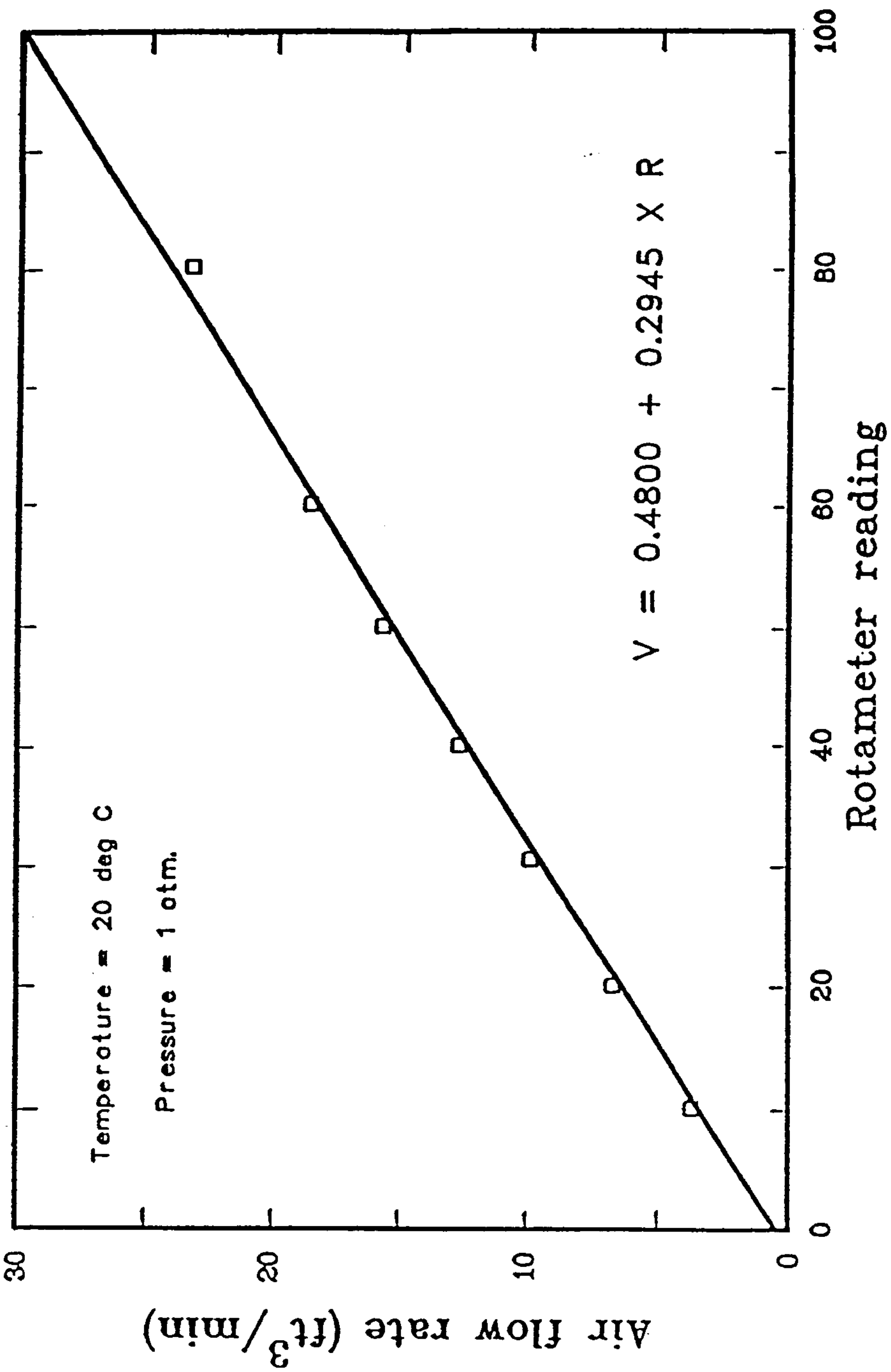

Figure A.38: Calibration curve (large rotameter).

Appendix B

Derivation of the Expression for $\frac{dH_m}{dAr}$

The McNab and Bridgwater Equation for predicting H_m is:

$$H_m = \left[\frac{D_c^2}{d_p}\right]\left[\frac{D_c}{D_i}\right]^{2/3}\left[\frac{568b_1^2}{Ar}\right](\sqrt{1+35.9\times 10^{-6}Ar}-1)^2 \tag{2.10}$$

The above equation can be rewritten as

$$H_m = C_1\left[\sqrt{\frac{1}{Ar}+35.9\times 10^{-6}}-\sqrt{\frac{1}{Ar}}\right]^2 \tag{B.92}$$

whence

$$\begin{aligned}\frac{dH_m}{dAr} &= 2C_1\left[\sqrt{\frac{1}{Ar}+35.9\times 10^{-6}}-\sqrt{\frac{1}{Ar}}\right]\\ &\times\left[\frac{1}{2\sqrt{\frac{1}{Ar}+35.9\times 10^{-6}}}\left(-\frac{1}{Ar^2}\right)-\frac{1}{2\sqrt{\frac{1}{Ar}}}\left(-\frac{1}{Ar^2}\right)\right]\\ &= C_1\left[\sqrt{\frac{1}{Ar}+35.9\times 10^{-6}}-\sqrt{\frac{1}{Ar}}\right]\\ &\times\left(\frac{\sqrt{Ar}}{Ar^2}-\frac{1}{Ar^2}\frac{Ar}{\sqrt{Ar+35.9\times 10^{-6}Ar^2}}\right)\\ &= C_1\left[\sqrt{\frac{1}{Ar}+35.9\times 10^{-6}}-\sqrt{\frac{1}{Ar}}\right]\\ &\times\left(\frac{1}{Ar\sqrt{Ar}}-\frac{1}{Ar\sqrt{Ar+35.9\times 10^{-6}Ar^2}}\right)>0 \quad for \quad Ar>0\end{aligned} \tag{B.93}$$

Appendix C

Experimental Conditions

Run No.	D_i (mm)	d_p (mm)	T($^\circ C$)
1	19.05	2.025	20
2	19.05	2.025	170
3	19.05	2.025	300
4	19.05	2.025	420
5	19.05	2.025	500
6	19.05	2.025	580
7	19.05	1.630	20
8	19.05	1.630	170
9	19.05	1.630	300
10	19.05	1.630	420
11	19.05	1.630	500
12	19.05	1.630	580
13	19.05	1.200	20
14	19.05	1.200	170
15	19.05	1.200	300
16	19.05	1.200	420
17	19.05	1.200	500
18	19.05	1.200	580
19	19.05	1.010	20
20	19.05	1.010	170
21	19.05	1.010	300
22	19.05	1.010	420
23	19.05	1.010	500
24	19.05	1.010	580
25	19.05	0.915	20
26*	19.05	0.915	170
27*	19.05	0.915	300
28*	19.05	0.915	420
29*	19.05	0.915	500
30*	19.05	0.915	580
31	26.64	2.025	20
32	26.64	2.025	170
33	26.64	2.025	300
34	26.64	2.025	420

35	26.64	2.025	500
36	26.64	2.025	580
37	26.64	1.630	20
38	26.64	1.630	170
39	26.64	1.630	300
40	26.64	1.630	420
41	26.64	1.630	500
42	26.64	1.630	580
43	26.64	1.200	20
44	26.64	1.200	170
45	26.64	1.200	300
46	26.64	1.200	420
47	26.64	1.200	500
48	26.64	1.200	580
49	26.64	1.010	20
50	26.64	1.010	170
51	26.64	1.010	300
52	26.64	1.010	420
53	26.64	1.010	500
54	26.64	1.010	580
55*	26.64	0.915	20
56*	26.64	0.915	170
57*	26.64	0.915	300
58*	26.64	0.915	420
59*	26.64	0.915	500
60*	26.64	0.915	580
61	12.70	2.025	20
62	12.70	2.025	170
63	12.70	2.025	300
64	12.70	2.025	420
65	12.70	2.025	500
66	12.70	2.025	580
67	12.70	1.630	20
68	12.70	1.630	170
69	12.70	1.630	300
70	12.70	1.630	420
71	12.70	1.630	500
72	12.70	1.630	580
73	12.70	1.200	20
74	12.70	1.200	170
75	12.70	1.200	300
76	12.70	1.200	420
77	12.70	1.200	500
78	12.70	1.200	580
79	12.70	1.010	20
80	12.70	1.010	170
81	12.70	1.010	300

82	12.70	1.010	420
83	12.70	1.010	500
84	12.70	1.010	580
85	12.70	0.915	20
86	12.70	0.915	170
87	12.70	0.915	300
88	12.70	0.915	420
89	12.70	0.915	500
90	12.70	0.915	580

* Scheduled runs which could not spout.

Appendix D

Experimental Data

Run No.	U_{ms} (m/s)	d_p (mm)	D_i (mm)	H (m)	ρ_f (kg/m^3)	μ $(kg/m \cdot s)$
1(7)	1.399	2.025	19.05	0.700*	1.268	0.0000184
	1.164	2.025	19.05	0.600	1.246	0.0000184
	1.036	2.025	19.05	0.500	1.245	0.0000184
	0.950	2.025	19.05	0.400	1.232	0.0000184
	0.886	2.025	19.05	0.300	1.225	0.0000184
	0.794	2.025	19.05	0.200	1.217	0.0000184
	0.408	2.025	19.05	0.100	1.213	0.0000184
2(7)	1.503	2.025	19.05	0.620*	0.834	0.0000248
	1.361	2.025	19.05	0.600	0.829	0.0000248
	1.190	2.025	19.05	0.500	0.823	0.0000248
	1.085	2.025	19.05	0.400	0.817	0.0000248
	0.989	2.025	19.05	0.300	0.812	0.0000248
	0.848	2.025	19.05	0.200	0.806	0.0000248
	0.441	2.025	19.05	0.100	0.802	0.0000248
3(6)	1.464	2.025	19.05	0.545*	0.637	0.0000300
	1.374	2.025	19.05	0.500	0.635	0.0000300
	1.261	2.025	19.05	0.400	0.631	0.0000300
	1.129	2.025	19.05	0.300	0.627	0.0000300
	0.971	2.025	19.05	0.200	0.622	0.0000300
	0.532	2.025	19.05	0.100	0.620	0.0000300
4(6)	1.453	2.025	19.05	0.520*	0.527	0.0000343
	1.408	2.025	19.05	0.500	0.525	0.0000343
	1.280	2.025	19.05	0.400	0.521	0.0000343
	1.141	2.025	19.05	0.300	0.518	0.0000343
	0.997	2.025	19.05	0.200	0.514	0.0000343
	0.549	2.025	19.05	0.100	0.512	0.0000343
5(5)	1.427	2.025	19.05	0.475*	0.470	0.0000365
	1.309	2.025	19.05	0.400	0.467	0.0000365
	1.133	2.025	19.05	0.300	0.464	0.0000365
	0.967	2.025	19.05	0.200	0.461	0.0000365
	0.523	2.025	19.05	0.100	0.459	0.0000365
6(5)	1.344	2.025	19.05	0.440*	0.424	0.0000379
	1.282	2.025	19.05	0.400	0.423	0.0000379
	1.180	2.025	19.05	0.300	0.420	0.0000379
	0.998	2.025	19.05	0.200	0.418	0.0000379
	0.609	2.025	19.05	0.100	0.416	0.0000379
7(9)	1.117	1.630	19.05	0.850*	1.269	0.0000184

	1.041	1.630	19.05	0.800	1.265	0.0000184
	0.972	1.630	19.05	0.700	1.259	0.0000184
	0.896	1.630	19.05	0.600	1.248	0.0000184
	0.813	1.630	19.05	0.500	1.241	0.0000184
	0.750	1.630	19.05	0.400	1.233	0.0000184
	0.679	1.630	19.05	0.300	1.226	0.0000184
	0.600	1.630	19.05	0.200	1.219	0.0000184
	0.301	1.630	19.05	0.100	1.213	0.0000184
8(6)	1.002	1.630	19.05	0.585*	0.826	0.0000248
	0.877	1.630	19.05	0.500	0.822	0.0000248
	0.784	1.630	19.05	0.400	0.819	0.0000248
	0.708	1.630	19.05	0.300	0.811	0.0000248
	0.623	1.630	19.05	0.200	0.805	0.0000248
	0.334	1.630	19.05	0.100	0.802	0.0000248
9(5)	1.043	1.630	19.05	0.475*	0.634	0.0000300
	0.872	1.630	19.05	0.400	0.631	0.0000300
	0.785	1.630	19.05	0.300	0.627	0.0000300
	0.643	1.630	19.05	0.200	0.623	0.0000300
	0.389	1.630	19.05	0.100	0.620	0.0000300
10(4)	1.141	1.630	19.05	0.370*	0.522	0.0000343
	0.876	1.630	19.05	0.300	0.518	0.0000343
	0.658	1.630	19.05	0.200	0.515	0.0000343
	0.399	1.630	19.05	0.100	0.512	0.0000343
11(4)	0.894	1.630	19.05	0.320*	0.465	0.0000365
	0.834	1.630	19.05	0.300	0.465	0.0000365
	0.737	1.630	19.05	0.200	0.462	0.0000365
	0.410	1.630	19.05	0.100	0.459	0.0000365
12(3)	0.876	1.630	19.05	0.270*	0.421	0.0000379
	0.683	1.630	19.05	0.200	0.418	0.0000379
	0.403	1.630	19.05	0.100	0.416	0.0000379
13(9)	0.882	1.200	19.05	0.900*	1.274	0.0000184
	0.814	1.200	19.05	0.800	1.263	0.0000184
	0.774	1.200	19.05	0.700	1.255	0.0000184
	0.722	1.200	19.05	0.600	1.245	0.0000184
	0.679	1.200	19.05	0.500	1.238	0.0000184
	0.622	1.200	19.05	0.400	1.230	0.0000184
	0.571	1.200	19.05	0.300	1.225	0.0000184
	0.452	1.200	19.05	0.200	1.217	0.0000184
	0.239	1.200	19.05	0.100	1.213	0.0000184
14(5)	0.765	1.200	19.05	0.510*	0.818	0.0000248
	0.646	1.200	19.05	0.400	0.814	0.0000248
	0.556	1.200	19.05	0.300	0.809	0.0000248
	0.472	1.200	19.05	0.200	0.805	0.0000248
	0.261	1.200	19.05	0.100	0.802	0.0000248
15(5)	0.696	1.200	19.05	0.415*	0.631	0.0000300
	0.655	1.200	19.05	0.400	0.630	0.0000300
	0.588	1.200	19.05	0.300	0.626	0.0000300

	0.501	1.200	19.05	0.200	0.622	0.0000300
	0.220	1.200	19.05	0.100	0.619	0.0000300
16(3)	0.732	1.200	19.05	0.285*	0.517	0.0000343
	0.563	1.200	19.05	0.200	0.515	0.0000343
	0.261	1.200	19.05	0.100	0.512	0.0000343
17(3)	0.592	1.200	19.05	0.255*	0.464	0.0000365
	0.521	1.200	19.05	0.200	0.461	0.0000365
	0.259	1.200	19.05	0.100	0.459	0.0000365
18(3)	0.657	1.200	19.05	0.225*	0.419	0.0000379
	0.592	1.200	19.05	0.200	0.418	0.0000379
	0.266	1.200	19.05	0.100	0.416	0.0000379
19(8)	0.701	1.010	19.05	0.730*	1.255	0.0000184
	0.680	1.010	19.05	0.700	1.254	0.0000184
	0.627	1.010	19.05	0.600	1.245	0.0000184
	0.571	1.010	19.05	0.500	1.237	0.0000184
	0.524	1.010	19.05	0.400	1.232	0.0000184
	0.478	1.010	19.05	0.300	1.225	0.0000184
	0.367	1.010	19.05	0.200	1.217	0.0000184
	0.185	1.010	19.05	0.100	1.213	0.0000184
20(5)	0.650	1.010	19.05	0.460*	0.815	0.0000248
	0.559	1.010	19.05	0.400	0.812	0.0000248
	0.456	1.010	19.05	0.300	0.808	0.0000248
	0.408	1.010	19.05	0.200	0.804	0.0000248
	0.229	1.010	19.05	0.100	0.801	0.0000248
21(3)	0.529	1.010	19.05	0.300*	0.627	0.0000300
	0.437	1.010	19.05	0.200	0.622	0.0000300
	0.193	1.010	19.05	0.100	0.619	0.0000300
22(3)	0.519	1.010	19.05	0.255*	0.517	0.0000343
	0.435	1.010	19.05	0.200	0.515	0.0000343
	0.180	1.010	19.05	0.100	0.512	0.0000343
23(3)	0.468	1.010	19.05	0.240*	0.463	0.0000365
	0.435	1.010	19.05	0.200	0.462	0.0000365
	0.189	1.010	19.05	0.100	0.459	0.0000365
24(3)	0.472	1.010	19.05	0.220*	0.419	0.0000379
	0.445	1.010	19.05	0.200	0.418	0.0000379
	0.200	1.010	19.05	0.100	0.416	0.0000379
25(6)	0.625	0.915	19.05	0.650*	1.250	0.0000184
	0.538	0.915	19.05	0.500	1.238	0.0000184
	0.483	0.915	19.05	0.400	1.230	0.0000184
	0.420	0.915	19.05	0.300	1.224	0.0000184
	0.329	0.915	19.05	0.200	1.217	0.0000184
	0.194	0.915	19.05	0.100	1.213	0.0000184
31(6)	1.556	2.025	26.64	0.620*	1.249	0.0000184
	1.229	2.025	26.64	0.500	1.240	0.0000184
	1.103	2.025	26.64	0.400	1.232	0.0000184
	1.036	2.025	26.64	0.300	1.225	0.0000184
	0.936	2.025	26.64	0.200	1.217	0.0000184

	0.450	2.025	26.64	0.100	1.213	0.0000184
32(7)	1.772	2.025	26.64	0.615*	0.838	0.0000248
	1.619	2.025	26.64	0.600	0.835	0.0000248
	1.343	2.025	26.64	0.500	0.826	0.0000248
	1.197	2.025	26.64	0.400	0.820	0.0000248
	1.049	2.025	26.64	0.300	0.814	0.0000248
	0.921	2.025	26.64	0.200	0.809	0.0000248
	0.496	2.025	26.64	0.100	0.804	0.0000248
33(6)	1.696	2.025	26.64	0.590*	0.644	0.0000300
	1.376	2.025	26.64	0.500	0.638	0.0000300
	1.236	2.025	26.64	0.400	0.633	0.0000300
	1.100	2.025	26.64	0.300	0.628	0.0000300
	0.975	2.025	26.64	0.200	0.625	0.0000300
	0.486	2.025	26.64	0.100	0.621	0.0000300
34(5)	1.768	2.025	26.64	0.540*	0.528	0.0000343
	1.350	2.025	26.64	0.400	0.523	0.0000343
	1.200	2.025	26.64	0.300	0.520	0.0000343
	1.024	2.025	26.64	0.200	0.516	0.0000343
	0.606	2.025	26.64	0.100	0.513	0.0000343
35(5)	1.639	2.025	26.64	0.500*	0.472	0.0000365
	1.385	2.025	26.64	0.400	0.468	0.0000365
	1.191	2.025	26.64	0.300	0.465	0.0000365
	1.025	2.025	26.64	0.200	0.462	0.0000365
	0.556	2.025	26.64	0.100	0.460	0.0000365
36(4)	1.612	2.025	26.64	0.440*	0.424	0.0000379
	1.212	2.025	26.64	0.300	0.420	0.0000379
	1.014	2.025	26.64	0.200	0.418	0.0000379
	0.531	2.025	26.64	0.100	0.417	0.0000379
37(6)	1.152	1.630	26.64	0.630*	1.247	0.0000184
	0.941	1.630	26.64	0.500	1.239	0.0000184
	0.845	1.630	26.64	0.400	1.230	0.0000184
	0.778	1.630	26.64	0.300	1.223	0.0000184
	0.689	1.630	26.64	0.200	1.217	0.0000184
	0.365	1.630	26.64	0.100	1.213	0.0000184
38(6)	1.315	1.630	26.64	0.585*	0.827	0.0000248
	1.157	1.630	26.64	0.500	0.824	0.0000248
	1.041	1.630	26.64	0.400	0.819	0.0000248
	0.881	1.630	26.64	0.300	0.814	0.0000248
	0.755	1.630	26.64	0.200	0.805	0.0000248
	0.367	1.630	26.64	0.100	0.802	0.0000248
39(5)	1.222	1.630	26.64	0.440*	0.635	0.0000300
	1.121	1.630	26.64	0.400	0.633	0.0000300
	0.895	1.630	26.64	0.300	0.628	0.0000300
	0.737	1.630	26.64	0.200	0.622	0.0000300
	0.378	1.630	26.64	0.100	0.620	0.0000300
40(4)	1.152	1.630	26.64	0.350*	0.522	0.0000343
	0.996	1.630	26.64	0.300	0.519	0.0000343

	0.804	1.630	26.64	0.200	0.516	0.0000343
	0.435	1.630	26.64	0.100	0.512	0.0000343
41(3)	1.036	1.630	26.64	0.305*	0.465	0.0000365
	0.797	1.630	26.64	0.200	0.461	0.0000365
	0.420	1.630	26.64	0.100	0.459	0.0000365
42(3)	0.911	1.630	26.64	0.265*	0.420	0.0000379
	0.805	1.630	26.64	0.200	0.418	0.0000379
	0.430	1.630	26.64	0.100	0.416	0.0000379
43(7)	0.817	1.200	26.64	0.650*	1.252	0.0000184
	0.790	1.200	26.64	0.600	1.249	0.0000184
	0.705	1.200	26.64	0.500	1.241	0.0000184
	0.647	1.200	26.64	0.400	1.234	0.0000184
	0.602	1.200	26.64	0.300	1.227	0.0000184
	0.495	1.200	26.64	0.200	1.218	0.0000184
	0.257	1.200	26.64	0.100	1.213	0.0000184
44(5)	0.710	1.200	26.64	0.475*	0.819	0.0000248
	0.641	1.200	26.64	0.400	0.815	0.0000248
	0.559	1.200	26.64	0.300	0.810	0.0000248
	0.491	1.200	26.64	0.200	0.805	0.0000248
	0.263	1.200	26.64	0.100	0.802	0.0000248
45(4)	0.731	1.200	26.64	0.390*	0.629	0.0000300
	0.618	1.200	26.64	0.300	0.626	0.0000300
	0.509	1.200	26.64	0.200	0.622	0.0000300
	0.220	1.200	26.64	0.100	0.620	0.0000300
46(3)	0.671	1.200	26.64	0.280*	0.518	0.0000343
	0.532	1.200	26.64	0.200	0.515	0.0000343
	0.265	1.200	26.64	0.100	0.512	0.0000343
47(3)	0.561	1.200	26.64	0.235*	0.464	0.0000365
	0.512	1.200	26.64	0.200	0.461	0.0000365
	0.239	1.200	26.64	0.100	0.459	0.0000365
48(2)	0.519	1.200	26.64	0.225*	0.419	0.0000379
	0.241	1.200	26.64	0.100	0.416	0.0000379
49(6)	0.674	1.010	26.64	0.545*	1.243	0.0000184
	0.637	1.010	26.64	0.500	1.240	0.0000184
	0.558	1.010	26.64	0.400	1.233	0.0000184
	0.499	1.010	26.64	0.300	1.226	0.0000184
	0.405	1.010	26.64	0.200	1.217	0.0000184
	0.209	1.010	26.64	0.100	1.213	0.0000184
50(5)	0.682	1.010	26.64	0.440*	0.815	0.0000248
	0.633	1.010	26.64	0.400	0.813	0.0000248
	0.519	1.010	26.64	0.300	0.810	0.0000248
	0.412	1.010	26.64	0.200	0.805	0.0000248
	0.232	1.010	26.64	0.100	0.802	0.0000248
51(3)	0.505	1.010	26.64	0.300*	0.627	0.0000300
	0.427	1.010	26.64	0.200	0.622	0.0000300
	0.180	1.010	26.64	0.100	0.620	0.0000300
52(3)	0.514	1.010	26.64	0.250*	0.516	0.0000343

	0.437	1.010	26.64	0.200	0.515	0.0000343
	0.178	1.010	26.64	0.100	0.512	0.0000343
53(3)	0.447	1.010	26.64	0.220*	0.463	0.0000365
	0.410	1.010	26.64	0.200	0.462	0.0000365
	0.190	1.010	26.64	0.100	0.459	0.0000365
54(3)	0.419	1.010	26.64	0.210*	0.418	0.0000379
	0.408	1.010	26.64	0.200	0.418	0.0000379
	0.191	1.010	26.64	0.100	0.416	0.0000379
61(7)	1.373	2.025	12.70	0.735*	1.265	0.0000184
	1.233	2.025	12.70	0.600	1.239	0.0000184
	1.138	2.025	12.70	0.500	1.247	0.0000184
	1.042	2.025	12.70	0.400	1.243	0.0000184
	0.953	2.025	12.70	0.300	1.233	0.0000184
	0.816	2.025	12.70	0.200	1.219	0.0000184
	0.409	2.025	12.70	0.100	1.213	0.0000184
62(6)	1.447	2.025	12.70	0.610*	0.829	0.0000248
	1.314	2.025	12.70	0.500	0.823	0.0000248
	1.228	2.025	12.70	0.400	0.821	0.0000248
	1.115	2.025	12.70	0.300	0.809	0.0000248
	0.975	2.025	12.70	0.200	0.804	0.0000248
	0.447	2.025	12.70	0.100	0.801	0.0000248
63(6)	1.476	2.025	12.70	0.555*	0.638	0.0000300
	1.382	2.025	12.70	0.500	0.635	0.0000300
	1.254	2.025	12.70	0.400	0.632	0.0000300
	1.078	2.025	12.70	0.300	0.625	0.0000300
	0.936	2.025	12.70	0.200	0.622	0.0000300
	0.490	2.025	12.70	0.100	0.619	0.0000300
64(5)	1.459	2.025	12.70	0.530*	0.526	0.0000343
	1.279	2.025	12.70	0.400	0.522	0.0000343
	1.200	2.025	12.70	0.300	0.517	0.0000343
	0.986	2.025	12.70	0.200	0.515	0.0000343
	0.501	2.025	12.70	0.100	0.512	0.0000343
65(5)	1.496	2.025	12.70	0.500*	0.473	0.0000365
	1.372	2.025	12.70	0.400	0.468	0.0000365
	1.169	2.025	12.70	0.300	0.466	0.0000365
	1.010	2.025	12.70	0.200	0.462	0.0000365
	0.497	2.025	12.70	0.100	0.459	0.0000365
66(5)	1.381	2.025	12.70	0.485*	0.425	0.0000379
	1.267	2.025	12.70	0.400	0.423	0.0000379
	1.156	2.025	12.70	0.300	0.420	0.0000379
	1.048	2.025	12.70	0.200	0.418	0.0000379
	0.510	2.025	12.70	0.100	0.416	0.0000379
67(9)	1.101	1.630	12.70	0.880*	1.274	0.0000184
	1.058	1.630	12.70	0.800	1.272	0.0000184
	1.019	1.630	12.70	0.700	1.266	0.0000184
	0.974	1.630	12.70	0.600	1.257	0.0000184
	0.925	1.630	12.70	0.500	1.248	0.0000184

	0.856	1.630	12.70	0.400	1.244	0.0000184
	0.774	1.630	12.70	0.300	1.230	0.0000184
	0.655	1.630	12.70	0.200	1.216	0.0000184
	0.230	1.630	12.70	0.100	1.212	0.0000184
68(6)	1.101	1.630	12.70	0.635*	0.826	0.0000248
	0.988	1.630	12.70	0.500	0.823	0.0000248
	0.855	1.630	12.70	0.400	0.819	0.0000248
	0.748	1.630	12.70	0.300	0.812	0.0000248
	0.637	1.630	12.70	0.200	0.805	0.0000248
	0.303	1.630	12.70	0.100	0.802	0.0000248
69(5)	1.287	1.630	12.70	0.545*	0.633	0.0000300
	1.071	1.630	12.70	0.400	0.630	0.0000300
	0.939	1.630	12.70	0.300	0.624	0.0000300
	0.849	1.630	12.70	0.200	0.622	0.0000300
	0.375	1.630	12.70	0.100	0.619	0.0000300
70(4)	1.117	1.630	12.70	0.435*	0.523	0.0000343
	0.982	1.630	12.70	0.300	0.518	0.0000343
	0.895	1.630	12.70	0.200	0.515	0.0000343
	0.379	1.630	12.70	0.100	0.512	0.0000343
71(4)	0.997	1.630	12.70	0.415*	0.464	0.0000365
	0.820	1.630	12.70	0.300	0.464	0.0000365
	0.751	1.630	12.70	0.200	0.462	0.0000365
	0.380	1.630	12.70	0.100	0.459	0.0000365
72(4)	0.960	1.630	12.70	0.395*	0.421	0.0000379
	0.872	1.630	12.70	0.300	0.419	0.0000379
	0.753	1.630	12.70	0.200	0.418	0.0000379
	0.371	1.630	12.70	0.100	0.416	0.0000379
73(9)	0.919	1.200	12.70	0.940*	1.273	0.0000184
	0.874	1.200	12.70	0.800	1.263	0.0000184
	0.819	1.200	12.70	0.700	1.261	0.0000184
	0.767	1.200	12.70	0.600	1.254	0.0000184
	0.704	1.200	12.70	0.500	1.246	0.0000184
	0.636	1.200	12.70	0.400	1.235	0.0000184
	0.563	1.200	12.70	0.300	1.226	0.0000184
	0.474	1.200	12.70	0.200	1.218	0.0000184
	0.239	1.200	12.70	0.100	1.213	0.0000184
74(6)	0.718	1.200	12.70	0.595*	0.826	0.0000248
	0.674	1.200	12.70	0.500	0.821	0.0000248
	0.605	1.200	12.70	0.400	0.816	0.0000248
	0.529	1.200	12.70	0.300	0.810	0.0000248
	0.437	1.200	12.70	0.200	0.804	0.0000248
	0.236	1.200	12.70	0.100	0.801	0.0000248
75(5)	0.608	1.200	12.70	0.490*	0.634	0.0000300
	0.560	1.200	12.70	0.400	0.630	0.0000300
	0.512	1.200	12.70	0.300	0.625	0.0000300
	0.478	1.200	12.70	0.200	0.622	0.0000300
	0.204	1.200	12.70	0.100	0.619	0.0000300

76(4)	0.604	1.200	12.70	0.400*	0.520	0.0000343
	0.565	1.200	12.70	0.300	0.518	0.0000343
	0.467	1.200	12.70	0.200	0.515	0.0000343
	0.212	1.200	12.70	0.100	0.512	0.0000343
77(4)	0.603	1.200	12.70	0.340*	0.465	0.0000365
	0.583	1.200	12.70	0.300	0.464	0.0000365
	0.476	1.200	12.70	0.200	0.462	0.0000365
	0.197	1.200	12.70	0.100	0.459	0.0000365
78(3)	0.570	1.200	12.70	0.295*	0.420	0.0000379
	0.467	1.200	12.70	0.200	0.418	0.0000379
	0.187	1.200	12.70	0.100	0.416	0.0000379
79(7)	0.655	1.010	12.70	0.700*	1.261	0.0000184
	0.615	1.010	12.70	0.600	1.251	0.0000184
	0.583	1.010	12.70	0.500	1.238	0.0000184
	0.510	1.010	12.70	0.400	1.233	0.0000184
	0.439	1.010	12.70	0.300	1.226	0.0000184
	0.356	1.010	12.70	0.200	1.217	0.0000184
	0.173	1.010	12.70	0.100	1.213	0.0000184
80(6)	0.568	1.010	12.70	0.535*	0.822	0.0000248
	0.541	1.010	12.70	0.500	0.820	0.0000248
	0.501	1.010	12.70	0.400	0.815	0.0000248
	0.429	1.010	12.70	0.300	0.810	0.0000248
	0.355	1.010	12.70	0.200	0.804	0.0000248
	0.190	1.010	12.70	0.100	0.801	0.0000248
81(4)	0.593	1.010	12.70	0.435*	0.630	0.0000300
	0.447	1.010	12.70	0.300	0.626	0.0000300
	0.397	1.010	12.70	0.200	0.623	0.0000300
	0.146	1.010	12.70	0.100	0.620	0.0000300
82(4)	0.483	1.010	12.70	0.355*	0.519	0.0000343
	0.465	1.010	12.70	0.300	0.519	0.0000343
	0.407	1.010	12.70	0.200	0.515	0.0000343
	0.167	1.010	12.70	0.100	0.512	0.0000343
83(3)	0.449	1.010	12.70	0.310*	0.464	0.0000365
	0.399	1.010	12.70	0.200	0.462	0.0000365
	0.170	1.010	12.70	0.100	0.459	0.0000365
84(3)	0.439	1.010	12.70	0.285*	0.420	0.0000379
	0.396	1.010	12.70	0.200	0.418	0.0000379
	0.175	1.010	12.70	0.100	0.416	0.0000379
85(7)	0.606	0.915	12.70	0.680*	1.257	0.0000184
	0.558	0.915	12.70	0.600	1.246	0.0000184
	0.519	0.915	12.70	0.500	1.237	0.0000184
	0.465	0.915	12.70	0.400	1.231	0.0000184
	0.389	0.915	12.70	0.300	1.224	0.0000184
	0.308	0.915	12.70	0.200	1.217	0.0000184
	0.178	0.915	12.70	0.100	1.213	0.0000184
86(5)	0.484	0.915	12.70	0.515*	0.820	0.0000248
	0.405	0.915	12.70	0.400	0.814	0.0000248

	0.356	0.915	12.70	0.300	0.808	0.0000248
	0.283	0.915	12.70	0.200	0.805	0.0000248
	0.157	0.915	12.70	0.100	0.802	0.0000248
87(5)	0.494	0.915	12.70	0.430*	0.635	0.0000300
	0.464	0.915	12.70	0.400	0.631	0.0000300
	0.419	0.915	12.70	0.300	0.625	0.0000300
	0.338	0.915	12.70	0.200	0.623	0.0000300
	0.161	0.915	12.70	0.100	0.619	0.0000300
88(4)	0.433	0.915	12.70	0.350*	0.520	0.0000343
	0.391	0.915	12.70	0.300	0.519	0.0000343
	0.339	0.915	12.70	0.200	0.516	0.0000343
	0.136	0.915	12.70	0.100	0.512	0.0000343
89(3)	0.379	0.915	12.70	0.305*	0.466	0.0000365
	0.297	0.915	12.70	0.200	0.462	0.0000365
	0.139	0.915	12.70	0.100	0.459	0.0000365
90(3)	0.341	0.915	12.70	0.280*	0.420	0.0000379
	0.287	0.915	12.70	0.200	0.419	0.0000379
	0.132	0.915	12.70	0.100	0.416	0.0000379

For all data, D_c = 156 mm, ρ_p = 2547 kg/m^3. The number in ( ) indicates the number of trials for different heights at each Run No.

* H = H_m

Appendix E

Fortran Programs

E.1 Program on U_{ms} correlation

```
C     This program is written to fit experimental data to a dimensionless
C     equation of the form
C
C         N1=b1*(N2**b2)*(N3**b3)*...*(Nn**bn)
C
C     b1,b2,b3,...bn are constants to be determined. Newton's Method
C     will be used. This method requires that the initial values of
C     b1,b2,b3,...bn are very close to the solution in order to
C     obtain convergence. The method of Multiple Linear Regression
C     is used to  provide this set of initial values of bi's. To apply
C     the latter method, the above equation has to be rewitten as
C
C          Y=f(X1,X2,X3,...Xn)=a1*X1+a2*X2+a3*X3+...+an*Xn
C      ie  lnN1=b1+b2*lnN2+b3*lnN3+...+bn*lnNn
C
C      This program is set to handle a maximum of 10 unknowns
C      (b1,b2,b3,...bn) and 305 sets of data points. To accomodate
C      more unknowns and/or sets of date points, change the dimensions
C      of the arrays accordingly and of course, the DATA statement in the
C      beginning of the MAIN program.
C
C      The data file should be in the form of
C
C             N11,N21,N31,...Nn1
C              .                .
C              .                .
C              .                .
C             N1m,N2m,N3m,...Mnm
C      where
C            m=number of sets of data points
C            n=number of unknowns sought
C
C
      DATA M,N,FACTOR,DB/305,5,1.,0.0001/
      DIMENSION X(10,384),XN(10,384),Y(384),YN1(384),A(384),B(384)
      DIMENSION PROD(384),DIFF1(384),DIFF2(384),DELB(10),COE(384),
     *         UMS(384),DP(384),DI(384),DC(384),SUM1(384),SUM2(384),
```

```
     *          H(384),RHOP(384),RHO(384),VISC(384),UIF(384),AR(384),
     *          W(384),RET(384)
C
C     Read input data
C
      READ(4,10)(UMS(I),DP(I),DI(I),DC(I),H(I),RHOP(I),RHO(I),VISC(I),
     *          I=1,M)
   10 FORMAT(F11.3,F8.3,F8.2,F8.1,F8.3,F8.0,F8.3,F11.7)
      NP=N+1
C
C     Give value to elements of the non-linear equations
C
      DO 20 K=1,M
      AR(K)=(DP(K)*1.E-3)**3*(RHOP(K)-RHO(K))*9.8067*RHO(K)/VISC(K)**2
      W(K)=ALOG10(4./3.*AR(K))
      RET(K)=10.**(-1.81391+1.34671*W(K)-0.12427*W(K)**2
     *         +0.006344*W(K)**3)
      YN1(K)=(RHO(K)*UMS(K)*DP(K)*1.E-3)/VISC(K)/RET(K)
      XN(2,K)=DI(K)/DC(K)
      XN(3,K)=H(K)/(DC(K)*1.E-3)
      XN(4,K)=DI(K)/DP(K)
      XN(5,K)=(RHOP(K)-RHO(K))/RHO(K)
   20 CONTINUE
C
C     Transform input data into x-values & y-values
C
      DO 40 MK=1,M
      Y(MK)=ALOG(YN1(MK))
      X(1,MK)=1
      DO 30 NK=2,N
      X(NK,MK)=ALOG(XN(NK,MK))
   30 CONTINUE
   40 CONTINUE
C
      CALL LSQM(X,Y,M,N,A,VAR)
C
C     Transform A to B
C
      B(1)=EXP(A(1))

      DO 50 IN=2,N
      B(IN)=A(IN)
   50 CONTINUE
C
C     Calculate the variance of the fit
C
      SSUMT1=0.
```

```
      SSUM1=0.
      RMST=0.
      RMS=0.
      DO 100 K=1,M
      SUM1(K)=B(1)
      DO 90 I=2,N
      SUM1(K)=SUM1(K)*XN(I,K)**B(I)
 90   CONTINUE
      SSUMT1=SSUMT1+(YN1(K)-SUM1(K))*(YN1(K)-SUM1(K))
      RMST=RMST+((SUM1(K)-YN1(K))*100./YN1(K))**2
      UIF(K)=SUM1(K)*VISC(K)/(DP(K)*1.E-3)/RHO(K)*RET(K)
      SSUM1=SSUM1+(UIF(K)-UMS(K))*(UIF(K)-UMS(K))
      RMS=RMS+((UIF(K)-UMS(K))*100./UMS(K))**2
100   CONTINUE
      VART1=SSUMT1/(M-N)
      VAR1=SSUM1/(M-N)
      RMST=SQRT(RMST/M)
      RMS=SQRT(RMS/M)

      WRITE(6,120)
120   FORMAT(5X,'INDIRECT APPROACH-Multiple Linear Regression')
      WRITE(6,130)
130   FORMAT(/,15X,'The fitting parameters are:-')
      WRITE(6,140)
140   FORMAT(15X,'___________________')
      WRITE(6,150)(I,B(I),I=1,N)
150   FORMAT(15X,'b',I1,'=',F10.4)
      WRITE(6,160) VART1,VAR1
160   FORMAT(/,15X,'Variance =',F9.5,5X,'V (Ums)  =',F9.5)
      WRITE(6,170) RMST,RMS
170   FORMAT(/,15X,'RMST     =',F9.5,5X,'RMS(ums) =',F9.5)

      B(1)=B(1)/FACTOR

      DO 180 I=1,M
      YN1(I)=YN1(I)/FACTOR
180   CONTINUE

      MM=0
250   IFLAG=0
      MM=MM+1
      IF(MM.GT.5000) GO TO 500

      DO 270 I=1,M
      PROD(I)=1.
      DO 260 J=2,N
      PROD(I)=PROD(I)*XN(J,I)**B(J)
```

```
 260  CONTINUE
      DIFF1(I)=YN1(I)-1.*B(1)*PROD(I)
      DIFF2(I)=YN1(I)-2.*B(1)*PROD(I)
 270  CONTINUE

      CALL LSQM2(X,XN,YN1,M,N,PROD,DIFF1,DIFF2,B(1),DELB)

      DO 280 I=1,N
      B(I)=B(I)+DELB(I)
      IF(ABS(DELB(I)).GT.DB) IFLAG=1
 280  CONTINUE
      IF(IFLAG.EQ.0) GO TO 290
      GO TO 250
 290  B(1)=B(1)*FACTOR
      DO 300 I=1,M
      YN1(I)=YN1(I)*FACTOR
 300  CONTINUE
C
C     Calculate the variance of the fit
C
      SSUMT2=0.
      SSUM2=0.
      RMST=0.
      RMS=0.
      DO 310 K=1,M
      SUM2(K)=B(1)*PROD(K)
      SSUMT2=SSUMT2+(YN1(K)-SUM2(K))*(YN1(K)-SUM2(K))
      RMST=RMST+((SUM2(K)-YN1(K))*100./YN1(K))**2
      UIF(K)=SUM2(K)*VISC(K)/(DP(K)*1.E-3)/RHO(K)*RET(K)
      SSUM2=SSUM2+(UIF(K)-UMS(K))*(UIF(K)-UMS(K))
      RMS=RMS+((UIF(K)-UMS(K))*100./UMS(K))**2
 310  CONTINUE
      VART2=SSUMT2/(M-N)
      VAR2=SSUM2/(M-N)
      RMST=SQRT(RMST/M)
      RMS=SQRT(RMS/M)

      WRITE(6,320)
 320  FORMAT(/,5X,'DIRECT APPROACH - Newton  s Method')
      WRITE(6,330) MM,DB
 330  FORMAT(/,15X,'No of Iterations =',I5,': Epsilon =',F7.6)
      WRITE(6,360)
 360  FORMAT(/,15X,'The fitting parameters are :-')
      WRITE(6,370)
 370  FORMAT(15X,'________________')
      WRITE(6,390)(I,B(I),I=1,N)
 390  FORMAT(15X,'B',I1,'=',F10.4)
```

```
      WRITE(6,400) VART2,VAR2
 400  FORMAT(/,15X,'Variance = ',F9.5,5X,'V (Ums)  =',F9.5)
      WRITE(6,410) RMST,RMS
 410  FORMAT(/,15X,'RMST     = ',F9.5,5X,'RMS(ums) =',F9.5)
      WRITE(7,470) (B(I),I=1,N)
 470  FORMAT(F9.5)
      CALL COMPAR(UIF,UMS,M)
      STOP
C
C     Print warning message!
C
 500  WRITE(6,600)
 600  FORMAT('**************WARNING*************')
      WRITE(6,650)
 650  FORMAT(12X,'Convergence  not achived after 5000 iterations')
      STOP
      END


      SUBROUTINE LSQM(X,Y,M,N,A,VAR)
C
C
C     Arguement:
C
C           X   real array of independent x-value
C           Y   real array of dependent y-value
C           M   interger number of pairs of (x,y) points
C           N   interger number of terms in fitting equation
C           A   fitting coefficients
C         VAR   variance of fit
C
C

      DIMENSION X(10,112),Y(M),A(N),COEFF(10,11)
      NP=N+1
C     Form the arguement coefficient matrix
C
      DO 80 I=1,N
      COEFF(I,NP)=0

      DO 50 K=1,M
      COEFF(I,NP)=COEFF(I,NP)+X(I,K)*Y(K)
  50  CONTINUE

      DO 70 J=1,N
      COEFF(I,J)=0
```

```
      DO 60 K=1,M
      COEFF(I,J)=COEFF(I,J)+X(I,K)*X(J,K)
   60 CONTINUE

      IF(I.EQ.J) GO TO 70
      COEFF(J,I)=COEFF(I,J)
   70 CONTINUE
   80 CONTINUE
C
C     Solve for the unknown A coefficients
C
      CALL GAUSS(COEFF,N,10,11,A,RNORM,IERROR)
C
C     Calculate variance of multiple linear regression
C
      SSUM=0
      DO 140 K=1,M
      SUM=A(1)
      DO 130 J=2,N
      SUM=SUM+A(J)*X(J,K)
  130 CONTINUE
      SSUM=SSUM+(Y(K)-SUM)**2
  140 CONTINUE
      VAR=SSUM/(M-N)
      RETURN
      END


      SUBROUTINE LSQM2(X,XN,YN,M,N,PROD,DF1,DF2,B1,DELB)
C
C
C     Arguement:
C
C           X   real array of independent LN(XN) values
C          XN   real array of independent Ni values (i=2,3....n)
C          YN   real array of dependent N1 values
C           M   interger number of pairs of (X,y) points
C           N   interger number of terms in fitting equation
C
C        PROD   (N2**b2)*(N3**b3)*...*(Nn**bn)
C         DF1   N1-1.0*(b1*PROD)
C         DF2   N1-2.0*(b1*PROD)
C          B1   b1
C        DELB   real array of unknowns to be sought
C
```

```
C
      DIMENSION X(10,112),XN(10,112),YN(112),PROD(112),DF1(112)
      DIMENSION DF2(112),DELB(112),COEFF(10,11)
      NP=N+1
C
C     Form the arguement coefficient matrix
C
      DO 80 I=1,N
      COEFF(I,NP)=0

      DO 50 K=1,M
      COEFF(I,NP)=COEFF(I,NP)+DF1(K)*B1*X(I,K)*PROD(K)
   50 CONTINUE

      DO 70 J=1,N
      COEFF(I,J)=0

      DO 60 K=1,M
      COEFF(I,J)=COEFF(I,J)+DF2(K)*(-PROD(K)*X(I,K)*X(J,K))
   60 CONTINUE

      IF(I.EQ.J) GO TO 70
      COEFF(J,I)=COEFF(I,J)
   70 CONTINUE
   80 CONTINUE
C
      COEFF(1,1)=0
      DO 90 K=1,M
      COEFF(1,1)=COEFF(1,1)+PROD(K)*PROD(K)
   90 CONTINUE

      COEFF(1,NP)=0
      DO 100 K=1,M
      COEFF(1,NP)=COEFF(1,NP)+DF1(K)*PROD(K)
  100 CONTINUE
C
C     Call subroutine GAUSS to solve for DELB's
C

      CALL GAUSS(COEFF,N,10,11,DELB,RNORM,IERROR)
      RETURN
      END

       SUBROUTINE GAUSS(A,N,NDR,NDC,X,RNORM,IERROR)
C
```

```
C     Purpose:
C          Uses Gauss elimination with partial pivot selection to
C          solve simultaneous linear equations of form [A]*{X}={C}.
C
C     Arguments:
C          A  Augmented coefficient matrix containing all coefficients
C             and r.h.s. constants of equations to be solved.
C          N  Number of equations to be solved.
C        NDR  First (row) dimension of A in calling program.
C        NDC  Second (column) dimension of A in calling program.
C          X  Solution vector.
C      RNORM  Measure of size of residual vector {C}-[A]*{X}.
C     IERROR  Error flag.
C             =1 Successful Gauss elimination.
C             =2 Zero diagonal entry after pivot selection.
C
      DIMENSION A(NDR,NDC),X(N),B(10,11),BIG(10)
      NM=N-1
      NP=N+1
C
C     Set up working matrix B
C
      DO 20 I=1,N
        DO 10 J=1,NP
          B(I,J)=A(I,J)
 10     CONTINUE
 20   CONTINUE
C
C     Carry out elimination process N-1 times
C
      DO 80 K=1,NM
C
C     Search for largest coefficient in column K, rows K through N
C     IPIVOT is the row index of the largest coefficient
C
        DO 22 I=K,N
        BIG(I)=ABS(B(I,1))
        DO 25 J=K,N
          AB=ABS(B(I,J))
          IF(AB.LE.BIG(I)) GOTO 25
            BIG(I)=AB
   25    CONTINUE
   22    CONTINUE
         KP=K+1
C
C     Search for the largest Si value in column K, rows K through N
C     IPIVOT is the row index of the largest Si
```

```
C
      SK=(ABS(B(K,K)))/BIG(K)
      IPIVOT=K
      DO 30 I=KP,N
      SI=(ABS(B(I,K)))/BIG(I)
      IF(SI.LE.SK) GO TO 30
      SK=SI
      IPIVOT=I
   30 CONTINUE
C
C     Interchange rows K and IPIVOT if IPIVOT.NE.K
C
         IF(IPIVOT.EQ.K) GO TO 50
           DO 40 J=K,NP
             TEMP=B(IPIVOT,J)
             B(IPIVOT,J)=B(K,J)
             B(K,J)=TEMP
 40        CONTINUE
 50      IF(B(K,K).EQ.0) GO TO 130
C
C     Eliminate B(I,K) from rows K+1 through N
C
         DO 70 I=KP,N
           QUOT=B(I,K)/B(K,K)
           B(I,K)=0.
           DO 60 J=KP,NP
             B(I,J)=B(I,J)-QUOT*B(K,J)
 60        CONTINUE
 70      CONTINUE
 80    CONTINUE
C
       IF(B(N,N).EQ.0.) GO TO 130
C
C     Back substitute to find solution vector
C
       X(N)=B(N,NP)/B(N,N)
       DO 100 II=1,NM
         SUM=0.
         I=N-II
         IP=I+1
         DO 90 J=IP,N
           SUM=SUM+B(I,J)*X(J)
 90      CONTINUE
         X(I)=(B(I,NP)-SUM)/B(I,I)
 100    CONTINUE
C
C     Calculate norm of residual vector, C-A*X
```

```
C     Normal return with IERROR=1
C
      RSQ=0.
      DO 120 I=1,N
        SUM=0.
        DO 110 J=1,N
          SUM=SUM+A(I,J)*X(J)
 110    CONTINUE
        RSQ=RSQ+(ABS(A(I,NP)-SUM))**2
 120  CONTINUE
      RNORM=SQRT(RSQ)
      IERROR=1
      RETURN
C
C     Abnormal return because of zero entry on diagonal
C     IEEROR=2
C
 130  IERROR=2
      RETURN
      END

      SUBROUTINE COMPAR(X,Y,M)
      IMPLICIT REAL*4(A-H,O-Z)
      DIMENSION X(M),Y(M),X0(2),Y0(2)
      DATA X0/0.,2./,Y0/0.,2./
      CALL DSPDEV('PLOT')
      CALL NOBRDR
      CALL COMPLX
      CALL PAGE(8.5,11.0)
      CALL AREA2D(4.5,5.0)
      CALL HEADIN('Ums (pred) vs Ums (exp)$',100,1.2,1)
      CALL XNAME('Predicted Ums (m/s)$',100)
      CALL YNAME('Experimental Ums (m/s)$',100)
      CALL GRAF(0.,0.2,2.,0.,0.2,2.)
      CALL THKFRM(.02)
      CALL FRAME
      CALL MARKER(15)
      CALL CURVE(X0,Y0,2,0)
      CALL CURVE(X,Y,M,-1)
      CALL ALNLEG(1.0,0.0)
      CALL ENDPL(0)
      CALL DONEPL
      RETURN
      END
```

E.2 Program to calculate average spout diameter

```
      IMPLICIT REAL*4(A-H,O-Z)
      DIMENSION Z(9),DS(9)
      DATA Z/0.,5.,10.,20.,30.,40.,50.,60.,70/
      DATA DS/2.34,3.48,3.24,3.00,3.14,3.30,3.48,3.72,4.14/
      N=9
      AREA=QINT4P(Z,DS,N,1,N)
      ADS=SQRT(AREA/DS(N))
      WRITE(6,10)ADS
   10 FORMAT(1X,F5.2)
      STOP
      END

      FUNCTION QINT4P(X,Y,N,IA,IB)
      DIMENSION X(N),Y(N)
C     WHERE:
C     QINT4P = THE RESULTING INTEGRAL
C     X = AN ARRAY CONTAINING THE "N" ABSCISSAE
C     Y = AN ARRAY CONTAINING THE CORRESPONDING ORDINATES
C     N = THE NUMBER OF POINTS
C     IA = X(IA) IS THE FIRST POINT OF INTEGRATION
C     IB = X(IB) IS THE LAST POINT OF INTEGRATION
      REAL*8 AC(64)
      DATA HALF,SIXTH,TWLVTH,TWO
     1/0.5,Z402AAAAB,Z40155555,2.0/
C     1/2 , 1/6 , 1/12 , 2
      DUM=ACSUM(AC,0.0,0)
      IF (N.LT.4.OR.IA.GE.IB.OR.IA.LT.1.OR.IB.GT.N) GO TO 60
      I1=IA
      IF (IA.LT.3) I1=3
      IF (IA.EQ.(N-1).AND.N.GT.4) I1=N-2
      I2=IB+1
      IF (IB.GT.(N-2)) I2=N-1
      IF (IB.EQ.2.AND.N.GT.4) I2=4
      DO 50 I=I1,I2
      IF (I.NE.I1) GO TO 10
C
C  INITIALIZATION
C
      H2=X(I-1)-X(I-2)
      D3=(Y(I-1)-Y(I-2))/H2
      H3=X(I)-X(I-1)
      D1=(Y(I)-Y(I-1))/H3
      H1=X(I)-X(I-2)
      D2=(D1-D3)/H1
      H4=X(I+1)-X(I)
```

```
      R1=(Y(I+1)-Y(I))/H4
      R2=(R1-D1)/(X(I+1)-X(I-1))
      H1=X(I+1)-X(I-2)
      R3=(R2-D2)/H1
      IF (IA.NE.1) GO TO 20
C
C  HANDLE THE FIRST SEGMENT WITH FORWARD DIFFERENCE FORMULA
C
      DUM=ACSUM(AC,
     1 H2*(Y(1)+H2*(D3*HALF-H2*(D2*SIXTH-(H2+TWO*H3)*R3*TWLVTH))))
      GO TO 20
10    H4=X(I+1)-X(I)
      R1=(Y(I+1)-Y(I))/H4
      R2=(R1-D1)/(X(I+1)-X(I-1))
      R3=(R2-D2)/(X(I+1)-X(I-2))
20    IF (I.LE.IA.OR.I.GT.IB) GO TO 30
C
C  HANDLE MOST WITH CENTRED DIFFERENCE FORMULA
C
      DUM=ACSUM(AC,
     1 H3*((Y(I)+Y(I-1))*HALF-H3*H3*(D2+R2+(H2-H4)*R3)*TWLVTH))
30    IF (I.NE.I2) GO TO 40
      IF (IB.NE.N) GO TO 50
C
C  HANDLE THE LAST SEGMENT WITH BACKWARD DIFFERENCE FORMULA
C
      DUM=ACSUM(AC,
     1 H4*(Y(N)-H4*(R1*HALF+H4*(R2*SIXTH+(TWO*H3+H4)*R3*TWLVTH))))
      GO TO 50
40    H1=H2
      H2=H3
      H3=H4
      D1=R1
      D2=R2
      D3=R3
50    CONTINUE
C
60    QINT4P=ACSUM(AC)
C
      RETURN
      END
```

Appendix F

Error % for the U_{ms} Values Predicted by Four Equations

U_{ms} in m/s

Run No.	U_{ms} expt.	U_{ms} Eq.(5.75)	% dev	U_{ms} Eq.(2.1)	% dev	U_{ms} Eq.(2.6)	% dev	U_{ms} Eq.(2.4)	% dev
1 - 1	1.399	1.393	-0.404	1.069	-23.573	1.425	1.838	1.056	-24.508
1 - 2	1.164	1.307	12.263	0.999	-14.210	1.345	15.507	1.061	-8.884
1 - 3	1.036	1.204	16.192	0.912	-11.973	1.249	20.566	1.039	0.310
1 - 4	0.950	1.092	14.937	0.820	-13.687	1.144	20.442	0.984	3.628
1 - 5	0.886	0.961	8.417	0.712	-19.622	1.020	15.107	0.871	-1.670
1 - 6	0.794	0.801	0.941	0.583	-26.527	0.867	9.176	0.683	-14.038
2 - 1	1.503	1.458	-2.961	1.241	-17.441	1.510	0.467	1.153	-23.261
2 - 2	1.361	1.440	5.778	1.224	-10.040	1.492	9.654	1.156	-15.079
2 - 3	1.190	1.329	11.658	1.122	-5.735	1.389	16.701	1.150	-3.332
2 - 4	1.085	1.204	10.965	1.007	-7.189	1.271	17.154	1.110	2.287
2 - 5	0.989	1.059	7.100	0.875	-11.550	1.133	14.571	1.004	1.530
2 - 6	0.848	0.884	4.237	0.717	-15.460	0.963	13.601	0.804	-5.146
3 - 1	1.464	1.456	-0.528	1.331	-9.069	1.536	4.889	1.179	-19.495
3 - 2	1.374	1.402	2.034	1.277	-7.052	1.484	8.013	1.179	-14.189
3 - 3	1.261	1.270	0.701	1.146	-9.129	1.358	7.697	1.160	-8.035
3 - 4	1.129	1.117	-1.048	0.996	-11.822	1.211	7.234	1.077	-4.640
3 - 5	0.971	0.932	-3.979	0.816	-15.952	1.029	6.018	0.886	-8.763
4 - 1	1.453	1.476	1.597	1.430	-1.606	1.582	8.850	1.172	-19.343
4 - 2	1.408	1.452	3.112	1.405	-0.244	1.558	10.666	1.173	-16.687
4 - 3	1.280	1.315	2.767	1.261	-1.477	1.426	11.432	1.161	-9.297
4 - 4	1.141	1.157	1.402	1.095	-4.005	1.271	11.423	1.088	-4.641
4 - 5	0.997	0.965	-3.163	0.898	-9.952	1.081	8.421	0.905	-9.261
5 - 1	1.427	1.448	1.483	1.447	1.395	1.570	10.022	1.169	-18.099
5 - 2	1.309	1.342	2.547	1.332	1.759	1.467	12.059	1.166	-10.933
5 - 3	1.133	1.181	4.223	1.157	2.144	1.308	15.418	1.114	-1.707
5 - 4	0.967	0.985	1.860	0.948	-1.965	1.111	14.943	0.946	-2.146
6 - 1	1.344	1.429	6.341	1.466	9.091	1.563	16.277	1.172	-12.764
6 - 2	1.282	1.370	6.854	1.400	9.173	1.504	17.355	1.172	-8.566
6 - 3	1.180	1.205	2.139	1.216	3.086	1.341	13.684	1.137	-3.640
6 - 4	0.998	1.005	0.686	0.996	-0.243	1.140	14.200	0.985	-1.276
7 - 1	1.117	1.212	8.527	0.948	-15.129	1.227	9.847	0.882	-21.012
7 - 2	1.041	1.181	13.414	0.921	-11.512	1.198	15.101	0.883	-15.163
7 - 3	0.972	1.113	14.522	0.864	-11.140	1.137	16.925	0.880	-9.461
7 - 4	0.896	1.041	16.190	0.803	-10.361	1.070	19.434	0.865	-3.436

7 - 5	0.813	0.960	18.132	0.735	-9.563	0.995	22.434	0.828	1.790
7 - 6	0.750	0.870	16.007	0.660	-12.032	0.911	21.451	0.759	1.264
7 - 7	0.679	0.765	12.720	0.573	-15.611	0.812	19.571	0.652	-4.038
7 - 8	0.600	0.638	6.401	0.469	-21.801	0.690	14.991	0.495	-17.483
8 - 1	1.002	1.116	11.392	0.967	-3.539	1.169	16.677	0.927	-7.525
8 - 2	0.877	1.049	19.650	0.903	3.020	1.106	26.127	0.926	5.575
8 - 3	0.784	0.950	21.139	0.810	3.263	1.012	29.018	0.903	15.150
8 - 4	0.708	0.836	18.131	0.705	-0.484	0.903	27.475	0.830	17.199
8 - 5	0.623	0.698	12.022	0.577	-7.316	0.767	23.163	0.675	8.305
9 - 1	1.043	1.073	2.845	1.003	-3.859	1.158	11.015	0.912	-12.525
9 - 2	0.872	0.994	13.974	0.922	5.776	1.081	24.009	0.910	4.336
9 - 3	0.785	0.874	11.372	0.801	2.082	0.964	22.802	0.869	10.709
9 - 4	0.643	0.729	13.413	0.656	2.082	0.819	27.426	0.738	14.840
10 - 1	1.141	0.986	-13.571	0.975	-14.517	1.100	-3.604	0.883	-22.602
10 - 2	0.876	0.899	2.606	0.882	0.645	1.012	15.560	0.878	0.280
10 - 3	0.658	0.750	13.915	0.722	9.720	0.860	30.742	0.800	21.515
11 - 1	0.894	0.940	5.155	0.961	7.502	1.068	19.489	0.868	-2.944
11 - 2	0.834	0.913	9.482	0.931	11.576	1.041	24.781	0.867	4.013
11 - 3	0.737	0.762	3.330	0.762	3.426	0.885	20.019	0.823	11.648
12 - 1	0.876	0.886	1.110	0.928	5.912	1.023	16.770	0.860	-1.799
12 - 2	0.683	0.775	13.444	0.801	17.331	0.907	32.870	0.846	23.895
13 - 1	0.882	0.893	1.292	0.717	-18.736	0.909	3.118	0.654	-25.824
13 - 2	0.814	0.849	4.329	0.679	-16.623	0.869	6.764	0.655	-19.522
13 - 3	0.774	0.801	3.489	0.637	-17.716	0.825	6.544	0.650	-16.013
13 - 4	0.722	0.749	3.720	0.592	-18.005	0.776	7.525	0.634	-12.121
13 - 5	0.679	0.691	1.736	0.542	-20.185	0.722	6.349	0.602	-11.327
13 - 6	0.622	0.626	0.601	0.486	-21.816	0.661	6.240	0.548	-11.906
13 - 7	0.571	0.550	-3.652	0.422	-26.092	0.589	3.108	0.466	-18.394
13 - 8	0.452	0.459	1.538	0.346	-23.517	0.500	10.714	0.351	-22.275
14 - 1	0.765	0.748	-2.247	0.673	-11.973	0.809	5.807	0.638	-16.602
14 - 2	0.646	0.671	3.865	0.598	-7.455	0.734	13.700	0.632	-2.127
14 - 3	0.556	0.590	6.147	0.519	-6.593	0.655	17.761	0.595	6.990
14 - 4	0.472	0.492	4.252	0.425	-9.938	0.556	17.861	0.496	5.172
15 - 1	0.696	0.702	0.838	0.692	-0.624	0.796	14.335	0.593	-14.761
15 - 2	0.655	0.691	5.425	0.680	3.753	0.784	19.742	0.593	-9.407
15 - 3	0.588	0.607	3.290	0.590	0.411	0.699	18.910	0.581	-1.131
15 - 4	0.501	0.507	1.100	0.484	-3.469	0.594	18.619	0.512	2.175
16 - 1	0.732	0.602	-17.702	0.633	-13.491	0.719	-1.749	0.552	-24.545
16 - 2	0.563	0.514	-8.733	0.532	-5.595	0.624	10.784	0.538	-4.455
17 - 1	0.592	0.578	-2.370	0.632	6.804	0.707	19.396	0.532	-10.145
17 - 2	0.521	0.519	-0.451	0.562	7.826	0.642	23.158	0.527	1.139
18 - 1	0.657	0.553	-15.841	0.625	-4.869	0.690	4.973	0.521	-20.757
18 - 2	0.592	0.525	-11.394	0.590	-0.343	0.658	11.139	0.520	-12.159
19 - 1	0.701	0.673	-3.966	0.547	-21.911	0.700	-0.154	0.540	-23.021
19 - 2	0.680	0.661	-2.837	0.536	-21.139	0.688	1.216	0.540	-20.632
19 - 3	0.627	0.618	-1.514	0.498	-20.531	0.648	3.318	0.538	-14.242
19 - 4	0.571	0.570	-0.225	0.456	-20.084	0.603	5.549	0.525	-8.103

19 - 5	0.524	0.516	-1.588	0.409	-21.951	0.551	5.187	0.492	-6.078
19 - 6	0.478	0.454	-5.112	0.355	-25.692	0.491	2.778	0.432	-9.611
19 - 7	0.367	0.378	3.094	0.291	-20.717	0.418	13.782	0.336	-8.502
20 - 1	0.650	0.581	-10.572	0.539	-17.035	0.648	-0.248	0.499	-23.265
20 - 2	0.559	0.546	-2.285	0.504	-9.874	0.613	9.711	0.498	-10.917
20 - 3	0.456	0.480	5.321	0.437	-4.082	0.547	19.852	0.478	4.928
20 - 4	0.408	0.400	-1.863	0.358	-12.252	0.464	13.812	0.410	0.399
21 - 1	0.529	0.489	-7.596	0.497	-6.137	0.583	10.245	0.450	-14.901
21 - 2	0.437	0.408	-6.690	0.407	-6.854	0.496	13.477	0.434	-0.714
22 - 1	0.519	0.457	-11.867	0.504	-2.862	0.574	10.539	0.411	-20.791
22 - 2	0.435	0.410	-5.698	0.447	2.839	0.520	19.644	0.407	-6.415
23 - 1	0.468	0.447	-4.457	0.517	10.435	0.576	23.038	0.393	-16.056
23 - 2	0.435	0.412	-5.292	0.472	8.578	0.535	23.018	0.391	-10.093
24 - 1	0.472	0.433	-8.168	0.520	10.206	0.570	20.822	0.382	-18.986
24 - 2	0.445	0.415	-6.656	0.497	11.586	0.549	23.375	0.382	-14.124
25 - 1	0.625	0.571	-8.635	0.469	-24.977	0.603	-3.584	0.477	-23.653
25 - 2	0.538	0.509	-5.474	0.413	-23.191	0.543	0.966	0.472	-12.199
25 - 3	0.483	0.461	-4.638	0.371	-23.228	0.497	2.916	0.452	-6.476
25 - 4	0.420	0.405	-3.568	0.322	-23.353	0.443	5.469	0.405	-3.654
25 - 5	0.329	0.338	2.664	0.264	-19.879	0.376	14.419	0.321	-2.483
31 - 1	1.556	1.388	-10.814	1.138	-26.840	1.494	-4.014	1.063	-31.706
31 - 2	1.229	1.258	2.321	1.022	-16.853	1.367	11.229	1.057	-13.975
31 - 3	1.103	1.139	3.287	0.917	-16.867	1.251	13.414	1.019	-7.641
31 - 4	1.036	1.002	-3.260	0.796	-23.130	1.115	7.626	0.920	-11.153
31 - 5	0.936	0.836	-10.659	0.652	-30.302	0.948	1.254	0.736	-21.343
32 - 1	1.772	1.520	-14.245	1.384	-21.879	1.649	-6.948	1.151	-35.020
32 - 2	1.619	1.499	-7.421	1.364	-15.736	1.629	0.595	1.153	-28.792
32 - 3	1.343	1.385	3.116	1.252	-6.766	1.517	12.949	1.149	-14.454
32 - 4	1.197	1.255	4.830	1.124	-6.095	1.388	15.992	1.108	-7.402
32 - 5	1.049	1.104	5.276	0.977	-6.861	1.238	18.022	1.003	-4.359
32 - 6	0.921	0.921	0.027	0.800	-13.116	1.052	14.247	0.803	-12.777
33 - 1	1.696	1.570	-7.434	1.540	-9.170	1.729	1.935	1.175	-30.736
33 - 2	1.376	1.461	6.161	1.425	3.545	1.621	17.777	1.174	-14.691
33 - 3	1.236	1.324	7.097	1.279	3.510	1.484	20.029	1.141	-7.655
33 - 4	1.100	1.165	5.916	1.112	1.126	1.323	20.280	1.043	-5.175
33 - 5	0.975	0.971	-0.363	0.910	-6.622	1.124	15.292	0.843	-13.541
34 - 1	1.768	1.566	-11.431	1.628	-7.938	1.755	-0.739	1.171	-33.746
34 - 2	1.350	1.371	1.557	1.408	4.263	1.558	15.398	1.154	-14.533
34 - 3	1.200	1.206	0.491	1.222	1.873	1.389	15.716	1.073	-10.602
34 - 4	1.024	1.006	-1.733	1.002	-2.147	1.181	15.296	0.884	-13.648
35 - 1	1.639	1.545	-5.760	1.657	1.070	1.751	6.810	1.168	-28.765
35 - 2	1.385	1.400	1.064	1.488	7.435	1.603	15.728	1.161	-16.206
35 - 3	1.191	1.231	3.387	1.293	8.545	1.429	19.975	1.097	-7.918
35 - 4	1.025	1.027	0.204	1.059	3.314	1.215	18.490	0.920	-10.243
36 - 1	1.612	1.491	-7.494	1.640	1.712	1.709	5.991	1.172	-27.267
36 - 2	1.212	1.258	3.755	1.360	12.234	1.467	21.010	1.137	-6.184
36 - 3	1.014	1.048	3.395	1.113	9.795	1.246	22.885	0.985	-2.834

37 - 1	1.152	1.111	-3.586	0.921	-20.077	1.194	3.608	0.888	-22.911
37 - 2	0.941	1.003	6.542	0.823	-12.553	1.089	15.697	0.882	-6.230
37 - 3	0.845	0.908	7.510	0.739	-12.581	0.996	17.928	0.849	0.495
37 - 4	0.778	0.799	2.719	0.642	-17.538	0.888	14.164	0.766	-1.549
37 - 5	0.689	0.666	-3.276	0.525	-23.786	0.755	9.527	0.611	-11.292
38 - 1	1.315	1.173	-10.780	1.090	-17.145	1.287	-2.149	0.926	-29.561
38 - 2	1.157	1.094	-5.438	1.009	-12.782	1.209	4.459	0.924	-20.101
38 - 3	1.041	0.991	-4.811	0.905	-13.032	1.106	6.232	0.900	-13.584
38 - 4	0.881	0.872	-1.054	0.786	-10.732	0.986	11.895	0.823	-6.577
38 - 5	0.755	0.728	-3.554	0.646	-14.475	0.839	11.112	0.668	-11.577
39 - 1	1.222	1.081	-11.563	1.078	-11.752	1.227	0.392	0.912	-25.367
39 - 2	1.121	1.036	-7.577	1.030	-8.133	1.181	5.378	0.912	-18.642
39 - 3	0.895	0.912	1.877	0.895	0.045	1.054	17.711	0.885	-1.117
39 - 4	0.737	0.761	3.284	0.735	-0.324	0.896	21.597	0.768	4.182
40 - 1	1.152	1.003	-12.897	1.061	-7.914	1.176	2.061	0.883	-23.341
40 - 2	0.996	0.937	-5.889	0.985	-1.107	1.106	11.065	0.882	-11.493
40 - 3	0.804	0.782	-2.777	0.807	0.318	0.940	16.926	0.815	1.423
41 - 1	1.036	0.960	-7.354	1.049	1.278	1.145	10.561	0.868	-16.247
41 - 2	0.797	0.795	-0.251	0.853	7.067	0.968	21.406	0.834	4.583
42 - 1	0.911	0.917	0.648	1.029	12.963	1.111	21.909	0.861	-5.537
42 - 2	0.805	0.808	0.426	0.896	11.323	0.992	23.251	0.849	5.404
43 - 1	0.817	0.803	-1.695	0.682	-16.547	0.870	6.486	0.658	-19.491
43 - 2	0.790	0.781	-1.188	0.661	-16.335	0.848	7.350	0.658	-16.698
43 - 3	0.705	0.720	2.163	0.605	-14.141	0.789	11.915	0.653	-7.427
43 - 4	0.647	0.652	0.813	0.543	-16.084	0.722	11.571	0.626	-3.269
43 - 5	0.602	0.574	-4.695	0.472	-21.671	0.643	6.879	0.563	-6.543
43 - 6	0.495	0.479	-3.283	0.386	-21.933	0.547	10.506	0.448	-9.539
44 - 1	0.710	0.755	6.386	0.726	2.296	0.860	21.065	0.638	-10.165
44 - 2	0.641	0.700	9.179	0.668	4.233	0.803	25.238	0.636	-0.782
44 - 3	0.559	0.616	10.121	0.580	3.830	0.716	28.017	0.607	8.653
44 - 4	0.491	0.513	4.564	0.475	-3.183	0.608	23.871	0.516	5.083
45 - 1	0.731	0.713	-2.522	0.751	2.735	0.849	16.154	0.594	-18.802
45 - 2	0.618	0.634	2.539	0.660	6.835	0.764	23.694	0.587	-5.066
45 - 3	0.509	0.528	3.827	0.541	6.251	0.650	27.648	0.526	3.305
46 - 1	0.671	0.623	-7.113	0.701	4.504	0.780	16.289	0.552	-17.704
46 - 2	0.532	0.536	0.774	0.594	11.722	0.682	28.178	0.540	1.445
47 - 1	0.561	0.576	2.598	0.672	19.698	0.741	32.112	0.532	-5.180
47 - 2	0.512	0.541	5.693	0.628	22.698	0.702	37.016	0.531	3.729
48 - 1	0.519	0.565	8.898	0.683	31.642	0.740	42.632	0.521	0.313
49 - 1	0.674	0.617	-8.430	0.531	-21.146	0.681	1.109	0.541	-19.735
49 - 2	0.637	0.594	-6.747	0.510	-19.988	0.659	3.377	0.541	-15.067
49 - 3	0.558	0.538	-3.599	0.457	-18.072	0.602	7.972	0.532	-4.674
49 - 4	0.499	0.473	-5.185	0.397	-20.433	0.537	7.616	0.494	-1.080
49 - 5	0.405	0.395	-2.528	0.325	-19.659	0.457	12.726	0.406	0.244
50 - 1	0.682	0.594	-12.839	0.590	-13.520	0.696	2.087	0.499	-26.865
50 - 2	0.633	0.570	-9.994	0.563	-11.052	0.670	5.892	0.499	-21.231
50 - 3	0.519	0.501	-3.509	0.489	-5.875	0.597	15.056	0.483	-6.897

50 - 4	0.412	0.418	1.367	0.400	-2.887	0.508	23.183	0.419	1.622
51 - 1	0.505	0.510	0.993	0.555	9.953	0.638	26.260	0.450	-10.857
51 - 2	0.427	0.425	-0.363	0.455	6.601	0.542	26.970	0.434	1.611
52 - 1	0.514	0.473	-7.939	0.559	8.708	0.623	21.113	0.411	-20.008
52 - 2	0.437	0.428	-2.059	0.500	14.475	0.569	30.209	0.408	-6.652
53 - 1	0.447	0.458	2.383	0.566	26.576	0.619	38.431	0.393	-12.112
53 - 2	0.410	0.430	4.841	0.528	28.823	0.585	42.697	0.392	-4.380
54 - 1	0.419	0.448	6.869	0.576	37.406	0.618	47.514	0.382	-8.727
54 - 2	0.408	0.433	6.224	0.555	36.099	0.600	47.118	0.382	-6.298
61 - 1	1.373	1.354	-1.375	0.958	-30.208	1.305	-4.926	1.057	-23.004
61 - 2	1.233	1.244	0.854	0.875	-29.049	1.209	-1.964	1.060	-14.070
61 - 3	1.138	1.143	0.435	0.796	-30.050	1.121	-1.503	1.029	-9.615
61 - 4	1.042	1.034	-0.728	0.713	-31.561	1.025	-1.643	0.964	-7.494
61 - 5	0.953	0.911	-4.442	0.620	-34.932	0.914	-4.087	0.847	-11.146
61 - 6	0.816	0.761	-6.743	0.509	-37.597	0.778	-4.669	0.659	-19.202
62 - 1	1.447	1.378	-4.778	1.078	-25.470	1.349	-6.786	1.156	-20.123
62 - 2	1.314	1.262	-3.939	0.980	-25.423	1.247	-5.117	1.152	-12.332
62 - 3	1.228	1.142	-6.998	0.878	-28.538	1.140	-7.187	1.112	-9.412
62 - 4	1.115	1.007	-9.656	0.766	-31.336	1.018	-8.680	1.013	-9.174
62 - 5	0.975	0.840	-13.813	0.627	-35.687	0.865	-11.241	0.813	-16.564
63 - 1	1.476	1.394	-5.543	1.173	-20.553	1.388	-5.948	1.178	-20.187
63 - 2	1.382	1.332	-3.633	1.116	-19.273	1.332	-3.591	1.179	-14.721
63 - 3	1.254	1.206	-3.847	1.000	-20.236	1.219	-2.814	1.156	-7.843
63 - 4	1.078	1.062	-1.463	0.871	-19.196	1.088	0.907	1.070	-0.709
63 - 5	0.936	0.886	-5.373	0.713	-23.831	0.924	-1.262	0.876	-6.369
64 - 1	1.459	1.415	-3.001	1.262	-13.497	1.432	-1.880	1.173	-19.635
64 - 2	1.279	1.249	-2.350	1.101	-13.947	1.280	0.068	1.158	-9.498
64 - 3	1.200	1.100	-8.359	0.958	-20.187	1.142	-4.840	1.082	-9.873
64 - 4	0.986	0.917	-7.032	0.784	-20.535	0.970	-1.628	0.894	-9.292
65 - 1	1.496	1.406	-6.049	1.293	-13.589	1.437	-3.962	1.167	-21.995
65 - 2	1.372	1.274	-7.111	1.162	-15.278	1.316	-4.070	1.161	-15.412
65 - 3	1.169	1.120	-4.153	1.009	-13.703	1.173	0.316	1.096	-6.232
65 - 4	1.010	0.935	-7.411	0.827	-18.094	0.997	-1.257	0.920	-8.910
66 - 1	1.381	1.418	2.669	1.343	-2.741	1.459	5.615	1.172	-15.145
66 - 2	1.267	1.301	2.709	1.223	-3.499	1.351	6.604	1.167	-7.913
66 - 3	1.156	1.145	-0.957	1.063	-8.077	1.204	4.180	1.110	-4.006
66 - 4	1.048	0.955	-8.915	0.870	-17.012	1.023	-2.367	0.937	-10.546
67 - 1	1.101	1.168	6.120	0.841	-23.615	1.116	1.363	0.881	-19.982
67 - 2	1.058	1.120	5.830	0.802	-24.150	1.074	1.529	0.881	-16.744
67 - 3	1.019	1.056	3.599	0.752	-26.159	1.019	-0.013	0.876	-14.081
67 - 4	0.974	0.987	1.316	0.699	-28.222	0.959	-1.545	0.857	-12.022
67 - 5	0.925	0.911	-1.535	0.640	-30.757	0.892	-3.532	0.816	-11.750
67 - 6	0.856	0.824	-3.704	0.574	-32.967	0.816	-4.685	0.745	-13.012
67 - 7	0.774	0.726	-6.156	0.500	-35.433	0.728	-5.908	0.637	-17.694
67 - 8	0.655	0.607	-7.341	0.410	-37.346	0.620	-5.374	0.483	-26.289
68 - 1	1.101	1.109	0.718	0.887	-19.409	1.093	-0.761	0.927	-15.840
68 - 2	0.988	0.996	0.858	0.789	-20.163	0.993	0.479	0.919	-7.014

68 - 3	0.855	0.902	5.522	0.707	-17.282	0.908	6.209	0.882	3.144
68 - 4	0.748	0.794	6.181	0.615	-17.764	0.810	8.288	0.795	6.230
68 - 5	0.637	0.663	4.078	0.504	-20.813	0.689	8.140	0.634	-0.537
69 - 1	1.287	1.085	-15.716	0.939	-27.036	1.099	-14.571	0.913	-29.082
69 - 2	1.071	0.945	-11.809	0.806	-24.705	0.971	-9.319	0.897	-16.288
69 - 3	0.939	0.832	-11.437	0.702	-25.270	0.867	-7.721	0.833	-11.325
69 - 4	0.849	0.693	-18.367	0.574	-32.406	0.736	-13.324	0.684	-19.427
70 - 1	1.117	1.007	-9.816	0.923	-17.369	1.054	-5.658	0.883	-20.969
70 - 2	0.982	0.854	-13.049	0.770	-21.569	0.909	-7.453	0.858	-12.627
70 - 3	0.895	0.712	-20.441	0.631	-29.532	0.772	-13.706	0.746	-16.665
71 - 1	0.997	1.005	0.786	0.957	-3.999	1.066	6.929	0.868	-12.938
71 - 2	0.820	0.868	5.837	0.814	-0.758	0.935	13.999	0.850	3.602
71 - 3	0.751	0.723	-3.671	0.666	-11.333	0.794	5.740	0.748	-0.417
72 - 1	0.960	0.999	4.077	0.980	2.117	1.071	11.595	0.860	-10.392
72 - 2	0.872	0.883	1.313	0.856	-1.792	0.960	10.038	0.849	-2.648
72 - 3	0.753	0.736	-2.251	0.700	-7.030	0.815	8.196	0.758	0.610
73 - 1	0.919	0.866	-5.798	0.640	-30.343	0.831	-9.556	0.654	-28.793
73 - 2	0.874	0.807	-7.695	0.593	-32.163	0.780	-10.732	0.654	-25.192
73 - 3	0.819	0.760	-7.219	0.555	-32.229	0.739	-9.715	0.645	-21.198
73 - 4	0.767	0.710	-7.443	0.515	-32.816	0.696	-9.300	0.626	-18.341
73 - 5	0.704	0.655	-6.959	0.472	-32.967	0.647	-8.066	0.591	-16.027
73 - 6	0.636	0.594	-6.646	0.424	-33.338	0.593	-6.819	0.535	-15.833
73 - 7	0.563	0.522	-7.195	0.369	-34.545	0.528	-6.138	0.453	-19.526
73 - 8	0.474	0.436	-8.041	0.302	-36.313	0.449	-5.238	0.340	-28.332
74 - 1	0.718	0.760	5.801	0.632	-11.933	0.772	7.459	0.637	-11.328
74 - 2	0.674	0.703	4.360	0.581	-13.737	0.720	6.853	0.635	-5.801
74 - 3	0.605	0.637	5.286	0.522	-13.781	0.659	8.924	0.616	1.796
74 - 4	0.529	0.560	5.948	0.453	-14.290	0.588	11.082	0.561	6.129
74 - 5	0.437	0.468	7.003	0.372	-14.969	0.500	14.321	0.453	3.662
75 - 1	0.608	0.718	18.063	0.655	7.730	0.763	25.527	0.593	-2.495
75 - 2	0.560	0.656	17.139	0.594	6.013	0.704	25.736	0.590	5.309
75 - 3	0.512	0.577	12.731	0.516	0.818	0.628	22.649	0.559	9.277
75 - 4	0.478	0.481	0.663	0.422	-11.615	0.534	11.615	0.471	-1.398
76 - 1	0.604	0.666	10.275	0.653	8.190	0.740	22.448	0.552	-8.615
76 - 2	0.565	0.585	3.617	0.567	0.356	0.659	16.618	0.544	-3.791
76 - 3	0.467	0.488	4.523	0.464	-0.576	0.560	19.902	0.484	3.534
77 - 1	0.603	0.625	3.636	0.637	5.657	0.713	18.172	0.532	-11.803
77 - 2	0.583	0.591	1.349	0.599	2.762	0.678	16.249	0.531	-8.906
77 - 3	0.476	0.492	3.459	0.490	2.988	0.576	20.952	0.495	3.994
78 - 1	0.570	0.593	4.089	0.624	9.551	0.691	21.145	0.521	-8.680
78 - 2	0.467	0.498	6.703	0.515	10.361	0.591	26.483	0.503	7.782
79 - 1	0.655	0.627	-4.324	0.467	-28.678	0.617	-5.799	0.539	-17.718
79 - 2	0.615	0.586	-4.744	0.434	-29.393	0.581	-5.552	0.539	-12.439
79 - 3	0.583	0.541	-7.189	0.398	-31.651	0.541	-7.212	0.529	-9.275
79 - 4	0.510	0.490	-3.968	0.357	-29.975	0.495	-2.995	0.499	-2.068
79 - 5	0.439	0.431	-1.875	0.310	-29.348	0.441	0.446	0.442	0.599
79 - 6	0.356	0.359	0.961	0.254	-28.600	0.375	5.305	0.346	-2.884

80 - 1	0.568	0.590	3.859	0.506	-10.936	0.617	8.708	0.498	-12.311
80 - 2	0.541	0.573	5.825	0.490	-9.491	0.601	11.118	0.498	-7.923
80 - 3	0.501	0.518	3.477	0.439	-12.315	0.550	9.793	0.491	-2.043
80 - 4	0.429	0.456	6.283	0.382	-11.045	0.490	14.298	0.457	6.520
80 - 5	0.355	0.380	7.145	0.313	-11.901	0.417	17.430	0.377	6.244
81 - 1	0.593	0.549	-7.487	0.521	-12.129	0.608	2.505	0.450	-24.126
81 - 2	0.447	0.465	3.921	0.434	-2.883	0.524	17.178	0.437	-2.284
81 - 3	0.397	0.387	-2.464	0.355	-10.503	0.445	12.093	0.379	-4.418
82 - 1	0.483	0.504	4.377	0.519	7.379	0.588	21.803	0.411	-14.913
82 - 2	0.465	0.467	0.481	0.477	2.532	0.550	18.180	0.409	-11.948
82 - 3	0.407	0.390	-4.254	0.391	-3.982	0.467	14.801	0.377	-7.373
83 - 1	0.449	0.477	6.149	0.513	14.161	0.573	27.637	0.393	-12.515
83 - 2	0.399	0.391	-1.913	0.413	3.410	0.480	20.405	0.375	-5.925
84 - 1	0.439	0.463	5.378	0.517	17.673	0.568	29.434	0.382	-12.908
84 - 2	0.396	0.395	-0.355	0.434	9.541	0.493	24.466	0.372	-5.988
85 - 1	0.606	0.553	-8.780	0.418	-31.057	0.550	-9.211	0.477	-21.362
85 - 2	0.558	0.524	-6.155	0.394	-29.359	0.524	-6.064	0.477	-14.561
85 - 3	0.519	0.483	-6.896	0.361	-30.416	0.488	-6.019	0.469	-9.544
85 - 4	0.465	0.437	-5.923	0.324	-30.366	0.446	-4.050	0.445	-4.205
85 - 5	0.389	0.385	-1.093	0.281	-27.707	0.398	2.231	0.396	1.757
85 - 6	0.308	0.321	4.177	0.230	-25.235	0.338	9.724	0.311	1.063
86 - 1	0.484	0.514	6.128	0.450	-6.983	0.548	13.315	0.428	-11.617
86 - 2	0.405	0.459	13.349	0.398	-1.673	0.496	22.475	0.423	4.553
86 - 3	0.356	0.404	13.441	0.346	-2.766	0.442	24.244	0.397	11.646
86 - 4	0.283	0.337	18.931	0.283	0.056	0.376	32.750	0.331	16.865
87 - 1	0.494	0.479	-3.001	0.467	-5.366	0.544	10.183	0.380	-23.066
87 - 2	0.464	0.464	0.089	0.452	-2.518	0.529	14.105	0.380	-18.073
87 - 3	0.419	0.409	-2.463	0.394	-6.064	0.472	12.738	0.370	-11.676
87 - 4	0.338	0.341	0.749	0.322	-4.768	0.401	18.689	0.322	-4.603
88 - 1	0.433	0.438	1.180	0.466	7.642	0.527	21.721	0.344	-20.479
88 - 2	0.391	0.409	4.553	0.432	10.468	0.495	26.700	0.343	-12.184
88 - 3	0.339	0.341	0.528	0.354	4.334	0.421	24.188	0.317	-6.379
89 - 1	0.379	0.412	8.823	0.460	21.271	0.513	35.269	0.328	-13.490
89 - 2	0.297	0.341	14.958	0.374	25.857	0.433	45.820	0.315	5.938
90 - 1	0.341	0.400	17.159	0.464	36.033	0.509	49.142	0.318	-6.611
90 - 2	0.287	0.343	19.630	0.393	36.764	0.444	54.723	0.311	8.384

Appendix G

Error % for the Spout Diameter

T °C	d_p (mm)	D_i (mm)	H_m (m)	U_{ms} (m/s)	d_s-exp (cm)	*McNab's* (cm)	% *dev*	*Wu's* (cm)	% *dev*
20	2.025	19.05	0.700	1.399	3.370	4.089	21.349	3.726	10.556
20	2.025	19.05	0.400	0.950	3.100	3.336	7.600	3.137	1.191
20	2.025	19.05	0.200	0.794	3.010	3.037	0.885	2.897	-3.754
20	1.630	19.05	0.850	1.117	3.580	3.664	2.340	3.380	-5.590
20	1.630	19.05	0.700	0.972	3.320	3.409	2.688	3.178	-4.262
20	1.630	19.05	0.500	0.813	3.020	3.102	2.701	2.935	-2.801
20	1.630	19.05	0.300	0.679	2.680	2.823	5.325	2.710	1.123
20	1.200	19.05	0.900	0.882	3.100	3.270	5.472	3.053	-1.520
20	1.200	19.05	0.700	0.774	2.930	3.044	3.906	2.878	-1.761
20	1.200	19.05	0.500	0.679	2.690	2.836	5.435	2.714	0.895
20	1.200	19.05	0.300	0.571	2.620	2.592	-1.071	2.514	-4.053
20	1.010	19.05	0.730	0.701	2.970	2.900	-2.351	2.757	-7.156
20	1.010	19.05	0.500	0.571	2.820	2.604	-7.647	2.517	-10.727
20	1.010	19.05	0.300	0.478	2.500	2.376	-4.971	2.327	-6.902
20	2.025	26.64	0.620	1.556	4.330	4.276	-1.236	3.893	-10.101
20	2.025	26.64	0.500	1.229	3.720	3.796	2.047	3.511	-5.630
20	2.025	26.64	0.300	1.036	3.750	3.471	-7.451	3.254	-13.222
20	1.630	26.64	0.630	1.152	3.970	3.688	-7.107	3.416	-13.944
20	1.200	26.64	0.650	0.817	2.690	3.123	16.078	2.946	9.501
20	1.200	26.64	0.500	0.705	2.890	2.892	0.081	2.760	-4.512
20	1.010	26.64	0.545	0.674	2.920	2.832	-3.030	2.707	-7.294
20	1.010	26.64	0.400	0.558	2.580	2.571	-0.347	2.491	-3.438
20	0.915	12.70	0.680	0.606	2.250	2.703	20.113	2.589	15.087
20	0.915	12.70	0.400	0.465	1.940	2.349	21.106	2.301	18.634
170	1.630	19.05	0.585	1.002	2.830	2.815	-0.540	3.142	11.016
170	1.630	19.05	0.400	0.784	2.650	2.485	-6.208	2.821	6.464
170	1.630	19.05	0.300	0.708	2.510	2.353	-6.254	2.695	7.386
170	1.200	19.05	0.510	0.765	2.710	2.454	-9.435	2.791	2.987
170	1.200	19.05	0.300	0.556	2.410	2.088	-13.373	2.427	0.685
170	1.010	19.05	0.460	0.650	2.380	2.262	-4.960	2.599	9.214
170	1.010	19.05	0.400	0.559	2.220	2.097	-5.540	2.434	9.618
170	1.010	19.05	0.300	0.456	1.930	1.893	-1.903	2.226	15.354
170	2.025	26.64	0.615	1.772	3.960	3.748	-5.348	4.031	1.788
170	2.025	26.64	0.500	1.343	3.790	3.249	-14.271	3.567	-5.887
170	2.025	26.64	0.300	1.049	3.570	2.858	-19.942	3.198	-10.427
170	1.630	26.64	0.500	1.157	3.200	3.017	-5.730	3.343	4.455
170	1.200	26.64	0.475	0.710	2.890	2.368	-18.075	2.703	-6.483

170	1.200	26.64	0.300	0.559	2.640	2.094	-20.663	2.433	-7.855
170	1.010	26.64	0.440	0.682	2.510	2.316	-7.735	2.654	5.737
170	1.010	26.64	0.300	0.519	3.100	2.020	-34.850	2.356	-24.013
170	0.915	12.70	0.515	0.484	2.190	1.964	-10.342	2.290	4.549
300	1.630	19.05	0.475	1.043	2.860	2.522	-11.833	3.165	10.677
300	1.630	19.05	0.300	0.785	2.560	2.182	-14.769	2.794	9.140
300	1.200	19.05	0.415	0.696	2.660	2.063	-22.429	2.655	-0.204
300	1.200	19.05	0.300	0.588	2.360	1.892	-19.815	2.465	4.432
300	1.010	19.05	0.300	0.529	2.190	1.798	-17.890	2.355	7.524
300	2.025	26.64	0.590	1.696	3.790	3.224	-14.921	3.917	3.345
300	2.025	26.64	0.500	1.376	3.560	2.897	-18.619	3.573	0.351
300	2.025	26.64	0.300	1.100	3.700	2.576	-30.374	3.235	-12.579
300	1.630	26.64	0.400	1.121	3.530	2.610	-26.055	3.265	-7.505
300	1.200	26.64	0.390	0.731	2.840	2.110	-25.693	2.710	-4.566
300	1.010	26.64	0.300	0.505	2.940	1.758	-40.212	2.308	-21.501
300	0.915	12.70	0.430	0.494	2.160	1.750	-18.994	2.290	6.033
420	2.025	19.05	0.520	1.453	3.370	2.709	-19.600	3.614	7.250
420	2.025	19.05	0.300	1.141	3.070	2.387	-22.261	3.247	5.750
420	1.630	19.05	0.370	1.141	2.660	2.396	-9.939	3.250	22.191
420	1.200	19.05	0.285	0.732	3.090	1.918	-37.920	2.678	-13.343
420	1.010	19.05	0.255	0.519	2.450	1.621	-33.845	2.307	-5.836
420	2.025	26.64	0.540	1.768	3.940	2.986	-24.221	3.936	-0.097
420	2.025	26.64	0.400	1.350	3.710	2.604	-29.815	3.497	-5.741
420	2.025	26.64	0.300	1.200	3.500	2.451	-29.974	3.320	-5.139
420	1.630	26.64	0.350	1.152	3.500	2.407	-31.231	3.264	-6.748
420	1.200	26.64	0.280	0.671	2.790	1.840	-34.052	2.579	-7.549
420	0.915	12.70	0.350	0.433	2.060	1.487	-27.799	2.135	3.626
500	1.630	19.05	0.320	0.894	2.660	2.009	-24.488	2.896	8.871
500	1.200	19.05	0.255	0.592	2.810	1.640	-41.654	2.422	-13.825
500	1.010	19.05	0.240	0.468	2.880	1.460	-49.318	2.186	-24.085
500	2.025	26.64	0.500	1.639	4.030	2.723	-32.429	3.774	-6.346
500	2.025	26.64	0.300	1.191	3.640	2.312	-36.491	3.279	-9.911
500	1.200	26.64	0.235	0.561	2.880	1.597	-44.553	2.366	-17.856
500	1.010	26.64	0.220	0.447	2.840	1.427	-49.748	2.143	-24.532
500	0.915	12.70	0.305	0.379	2.010	1.320	-34.305	1.997	-0.631
580	2.025	19.05	0.440	1.344	3.240	2.344	-27.645	3.421	5.572
580	2.025	19.05	0.300	1.180	3.110	2.189	-29.605	3.228	3.807
580	1.630	19.05	0.270	0.876	2.700	1.894	-29.846	2.838	5.128
580	1.200	19.05	0.225	0.657	2.720	1.641	-39.659	2.504	-7.940
580	1.010	19.05	0.220	0.472	2.900	1.396	-51.871	2.170	-25.182
580	2.025	26.64	0.440	1.612	3.790	2.563	-32.381	3.701	-2.350
580	2.025	26.64	0.300	1.212	3.680	2.218	-39.723	3.266	-11.248
580	1.200	26.64	0.225	0.519	2.960	1.462	-50.602	2.261	-23.620
580	0.915	12.70	0.280	0.341	2.050	1.192	-41.873	1.885	-8.033